ENERGY

CONSERVATION

ORNL/Sub/83-47985/1

Free-Piston Stirling Engine Diaphragm-Coupled Heat-Actuated Heat Pump Component Technology Program

Phase 1B Final Report

R. A. Ackermann

Report Prepared by

MECHANICAL TECHNOLOGY, INC.
968 Albany-Shaker Road
Latham, New York 12110

under
Subcontract 86X-47985V

for

OAK RIDGE NATIONAL LABORATORY
operated by
MARTIN MARIETTA ENERGY SYSTEMS, INC.
for the

U.S. DEPARTMENT OF ENERGY

OFFICE OF BUILDINGS
AND COMMUNITY SYSTEMS

Printed in the United States of America. Available from
National Technical Information Service
U.S. Department of Commerce
5285 Port Royal Road, Springfield, Virginia 22161
NTIS price codes—Printed Copy: A07 Microfiche A01

This report was prepared as an account of work sponsored by an agency of the United States Government. Neither the United States Government nor any agency thereof, nor any of their employees, makes any warranty, express or implied, or assumes any legal liability or responsibility for the accuracy, completeness, or usefulness of any information, apparatus, product, or process disclosed, or represents that its use would not infringe privately owned rights. Reference herein to any specific commercial product, process, or service by trade name, trademark, manufacturer, or otherwise, does not necessarily constitute or imply its endorsement, recommendation, or favoring by the United States Government or any agency thereof. The views and opinions of authors expressed herein do not necessarily state or reflect those of the United States Government or any agency thereof.

ORNL/Sub/83-47985/1

FREE-PISTON STIRLING ENGINE DIAPHRAGM-COUPLED HEAT-ACTUATED HEAT PUMP COMPONENT TECHNOLOGY PROGRAM

PHASE 1B FINAL REPORT

R. A. Ackermann

Date Published—September 1987

Report Prepared by

MECHANICAL TECHNOLOGY, INC.
968 Albany-Shaker Road
Latham, New York 12110

under
Subcontract 86X-47985V

for

OAK RIDGE NATIONAL LABORATORY
Oak Ridge, Tennessee 37831
operated by
MARTIN MARIETTA ENERGY SYSTEMS, INC.
for the
U.S. DEPARTMENT OF ENERGY
under contract DE-AC05-84OR21400

ABSTRACT

In Phase I of the Diaphragm-Coupled Heat Pump Compressor Development Program, a free piston Stirling engine (FPSE) driven heat pump power module was designed, fabricated, and tested. The power module consisted of a natural gas combustor, FPSE, hydraulic transmission, and refrigerant compressor. A major problem encountered with this hardware was the shortfall in rated heating and cooling capacity. To determine the causes of the shortfall, an analytical investigation was conducted during Phase IA.

In Phase IA, it was identified that the heating and cooling capacity of the heat pump was limited by the higher-than-predicted power loss in the hydraulic transmission. The hydraulic transmission losses are manifested in a loss of engine pressure volume (PV) power because they limit the compressor piston stroke which in turn limits the engine's compression space swept volume and, therefore, the PV power generated. It was concluded that by reducing the hydraulic transmission losses, the capacity could be increased, and the design capacity of 3.0 tons of refrigeration at 95°F could possibly be achieved.

During Phase IB of the program, described herein, several of the more important losses identified in Phase IA were investigated experimentally. In particular, hardware associated with the critical clearance seals in the hydraulic transmission was modified, and several different hydraulic transmission fluids were tried. The results were encouraging in that improvements made to the hydraulic transmission produced a capacity increase from 1.0 to over 2.0 tons of cooling. However, the increase to 3.0 tons was not achieved. The testing did show conclusively, though, that the internal counterweight was responsible for the largest loss in the hydraulic transmission and, in order to achieve a significant increase in capacity, the internal counterweight would have to be removed.

TABLE OF CONTENTS

Section		Page
	ABSTRACT	iii
1.0	INTRODUCTION	1-1
2.0	EXECUTIVE SUMMARY	2-1
3.0	TECHNICAL DISCUSSION	3-1
	3.1 Milestone No. 1 - Reduction of Hydraulic Transmission Losses	3-5
	3.1.1 Work Element 1A - Rod Seals	3-5
	3.1.2 Work Element 1B - Clearance Seal	3-12
	3.1.3 Work Element 1C - Pumping Loss	3-21
	3.1.4 Work Element 1D - Viscous Loss	3-24
	3.1.5 Work Element 1E - Compressor Seal Loss	3-26
	3.1.6 Work Element 1F - Porting Loss	3-28
	3.2 Milestone No. 2 - Improvement of Mechanical Operating Characteristics	3-32
	3.2.1 Work Element 2A - Counterweight (Balancer)	3-32
	3.2.2 Work Element 2B - Piston Centering and Centerporting	3-32
	3.2.3 Work Element 2C - Gas Spring	3-42
	3.2.4 Work Element 2D - Mechanical Springs	3-45
	3.2.5 Work Element 2E - Refrigerant Shuttling	3-46
	3.2.6 Work Element 2F - Life Tests	3-47
	3.3 Summary of Breadboard Heat Pump Performance Improvements for Phase IB	3-47
	3.4 Milestone No. 3 - Oil Management System Development	3-54
	3.4.1 Overall System Description	3-54
	3.4.2 Control Logic	3-56
	3.4.3 System Hardware	3-59
4.0	EVALUATION OF NEW CONCEPTS	4-1
	4.1 Concept Selection	4-18
	APPENDIX A - HAHP BREADBOARD HEAT PUMP INSTRUMENTATION	A-1
	APPENDIX B - REFRIGERANT TEST LOOP AND COMPRESSOR LOADING CONTROL	B-1

LIST OF FIGURES

Number		Page
1-1	Compressor and Hydraulic Transmission Layout	1-2
1-2	Breadboard HAHP Power Module and Compressor Assembly	1-3
1-3	Representative Lower End and Engine (EM 4) Power Characteristics	1-6
3-1	HAHP Engine/Compressor Layout	3-3
3-2	Free-Piston Stirling Engine Heat Pump Power Module	3-4
3-3	Effect of Compressor Rod Oil Seals on Piston Power Loss	3-6
3-4	Change in Displacer/Piston Stroke Ratio	3-7
3-5	Push-Pull Static Test Summary	3-9
3-6	Rod Oil Seal Dynamic Tests	3-11
3-7	Rod Oil Seal Dynamic Tests	3-13
3-8	0.75 in. Diameter Rod Seal Static Leakage	3-14
3-9	Compressor (Direct Drive)	3-15
3-10	HAHP Direct Drive Compressor - Center Bearing Leakage	3-17
3-11	HAHP Counterweight Transmission Porting Layout	3-18
3-12	Snap-Back Test Results with 0.003 in. Clearance	3-19
3-13	Snap-Back Test Results with 0.001 in. Clearance	3-20
3-14	Compressor and Hydraulic Transmission Layout	3-22
3-15	Fluid Dynamically Shaped Fairings Mounted on Counterweight	3-23
3-16	FPSE Diaphragm-Coupled Compressor Development Total Hydraulic Transmission Loss	3-25
3-17	FPSE Diaphgram-Coupled Compressor Development	3-27
3-18	Refrigerant Compressor Cylinder PV Diagram with New Backer Ring	3-29
3-19	Outboard Counterweight Centerport Geometry	3-30
3-20	Counterweight Centerport Characteristics	3-31
3-21	HAHP Transmission with Original Oil Centerporting Layout	3-34
3-22	Transmission Phasor Diagram for Pressure and Displacements	3-35
3-23	Port 1: Port between Upper and Lower Oil Cavities Provides Stabilizing Force Resulting from Net Flow from Volume B to Volume A	3-36
3-24	Port 2: Port between Lt.H. Oil and Lower Oil Cavities Results in Net Flow from Volume B to Volume C	3-37
3-25	Port 3: Port between Upper Oil and Rt.H. Oil Cavities Results in Net Flow from Volume D to Volume A	3-38
3-26	HAHP Transmission Cross-Porting Layout	3-40
3-27	HAHP Counterweight Compressor Oil Pressure Interactions	3-41
3-28	Original Gas Spring Assembly	3-43
3-29	Improved Gas Spring Assembly	3-44
3-30	Shuttle Loss Test (1/8/85)	3-48
3-31	Oil Management System Block Diagram	3-55
3-32	Oil Management System Piping Diagram	3-57
3-33	Oil Management System Control Logic	3-58
3-34	Oil Management System Control Panel	3-60
3-35	Oil Management System Logic Electric Circuit	3-61
3-36	Oil Management System Relay Package	3-62
3-37	Oil and Nitrogen Control Solenoids	3-63

LIST OF FIGURES (Cont'd)

Number		Page
4-1a	Improved Counterweight Version	4-5
4-1b	Existing Counterweight Version	4-6
4-2	Direct Acting with External Vibration Absorbers	4-7
4-3	Linkage-Driven Oscillating Shaft	4-8
4-4	Hydraulically Driven Twin Pistons	4-9
4-5	Single Vertical Cylinder with External Absorber	4-10
4-6	Opposed Pistons - Series Actuation	4-11
4-7	Opposed Pistons - Parallel Actuation	4-12
4-8	Direct Acting with Internal Parallel Counterweight	4-13
4-9	Direct Acting with Inherent Oil Balance	4-14
4-10a	Metal Bellows Replacing Engine Diaphragm	4-15
4-10b	Existing Engine Diaphragm and Transition Plate	4-16
4-11	Improved Counterweight Version	4-20
4-12a	Direct Acting with External Vibration Absorbers (Side View)	4-21
4-12b	Direct Acting with External Vibration Absorbers (Top View)	4-22
4-12c	End View - Left Side Absorber	4-23
4-13a	Linkage Drive Twin Pistons; Oscillating Shaft (Rear View)	4-24
4-13b	Linkage Drive Twin Pistons; Oscillating Shaft (Side View)	4-25
4-13c	Section Through Compressor Pistons	4-26
4-14	Hydraulically Driven Twin Piston - Series Actuation	4-27
A-1	HAHP Instrumentation Schematic	A-5
A-2	Heat Pump Compressor and Hydraulic Transmission Layout	A-6
A-3	Hydraulic Transmission Energy Flow Diagram	A-10
A-4	"Direct Drive" Compressor Measured Energy Flow	A-11
B-1	HAHP Refrigerant Calorimeter	B-5
B-2	Refrigerant Test Loop State Points	B-5

LIST OF TABLES

Number		Page
3-1	HAHP Breadboard Performance	3-2
3-2	HAHP Breadboard Performance Comparison	3-50
3-3	HAHP Breadboard Performance Comparison	3-51
3-4	HAHP Breadboard Performance Comparison	3-52
3-5	Compressor Efficiency and Capacity Development	3-53
4-1	Comparison between the Diaphragm-Coupled Compressor and Resonant Piston Compressor Design	4-3
4-2	Comparison of Alternative Design Concepts for Hermetic Coupling of Refrigerant Compressor to Free Piston Engine	4-4
4-3	Advanced Concepts - HAHP Transmission/Compressor	4-17
4-4	Concept Ratings - HAHP Transmission/Compressor	4-28
A-1	HAHP System Measurement Points	A-4
A-2	HAHP System Measurement Points	A-4
A-3	Hydraulic Transmission and Compressor Measurement Probes	A-7
A-4	Definition of Power and Efficiency Terms	A-9
A-5	Comparison of Breadboard Heat Pump Performance Results with and without the Counterweight	A-12

1.0 INTRODUCTION

During 1980, Mechanical Technology Incorporated (MTI) identified the diaphragm-coupled compressor as the best means for providing hermetic coupling between a free-piston Stirling engine (FPSE) and a refrigerant compressor. The essential features of the MTI design are the positive seal (diaphragm), hydraulically powered transmission, and vibration balance (counterweight).

A layout drawing of the compressor is shown in Figure 1-1. The compressor is coupled to the engine via a hydraulic transmission that transfers the power from the engine to the compressor through the force link provided by the hydraulic fluid. The breadboard heat-actuated heat pump, consisting of the combustor, FPSE, hydraulic transmission, and compressor, is shown in Figure 1-2. The operation of the unit proceeds as the engine pressure forces the power diaphragm to deflect, and an equal volume of hydraulic fluid is displaced which forces the compressor piston into motion proportional to the displaced volume of the power diaphragm. The lower oil cavity is also displaced by this amount, causing the lower (gas spring) diaphragm to deflect into the compressor gas spring cavity, which assists in reversing the motion of the compressor piston.

Physically, the compressor housing is approximately 15 in. × 15 in. × 15 in. The compressor weighs approximately 120 lb when filled with oil.

An important design feature offered by the compressor is that it is dynamically balanced. The inertia of the compressor piston is balanced by the inertia (180° out-of-phase) of a compressor counterweight.

The first generation diaphragm-coupled compressor has been under development in a breadboard configuration with a FPSE driver to prove the technical feasibility of the design approach. The initial development program, Phase I, addressed the following points:

- Efficiency
- Stability
- Capacity
- Vibration balance

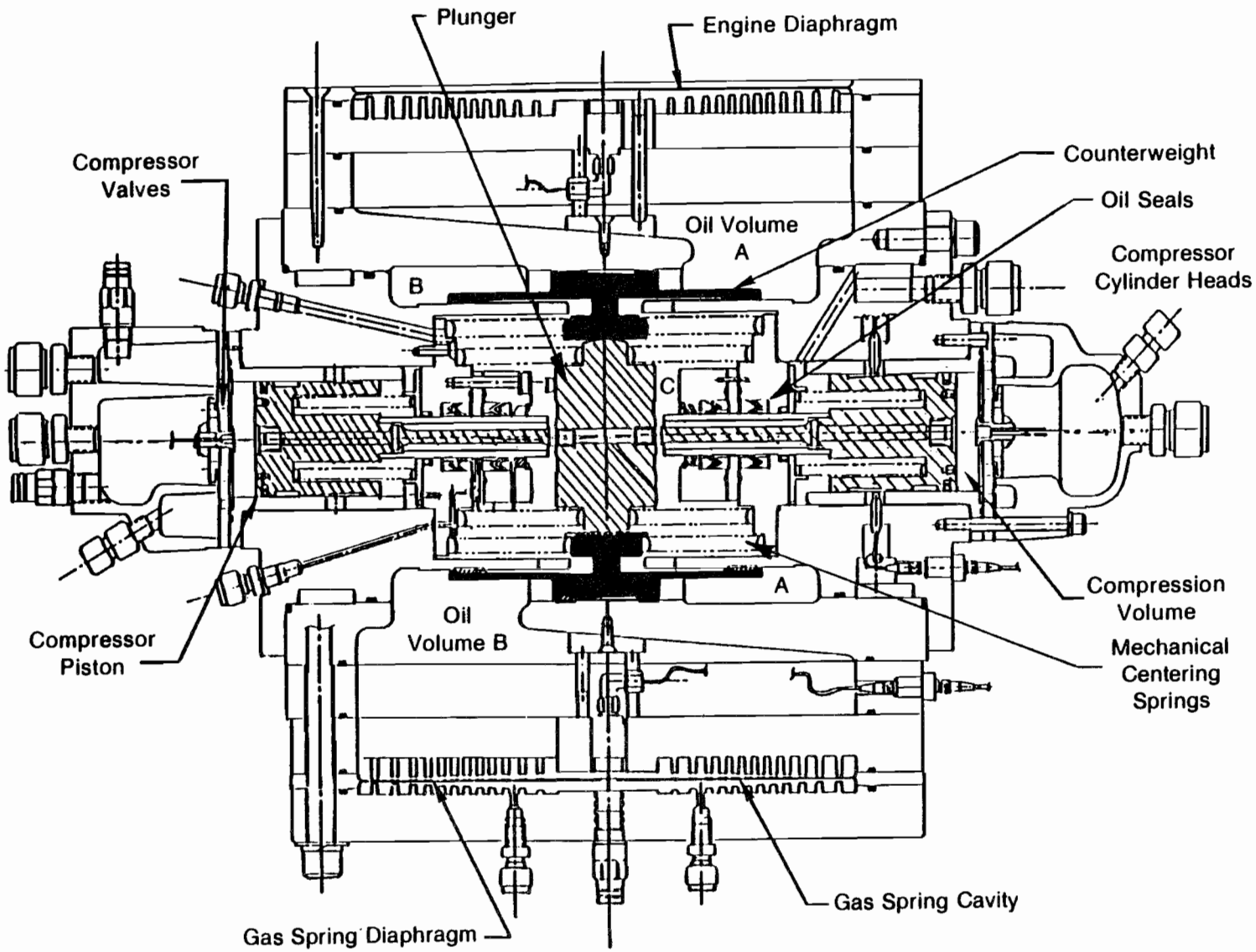

Figure 1-1 Compressor and Hydraulic Transmission Layout

831741-1

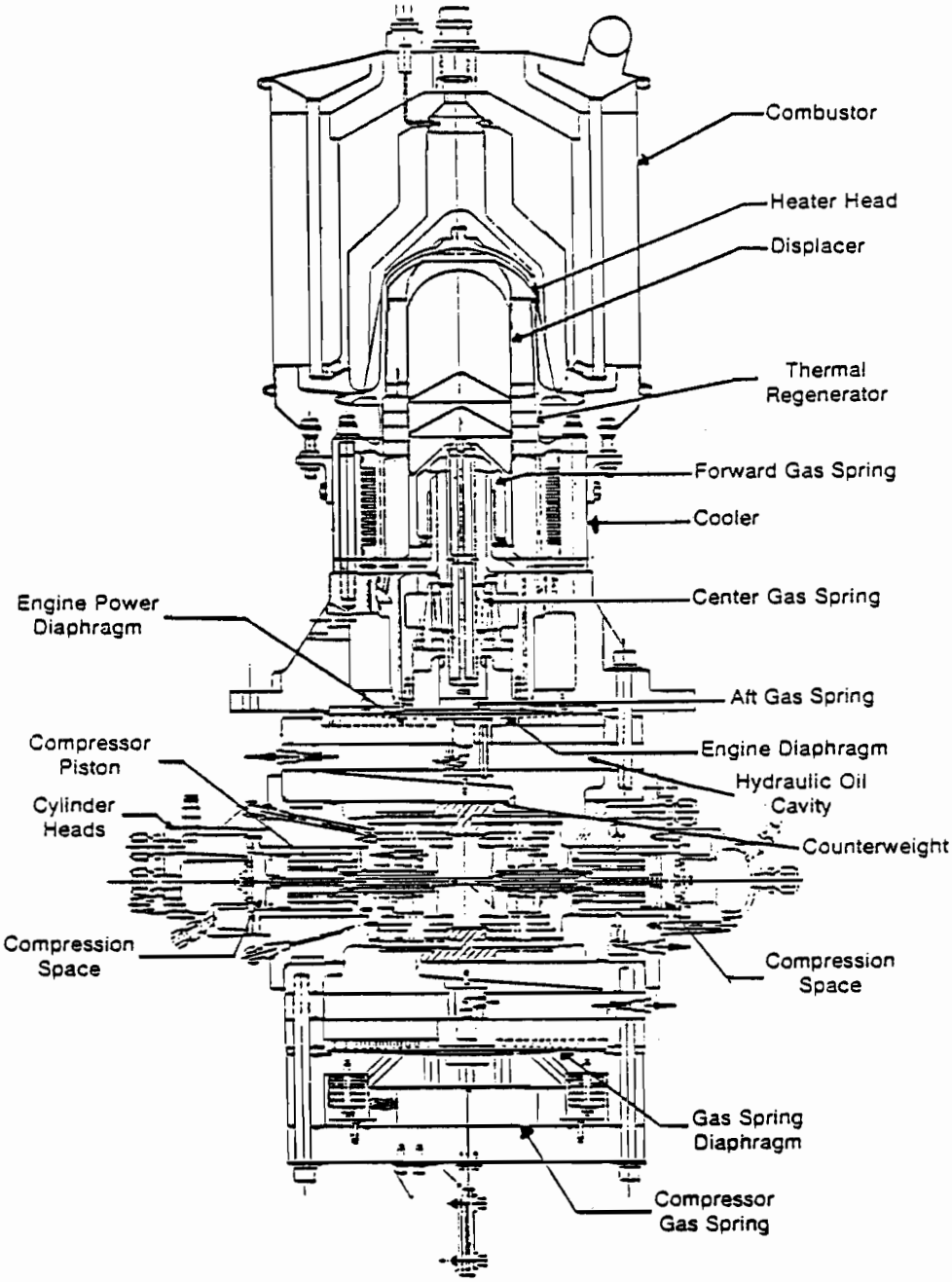

Figure 1-2 Breadboard HAHP Power Module and Compressor Assembly

841843

- Capacity modulation
- Durability.

The Phase I program resulted in good technical progress, which has verified the technical feasibility of the diaphragm-coupled hydraulic design and provided operational data on several key items; namely:

- Stable operation of the engine and compressor
- Vibration-free operation
- Capacity modulation
- Durability of the diaphragms.

To a limited extent, the machine's durability and efficiency has also been demonstrated, in that good hardware reliability has been experienced during experimental operation and good efficiency has been measured in a simpler unbalanced compressor design. The major outstanding problem with the balance design has been the difficulty in achieving the 3-ton full-rated capacity with the compressor at 95°F ambient conditions.

During Phase IA, a subsequent portion of the program, several conditions were examined as possible causes for the capacity shortfall:

- Inherent geometric or thermodynamic limitations
- Underpowered engine
- Excessive transmission losses
- Engine and compressor mismatch.

Extensive analysis and experimentation at MTI has convinced the MTI program team that the compressor design is neither geometrically nor thermodynamically limited from achieving its rated capacity. Further, the engine has been demonstrated (with an alternator load) to provide ample power output to drive the compressor to its rated capacity. More specifically, the compressor requires approximately 3500 watts of pressure volume (PV) at rated capacity, and the engine has been measured to provide up to 4200 watts of PV power when coupled to an electric alternator load.

Analysis and test data, in the current state, have shown that the hydraulic transmission does not meet its design specification because of excessive losses. That is, the hydraulic transmission, with high loss, absorbs too much energy and does not allow the engine/compressor system to operate at the design operating point. This is shown in Figure 1-3, where the hydraulic transmission and compressor load characteristics are plotted along with the engine's power output characteristics. The intersection of these two curves represents the operating point for the system. The result of the increased transmission losses is seen to raise the load line of the transmission and compressor producing a lower operating point and a reduced engine PV power output. This result is analogous to a rotary prime mover where too high a starting load will prevent the machine from reaching its full speed. By reducing the load, the speed will increase and the machine will produce its rated power.

Early development during Phase IB of the unbalanced, direct-drive compressor/transmission without its internal counterweight supports the hypothesis that the transmission efficiency is an important problem preventing operation at design capacity. That is, as the compressor/transmission losses were reduced through hardware modifications, the engine/compressor operating characteristics approached design specifications and higher levels of capacity were achieved.

Phase IB was directed specifically toward improvement of the compressor and transmission to achieve their full performance potential. The program plan has been to conduct testing on the existing compressor to reduce transmission losses; evaluate the performance of the oil seals and diaphragms; and evaluate centerporting and centering of the counterweight and compressor piston. The major tasks in the Phase IB program were:

- Reduction of hydraulic transmission losses
- Reduction of mechanical losses and improvement of mechanical operation characteristics
- Oil-management system development
- Evaluation of new concepts.

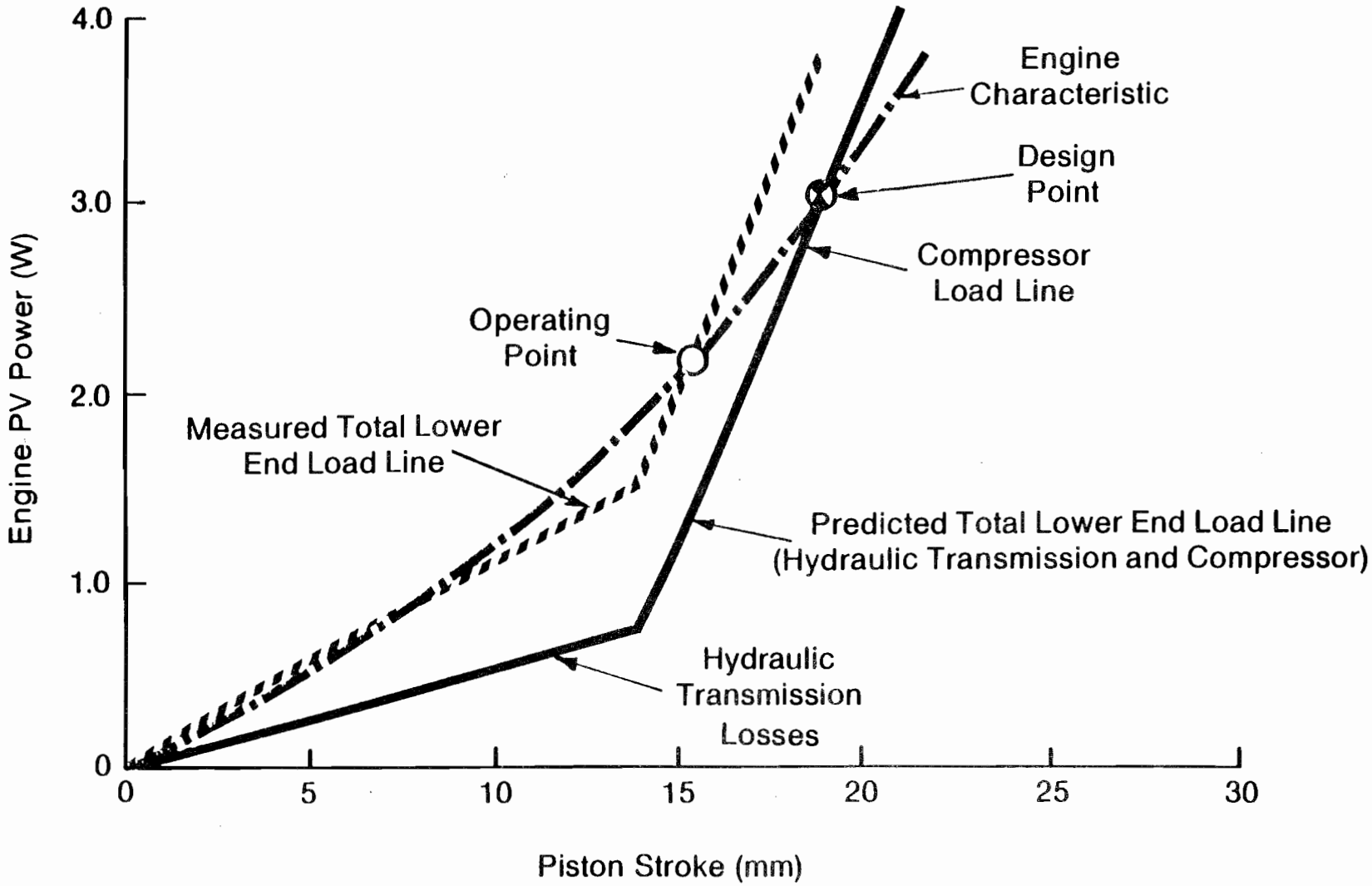

Figure 1-3 Representative Lower End and Engine (EM 4) Power Characteristics

852206-1

2.0 EXECUTIVE SUMMARY

During Phase I of the Diaphragm-Coupled Heat Pump Compressor Development Program, a breadboard heat pump power module (FPSE, hydraulic transmission, and refrigerant compressor) was designed and fabricated. The essential ground rule of the development, imposed by the Department of Energy (DOE), was the use of an existing MTI FPSE. The breadboard heat pump represented a coupling of this engine with a linear resonant refrigerant compressor. During testing in Phase I, this breadboard heat pump fell far short of its design capacity of 3.0 tons of cooling at 95°F ambient conditions. In addition, mechanically the compressor was not achieving stable, centered operation of the compressor piston; therefore good steady-state data for analytical validation and troubleshooting could not be obtained.

To better understand the breadboard heat pump's deficiencies, an analytical effort was started in Phase IA to identify the shortfalls in the breadboard design. The result was that, with proper modifications to the hydraulic transmission and compressor hardware, the system's performance could be significantly improved, and the design goal of 3.0 tons of cooling could be achieved. The analysis also concluded that the shortfall in capacity was the result of losses in the hydraulic transmission and compressor and was not an engine problem related to its being underpowered.

The work elements of Phase 1B addressed the losses in both the hydraulic transmission and the compressor as well as improved mechanical operation of the breadboard heat pump. Tasks were established to:

- Evaluate losses due to leakage and friction of all close clearance seals in the hydraulic transmission

- Evaluate blow-by and friction from the compressor piston ring seal

- Evaluate viscous losses associated with the movement of the hydraulic oil

- Evaluate effectiveness of the centerports for maintaining stable, centered piston operation

- Evaluate centerport flow loss

- Evaluate refrigerant shuttling loss from the backside of each compressor piston.

- Evaluate friction loss in the rod seals.

In addition, two tasks were established to improve and further develop the oil management system and to investigate and evaluate alternative coupling concepts for an advanced FPSE heat pump to arrive at a preferred approach.

The results of this program may be summarized as follows:

1. The hydraulic transmission losses were reduced significantly allowing the compressor piston stroke to be increased from 10.7 to 16.8 mm, thus increasing the cooling capacity from $\sim$1 to 2 tons of cooling at 95°F ambient conditions. The two most important effects in achieving this improvement were first, a change in hydraulic oil from an oil with a viscosity of 33 cs to a 2 cs oil; and second, a new piston ring seal backer spring that reduced blowby by more than 30%.

2. The internal counterweight was identified as the major loss producing component in the hydraulic transmission. The numerous close clearance seals formed by the counterweight and the movement of oil produced by the counterweight motion are responsible for the loss this element produces. Figure 1-1 shows the four clearance seals formed by the counterweight. The counterweight forms the seals between volumes A and B, B and D, C and D, and A and C.

3. In a separate experiment the counterweight was removed and the system run for short periods of time in this unbalanced mode to determine the effect of the counterweight on the hydraulic losses. The results were quite conclusive in that the hydraulic losses were reduced by 700 W and the capacity increased to 2-1/2 tons. Because of the unbalanced operation, run times were severely limited by

damage to the combustor, and good steady state data could not be obtained.

4. An electronic-based oil-management system was designed under this program. However, fabrication and testing of the oil-management system was not a scheduled task in this program and will have to be performed under an MTI-sponsored internal R&D program.

5. A variety of alternative compressor and transmission concepts were evaluated and an evolutionary approach to the current design, primarily involving an external balancer, was identified as the most promising configuration for future development.

The following sections detail the results and conclusions obtained from this phase of the program.

3.0 TECHNICAL DISCUSSION

This section details the development work that has been accomplished under the work plan of the Phase IB program. This development work proceeded from the baseline tests results obtained from the breadboard heat pump at the end of Phase I. The highest capacity achieved at the 95°F ambient conditions at that time was 16,238 Btu/hr with a maximum piston stroke of 10.68 mm. The baseline data, recorded on 1 September 1983, are given in Table 3-1, along with a comparison of the design point specifications. As shown, a significant shortfall in capacity existed at the end of Phase I.

The breadboard configuration tested during Phase I is shown in Figure 3-1. It consisted of the Engineering Model (EM) No. 4, FPSE, hydraulic transmission with the internal counterweight, and refrigerant compressor. The transmission fluid was Suniso 3GS, and the refrigerant was R-22. To further the understanding of the loss mechanisms that were limiting the piston stroke, two changes, designed to enable larger strokes, were made to the breadboard system.

1. The counterweight was removed from the hydraulic transmission, and the breadboard heat pump was run in the unbalanced mode. The system configuration for this "direct drive" mode of operation is shown in Figure 3-2. The major disadvantage of this mode of operation was that the combustor was frequently damaged due to severe vibrations, and good long-term, steady-state data could not be obtained. However, even with its shortcomings, this mode of operation did allow larger larger piston strokes and a great deal was learned about the loss mechanisms.

2. Refrigerant R-500 was substituted for R-22. This had the desirous effect of reducing the refrigerant work of compression for the same evaporator and condensor temperatures. The reduced compressor work, in turn, allowed greater piston strokes to be achieved.

The lower end, hydraulic transmission, and compressor, loss investigations conducted in Phase IB were done primarily with the direct drive breadboard configuration.

Table 3-1

HAHP Breadboard Performance
(with Internal Counterweight)

		Design	9/1/83[1]
Date		Design	9/1/83[1]
Refrigerant		R-22	R-22
Transmission Fluid		--	Suniso 3GS
X_d	(mm)	20.84	19.51
X_p	(mm)	19.05	10.68
$\Theta_{d,p}$	(°)	69.3	56.71
P(mean)	(bar)	60.0	56.3
Frequency	(Hz)	60.0	57.1
P(Suction)	(psia)	90.7	91.7
T(Suction)	(°F)	45.0	104.4
P(Discharge)	(psia)	277.4	279.9
T(Discharge)	(°F)	158.0	203.5
Refrigerant Flow	(lb_m/hr)	570	216.8
Capacity	(Btu/hr)	-36,000	-16,238
P(Motor)	(W)	313.0	527.1
Engine PV	(W)	2,907.0	1,191.0
Q(Head)	(W)	8,813.0	7,072.0
Total Lower End Loss[2]	(W)	502.0	598.1
Piston + CW Loss	(W)	356.0	378.1
Gas Spring Loss	(W)	114.0[3]	77.2[4]
Hydraulic Loss	(W)	2.1	142.8

[1] - Base run used to establish performance at the end of the Phase I, HAHP Program, September 30, 1984
[2] - Terms defined in Table A-4
[3] - Using helium gas
[4] - Using nitrogen gas

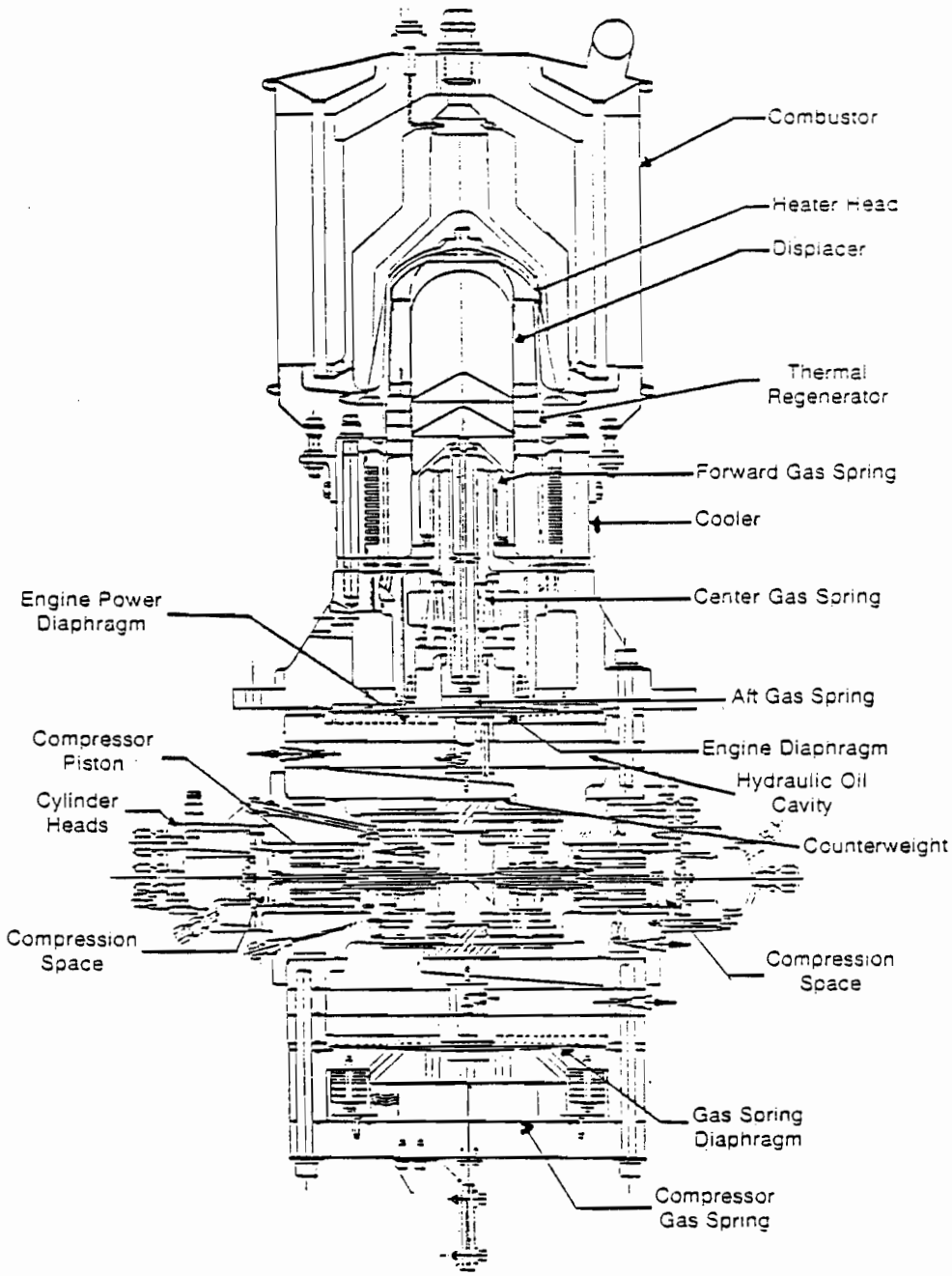

Figure 3-1 HAHP Engine/Compressor Layout (with Internal Counterweight)

841843

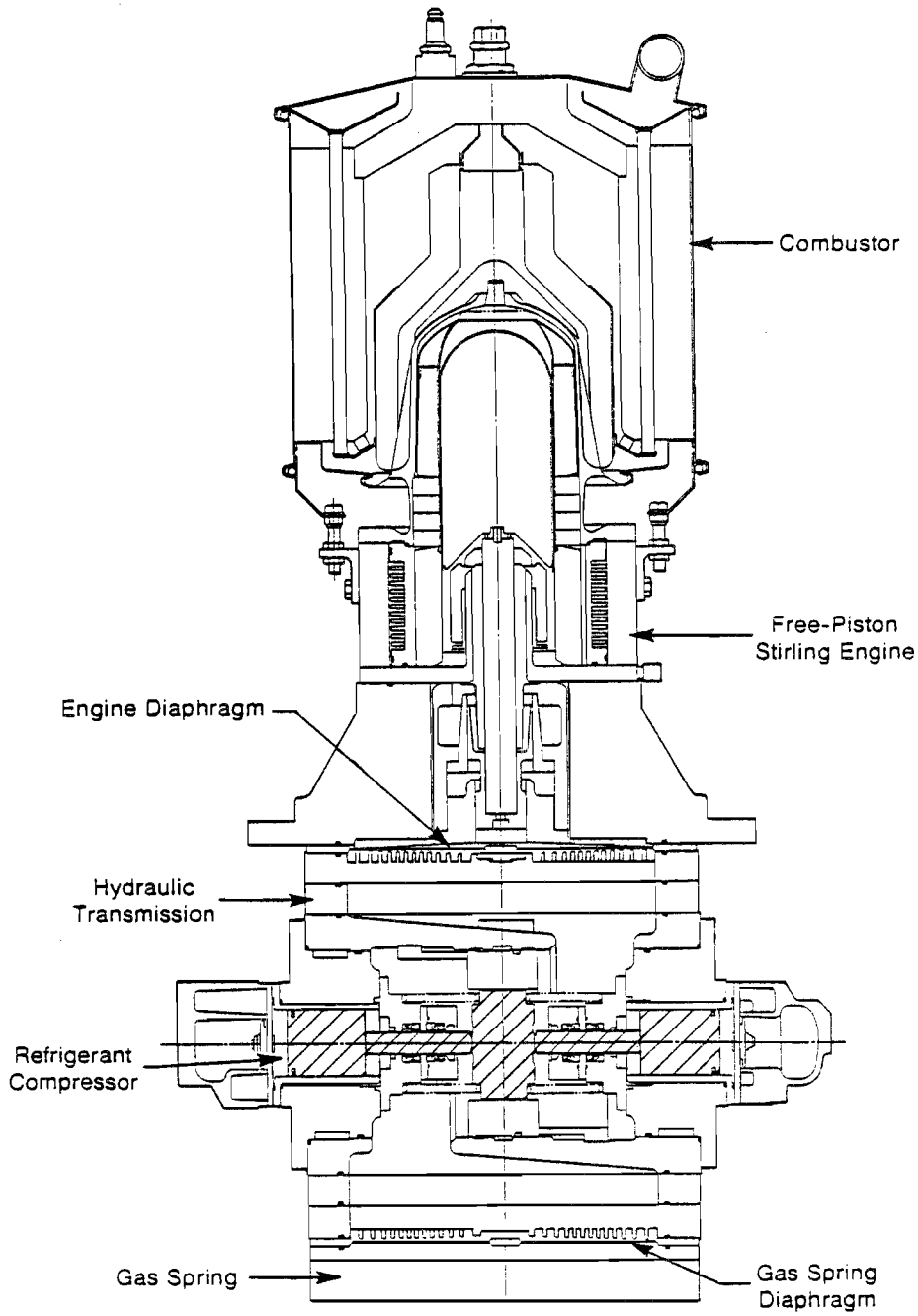

Figure 3-2 Free-Piston Stirling Engine Heat Pump Power Module (without Inernal Counterweight)

852775

3.1 Milestone No. 1 - Reduction of Hydraulic Transmission Losses

3.1.1 Work Element 1A - Rod Seals

The work plan specified that this effort will involve an investigation of alternative rod oil-seal configurations to include at least two seal designs which show promise for improved performance. Based on the results of this investigation, the most promising configuration will be fabricated and tested.

Tests were conducted with the breadboard system to evaluate the power loss associated with the chevron rod seals. Both dynamic and static tests were performed. The dynamic tests consisted of operating the machine with both single and double seals. (It should be noted that the standard configuration involves a double seal pack.)

Dynamic seal pack tests were run on the direct drive breadboard unit. The unit was run with refrigerant R-500 and at several mean operating pressures. The operating conditions were:

Refrigerant	R-500
Suction Pressure	45 psia
Discharge Pressure	150 psia
Displacer Strokes	5 to 18 mm
Piston Strokes	10 to 18 mm
Mean Operating Pressures	40, 50, 55, 60 bar

The purpose of this testing was to determine if the compressor losses were strongly affected by chevron seal friction. By eliminating one seal pack, the effective rubbing area was cut in half. The tests run at 55 bar showed a reduction of 30% in the piston power loss (see definition in Appendix A) at 18-mm stroke and a reduction of 43% in the stroke ratio (displacer stroke/ piston stroke). The results are shown in Figures 3-3 and 3-4. Results at other mean pressures were not as conclusive, and data scatter was more pronounced. No explanation for this was arrived at; however, the data at 55 bar were reproduced on several occasions with excellent reproducibility. It

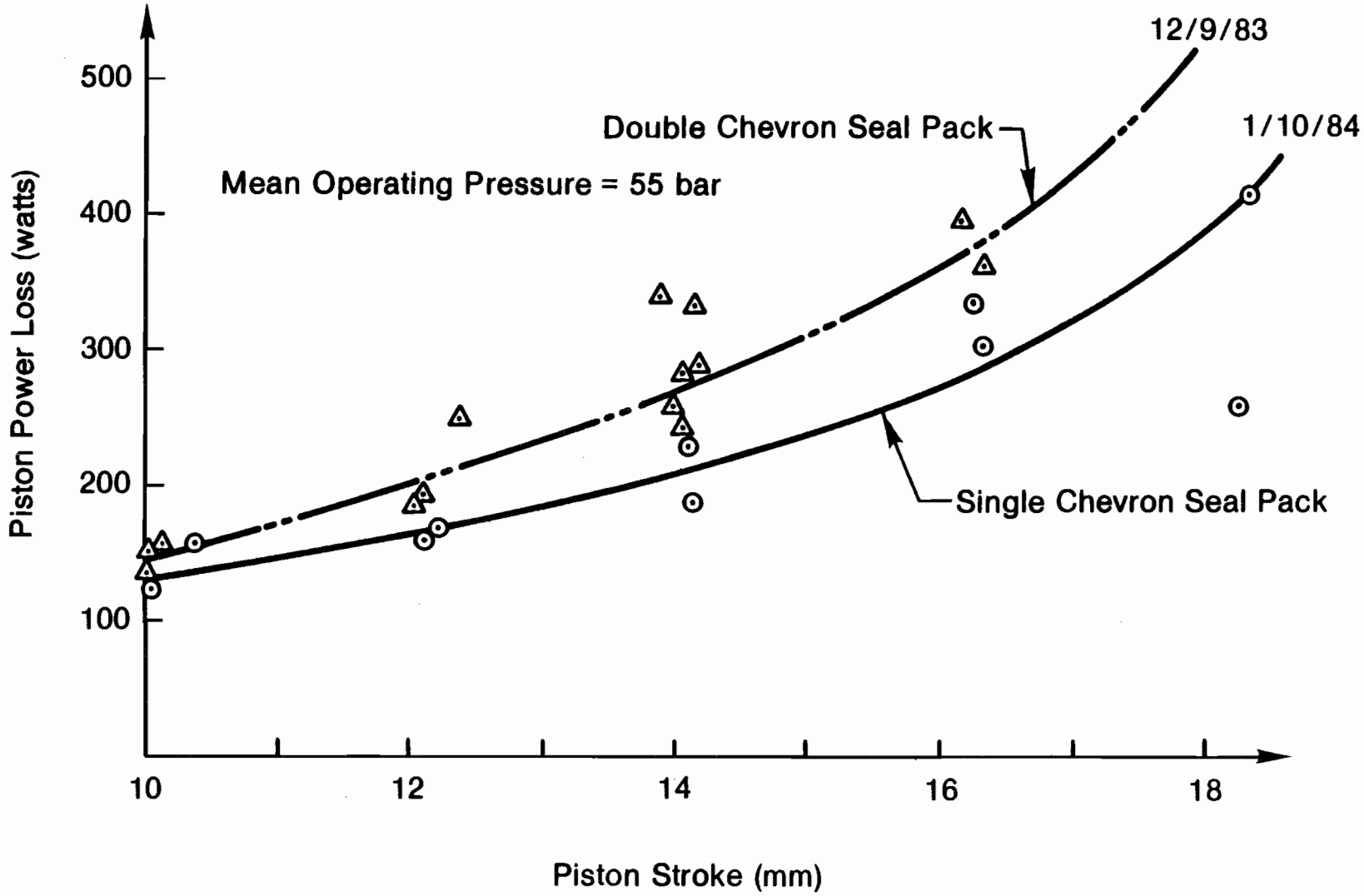

Figure 3-3 Effect of Compressor Rod Oil Seals on Piston Power Loss (Direct Drive Breadboard Unit)

841925

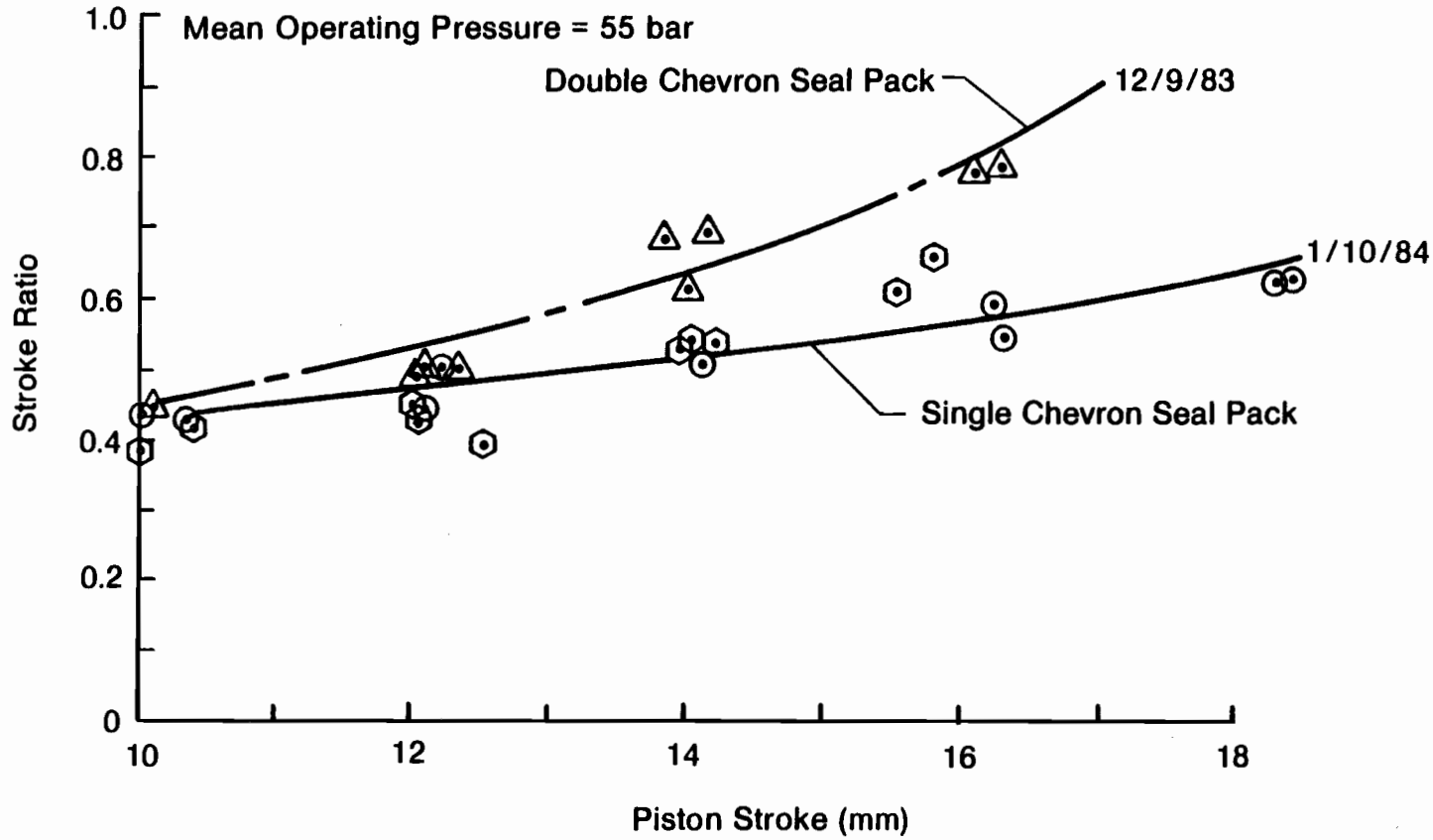

Figure 3-4 Change in Displacer/Piston Stroke Ratio (Direct Drive Breadboard Unit)

852063

appears that a reduction in the compressor loss is possible through redesign of the seals.

As a result of these tests, a modified design was established for an upgraded seal configuration. The current seal surface diameter is 0.75 in. The selection of this dimension was established because a 0.75-in. chevron seal design was available from the Automotive Stirling Engine (ASE) Program. The modified design employs a seal diameter of 0.375 in. Being pressure-actuated seals, the reduced diameter should reduce the frictional load imposed on the piston rod. The small diameter seals have been conceptually designed but have not been fabricated because the design requires the machining of new pistons as well. This new design will be taken into account for the next generation compressor.

Static tests on the rod seal were also performed. Frictional measurements were made with the double seal pack in place to assess the measured loss versus the predicted seal loss. The data were taken by moving the compressor piston with a test fixture which incorporates a force transducer. The compressor was pressurized to various levels, and the resulting force imposed by the chevron seals was measured. The line labeled "chevron seals only" in Figure 3-5 illustrates the results of this test. As shown in the figure, additional loss data were also taken for the clearance seals to evaluate this performance.

The friction power dissipation can be calculated as follows:

$$E\ \text{friction} = E_f \times V_{RMS} \times \text{unit conversion factor}$$

where:

$$V_{RMS} = (Xp)_{max} \times \text{frequency} \times 0.707$$

$$E\ \text{friction} = 20\ \text{lb} \times (0.75\ \text{in.} \times 60\ \text{cycles/sec} \times 0.707) \times \text{unit conversion factor}$$

$$= 636\ \frac{\text{in. lb}}{3} \times \frac{\text{ft}}{12\ \text{in.}} \times \frac{\text{hp/s}}{550\ \text{ft lb}} \times \frac{740\ \text{W}}{\text{hp}}$$

$$= 71\ \text{W}$$

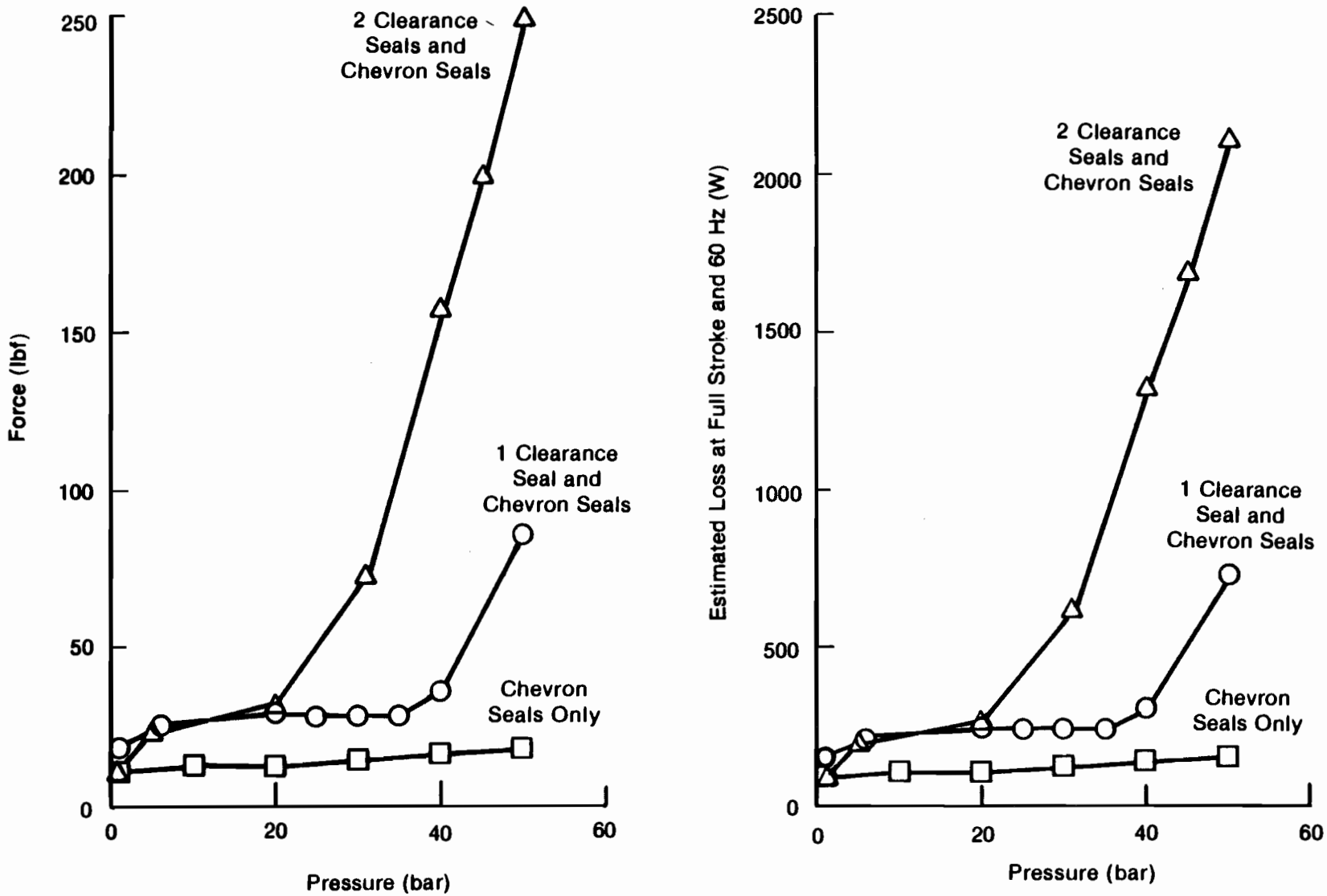

Figure 3-5 Push-Pull Static Test Summary

852073

The prediction for friction power in the chevron seals is for 92 W loss. This is in good agreement with the calculation based on test results as described above.

Independent dynamic tests of the direct-drive transmission were conducted on the hydraulic simulator to evaluate the performance of chevron and pumping oil seals. These tests involved the experimental evaluation of four rod seals:

1. Single chevron seal without bearing
2. Single chevron seal with bearing
3. Double chevron seal with bearing
4. Pumping-ring seal with bearing.

The results of testing the first three seals are shown in Figure 3-6. This plot shows the piston power losses as a function of piston stroke for seals 1 through 3. The results show that:

- They are reproducible; each seal configuration was tested three separate times.

- There is a large scatter in data.

- There is no performance difference between the single chevron and the double chevron seals when the rod bearing is in place. This conclusion contradicts the test results reported in Figures 3-3 and 3-4. The latest test is considered to have a higher level of validity and repeatability than the results previously obtained; the conclusion is, there is no difference in efficiency for operation with one or with two chevron seals.

- The losses of the single chevron seal without bearings is $\sim$100 W less on the mean as compared with the other two seals. This indicates that the bearing is a more significant loss mechanism than the chevron seals.

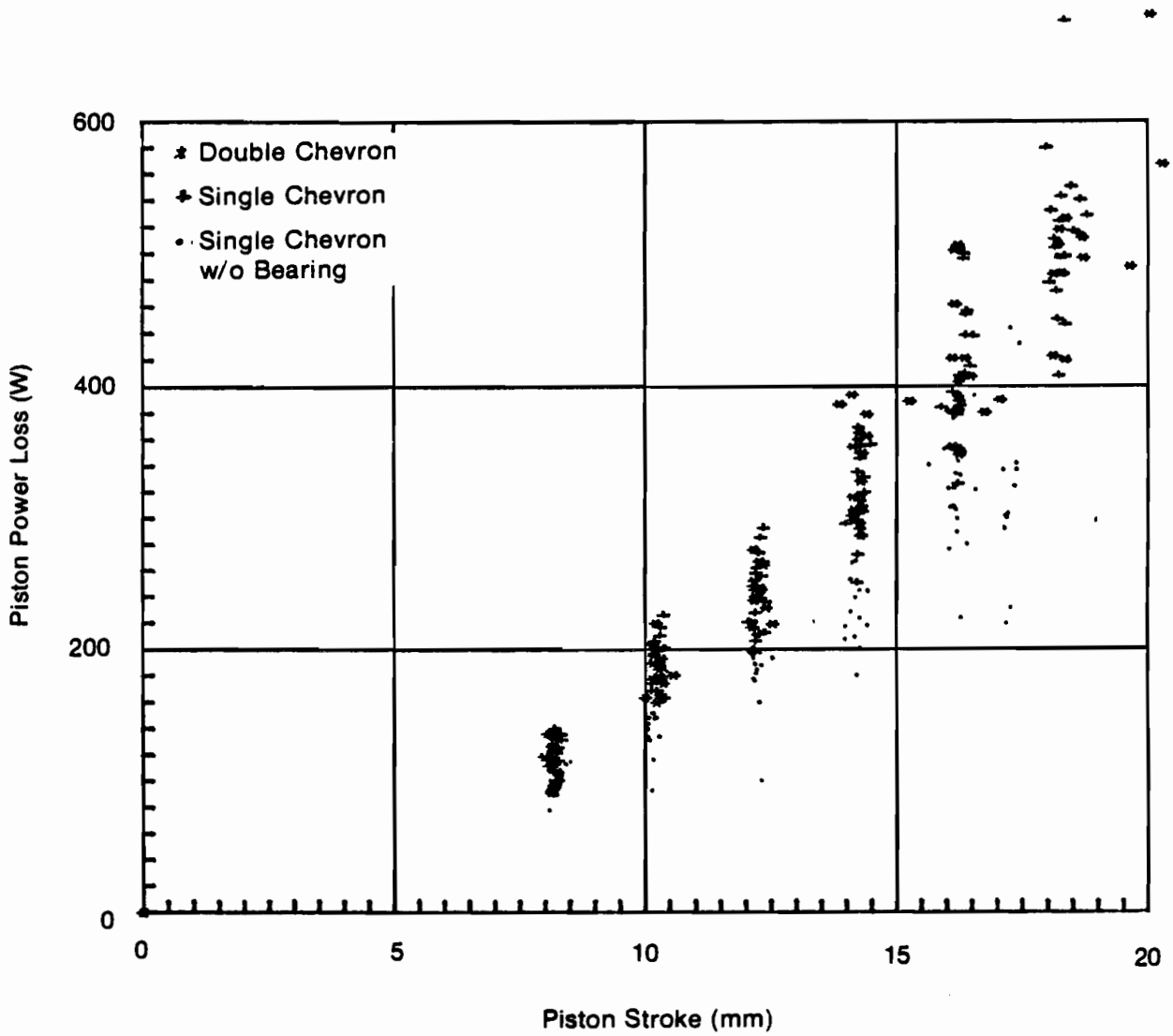

Figure 3-6 Rod Oil Seal Dynamic Tests
(Direct-Drive Transmission-Hydraulic Simulator)

852075

With regard to the pumping ring seals, the results of the initial tests were that the pair of seals tested did not hold a seal well under dynamic operation conditions of the HAHP compressor. It is suspected that the reason is that the clamping pressure which preloads the seal o-ring was not high enough to effectively close the radial gap (1.1 mils) between the pumping rod and pumping ring. In addition, inspection of the pumping-ring seal showed the pumping rings were fabricated with a tapered opening in both axial directions from a midpoint on the working surface. This would cause pumping of oil in both directions with no sealing capacity. Hence, a combination of an incorrectly machined pumping ring working surface and a large radial gap between the rod and ring for the clamping pressure available from the compressor are suspected to have caused the poor performance of the pumping ring.

Performance data from the pair of pumping rings tested indicate that the transmission loss difference between operation with pumping ring seals and operation with chevron seals is negligible. Figure 3-7 illustrates the measured losses with the two types of oil seals.

Tests were performed to evaluate rod seal leakage. These tests were performed with a fully assembled compressor under static conditions. The measured oil leakage past a single chevron seal pack at various crankcase pressures is shown in Figure 3-8. Leakage increases linearly with Δp, but at a higher rate than calculated for the 50 microinch assumed design clearance. Although the measured leakage was greater than the design predictions, the flow would be balanced through the centerports with only a small offset.

3.1.2 Work Element 1B - Clearance Seal

The work plan specified that the clearance seal on the counterweight will be analyzed and tests conducted to identify the potential for oil leakage between adjacent oil cavities. Other loss mechanisms will also be considered. If necessary, the seal regions will be redesigned and tests will be performed with new or modified hardware.

This section deals with static tests that were made to assess clearance seal performance with both direct-drive and counterweight compressor configurations. The direct-drive configuration is discussed first. Figure 3-9 schematically

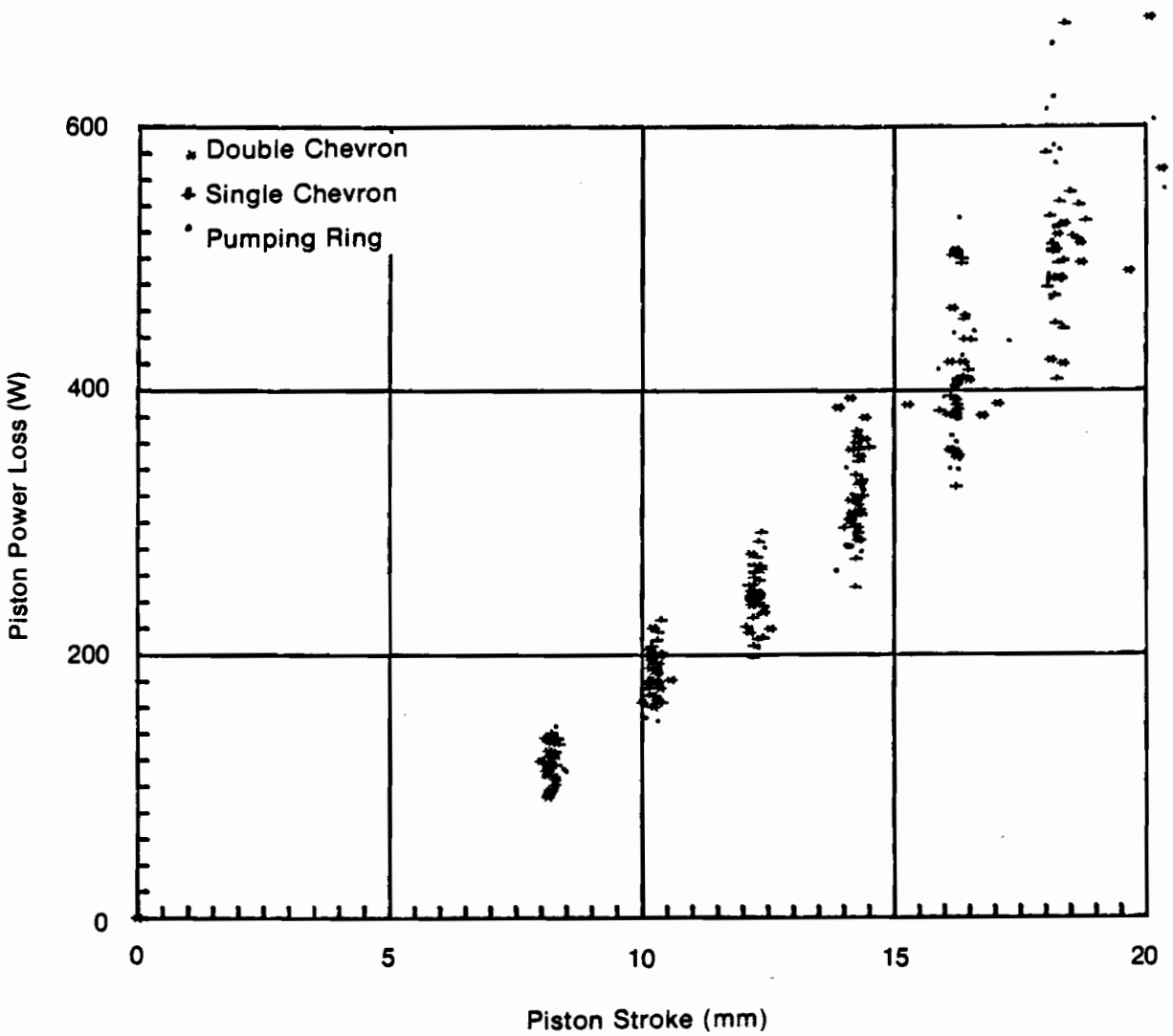

Figure 3-7 Rod Oil Seal Dynamic Tests
(Direct-Drive Transmission - Hydraulic Simulator)

852076

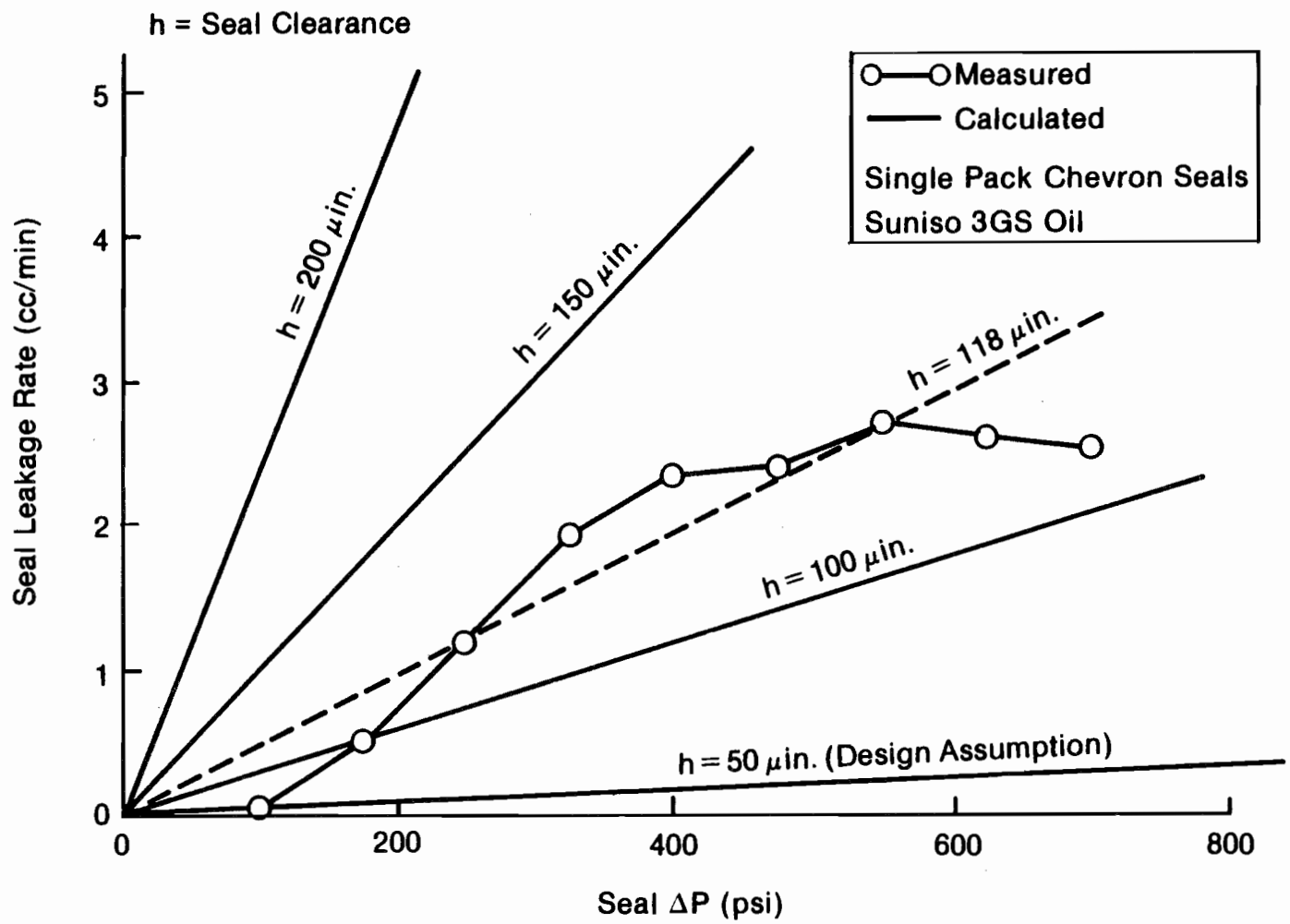

Figure 3-8 0.75 in. Diameter Rod Seal Static Leakage

851650

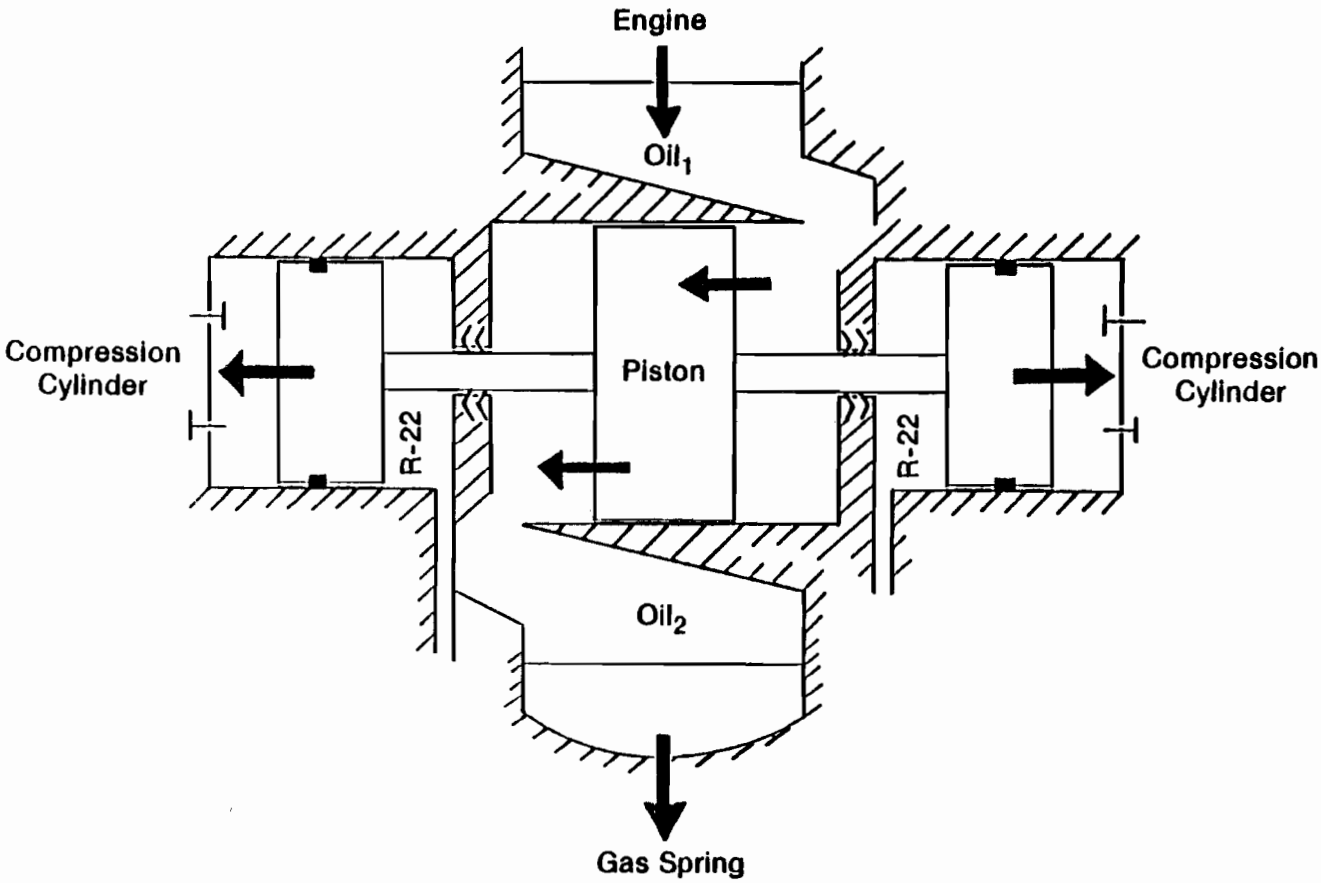

Figure 3-9 Compressor (Direct Drive)

841844

illustrates the direct-drive compressor. As indicated in the figure, there is only one clearance seal to contend with in the direct-drive configuration.

Static tests were performed to evaluate clearance seal leakage in the HAHP direct-drive compressor. The fully assembled compressor was employed with steel plates replacing the diaphragms to allow pressurization. Measured leakage compares closely with calculated leakage as shown in Figure 3-10. The measured flow peaks near the center position where the centerports are designed to open and the seal length is minimum. As the piston moves to either side of the center, the seal length increases to a maximum at Xp = ± 0.24 in. The slight offset of the flow peak to the left may indicate a physical effect of the centerports.

In contrast to the direct-drive compressor, the counterweight configuration incorporates five clearance seals. Figure 3-11 identifies each of these seals. To investigate the effectiveness of these clearance seals, a static test was devised in which the piston is displaced manually, producing corresponding displacement of the counterweight and diaphragm components. The piston is held in a displaced position while the diaphragm and counterweight are allowed to return to a centered position due to mechanical spring forces and leakage by the clearance seals. (Note that if the clearance seals allowed no leakage, the diaphragm and counterweight would be constrained from returning to a centered position.) By evaluating the relative motion of the moving components, one can deduce the relative effectiveness of the various seals.

Figure 3-12 shows test data that were taken with the original seal clearances. As indicated, the diaphragm returns to its center position much faster than does the counterweight. This condition would result if either the outboard counterweight seals were leaking excessively or if both the inboard counterweight and counterweight/piston seals were leaking excessively. Upon inspection of the hardware, it was found that the outboard counterweight seals had a radial gap of 0.003 in., although the design specified 0.001 in. New seals were machined to the design specification, and the static leakage test was repeated. Figure 3-13 shows the result of this test. As shown, the "snap back" response of the diaphragm was much slower. It can be calculated from the displacement traces shown in Figures 3-12 and 3-13 that the leakage rate across the counterweight was reduced by a factor of 20. If the only leakage that occurred was across the outboard seals, then the leakage rate should have been reduced by the cube of the change in clearance - a

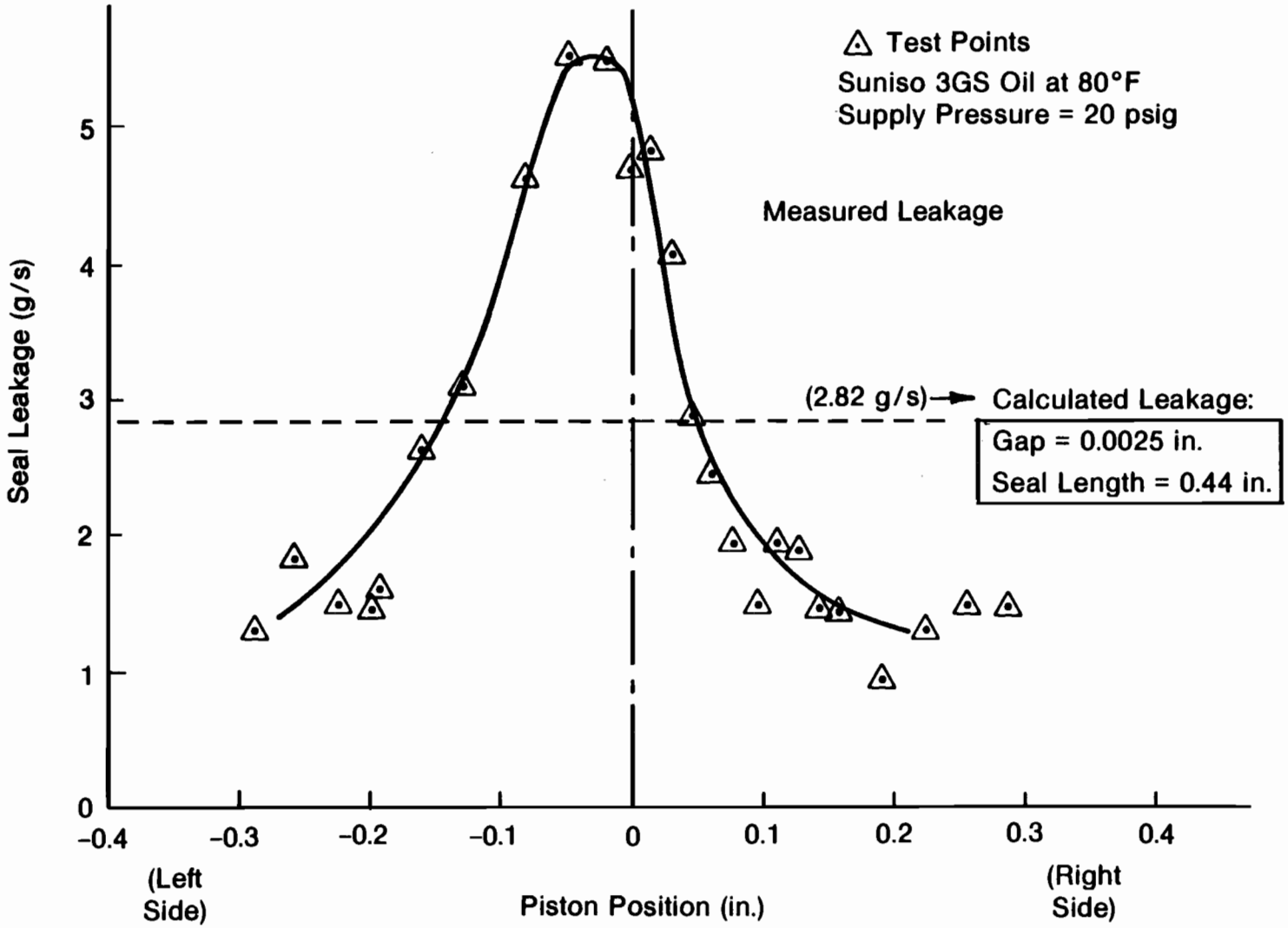

Figure 3-10 HAHP Direct Drive Compressor - Center Bearing Leakage

852047

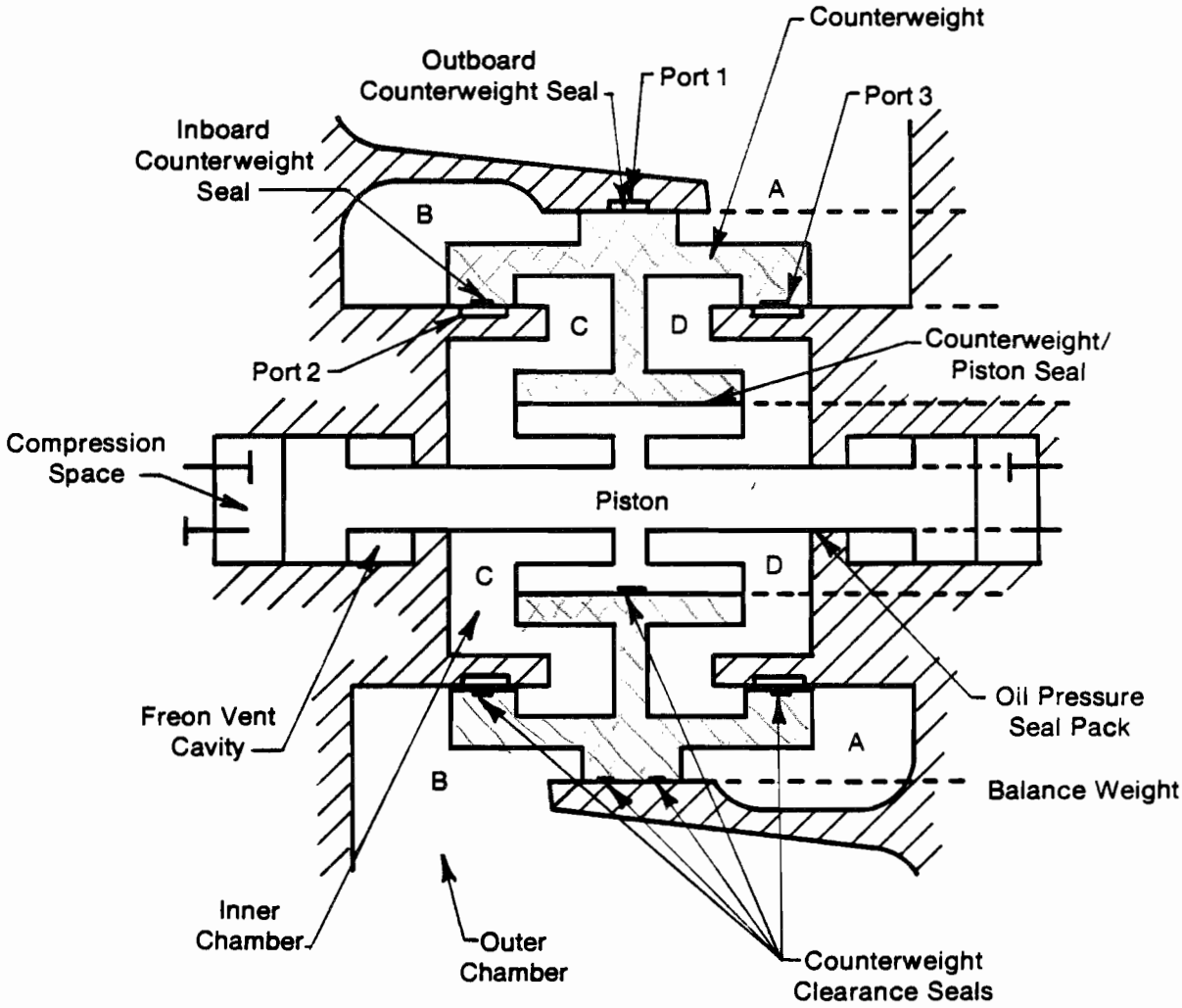

Figure 3-11 HAHP Counterweight Transmission Porting Layout

852062

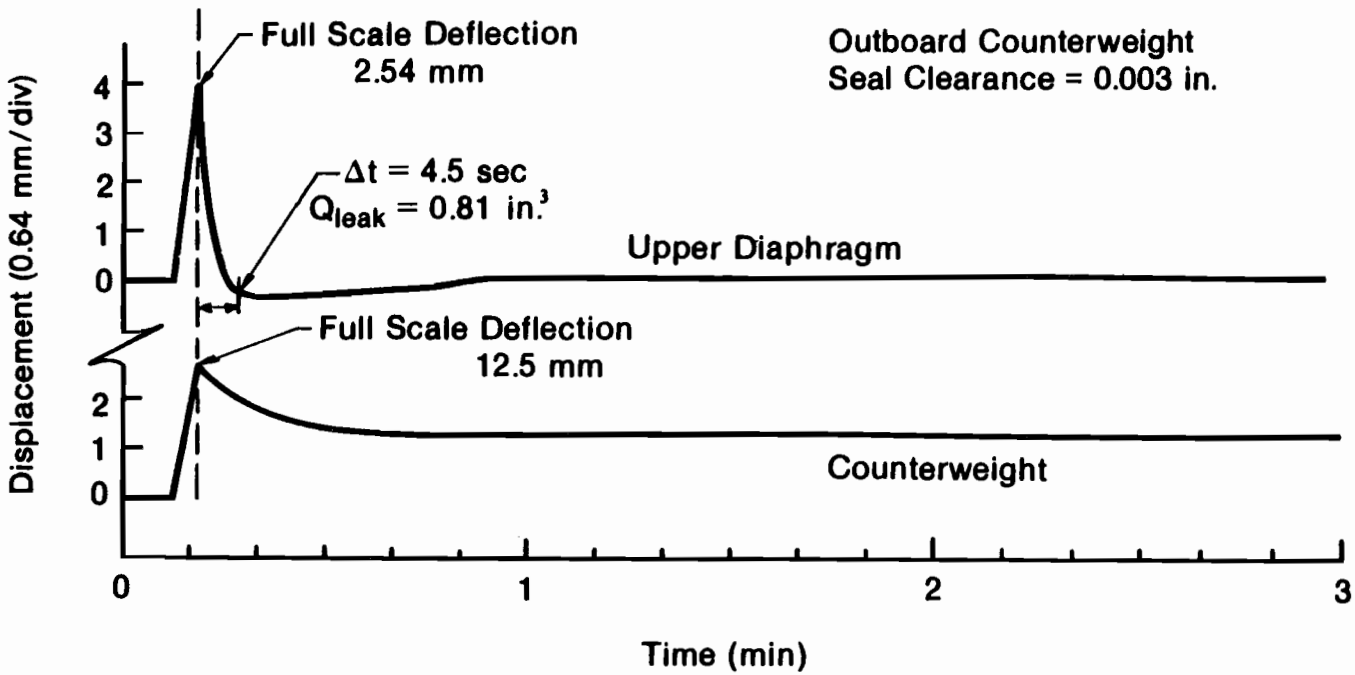

Figure 3-12 Snap-Back Test Results with 0.003 in. Clearance

851686-1

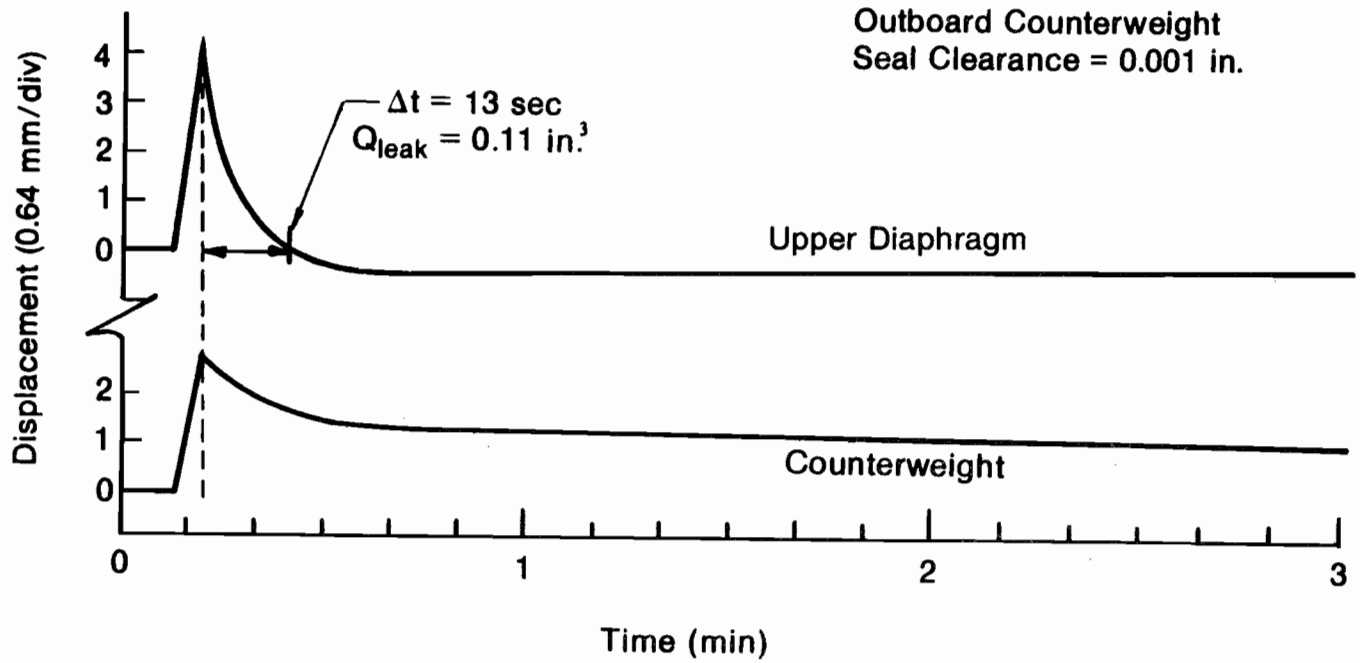

Figure 3-13 Snap-Back Test Results with 0.001 in. Clearance

851664

factor of 27. The data clearly indicate that the outboard seals were a major loss source to the overall transmission. In fact, the calculated loss due to the 0.003-in. clearance is over 300 W versus 12 W for the 0.001-in. configuration.

Unfortunately, full dynamic operation of the compressor with the 0.001-in. seal was not possible because the counterweight bound-up at normal engine charge pressure. Operation was possible, however, at charge pressures below 40 bar. It is suspected that at elevated pressure, the housing is distorting enough to seize the counterweight seals. To resolve this, it is speculated that a compliant seal will be required.

3.1.3 Work Element 1C - Pumping Loss

The work plan specified that in this task, the entire system will be examined and further tests will be performed to identify the cause of any oil pumping throughout the compressor. If necessary, components, including the piston and counterweight, will be redesigned to eliminate pumping, and new components will be fabricated and tested.

The hydraulic transmission was examined for abrupt geometries that could result in pumping losses or viscous dissipation. Two such regions were identified whereby excessive pumping losses could result. These two regions, indicated in Figure 3-14, were determined as regions which could be modified to achieve improvements in the current hardware.

The first region is in the space between the center-drive piston and the chevron seal pack. As the compressor stroke increases, the fluid tends to be forced out from between the piston and seal pack, resulting in unnecessary fluid flow loss. To alleviate this problem, the seal pack cartridge will be scalloped so as to provide smoother flow-passage for the entrapped fluid. This configuration will be incorporated in the next generation of transmission equipment.

The second region to be improved is the counterweight face area. The current configuration requires hydraulic fluid to turn a sharp corner in order to move the counterweight. A design modification has been established, whereby a fluid dynamically shaped fairing was mounted to the counterweight to smooth the hydraulic flow path. Figure 3-15 illustrates the counterweight design modification. The

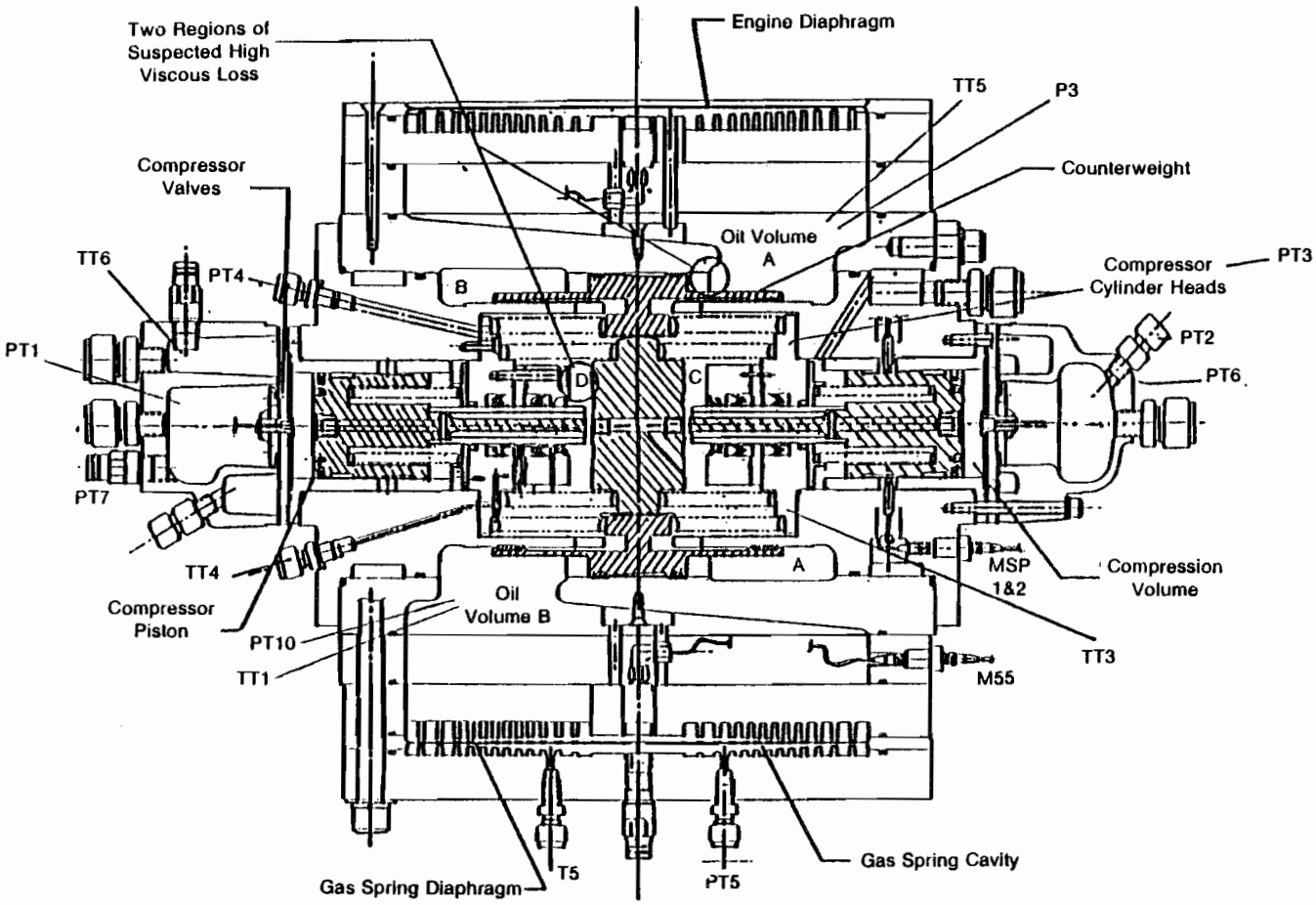

Figure 3-14 Compressor and Hydraulic Transmission Layout

831741-2

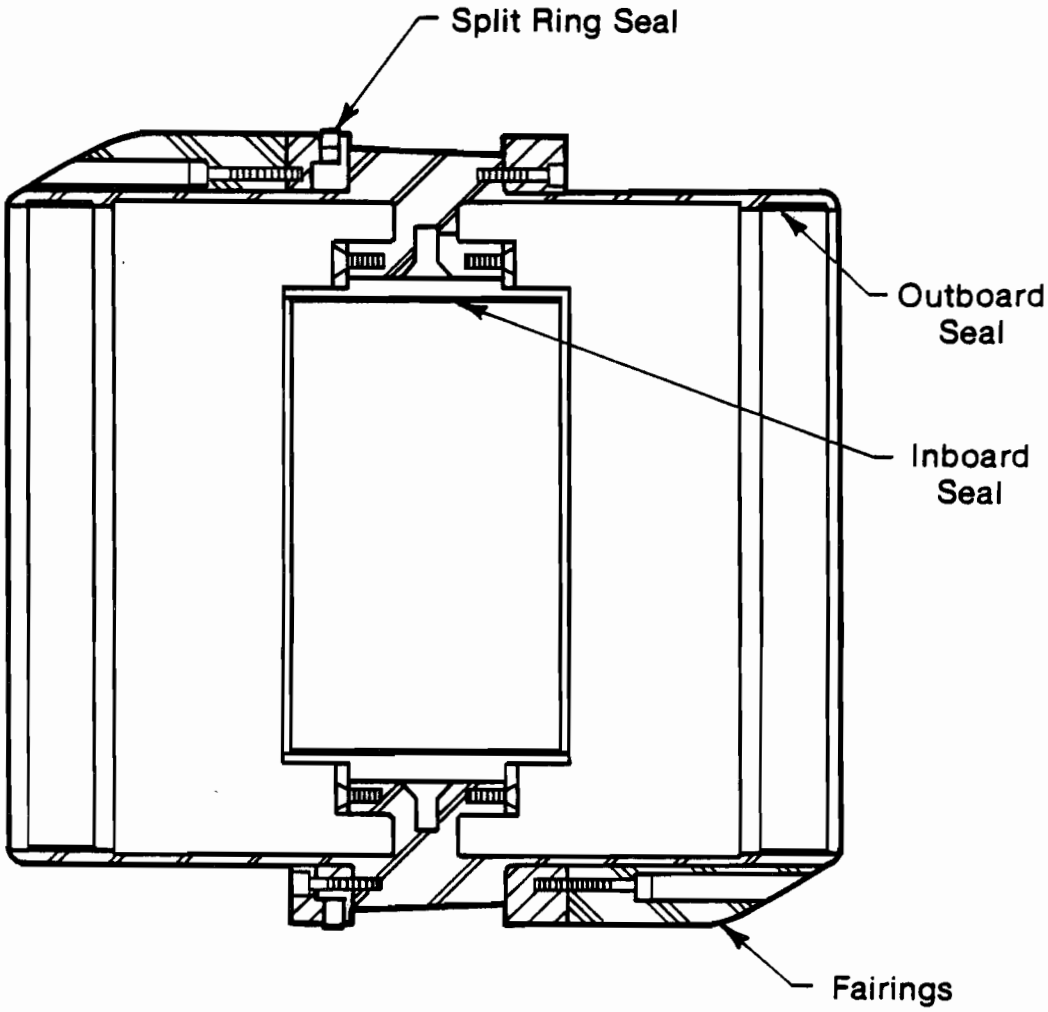

Figure 3-15 Fluid Dynamically Shaped Fairings Mounted on Counterweight

852077

modified design was tested during December 1984 and showed no overall change in transmission efficiency, indicating that perhaps flow losses in other regions dominate the viscous dissipation losses.

3.1.4 Work Element 1D - Viscous Loss

The work plan stated that the viscous loss will be quantified by means of analysis, hardware modification, and testing. Based on analysis and test results, improved components that can be implemented with the existing hardware will be designed, fabricated, and tested.

To investigate the impact of viscous losses, the "direct drive" breadboard system was operated with three hydraulic fluids: a silicone lubrication - Dow Corning 510 fluid; a refrigerant compressor oil - Suniso 3GS; and brake fluid. The viscosity for each of these fluids is given as:

- Dow Corning 510 Fluid
  ν = 500 cs @ 25°C (77°F)
  ν = 150 cs @ 100°C (212°F)

- Suniso 3GS
  ν = 33 cs @ 37.8°C (100°F)
  ν = 4.4 cs @ 99°C (210°F)

- Brake Fluid
  ν = 1.5 cs @ 100°C (212°F)

The results of these tests indicate that brake fluid significantly reduces the hydraulic transmission loss providing for reduced displacer/piston stroke ratio in the engine and larger refrigerant mass flow. The comparison of the three fluids and their effect on the total transmission loss (see definition in Appendix A) is given in Figure 3-16. Two observations may be made from this figure. First, only with the brake fluid could piston stroke above 17 mm be attained; and second, at 16 mm, the brake fluid reduced the total transmission loss by 25% over the Suniso 3GS and 38% over the Dow Corning 510 fluid. In subsequent heat pump performance testing, which will be presented in Section 3.3, it was found that the lower viscosity fluids do produce a significant improvement in heat pump capacity.

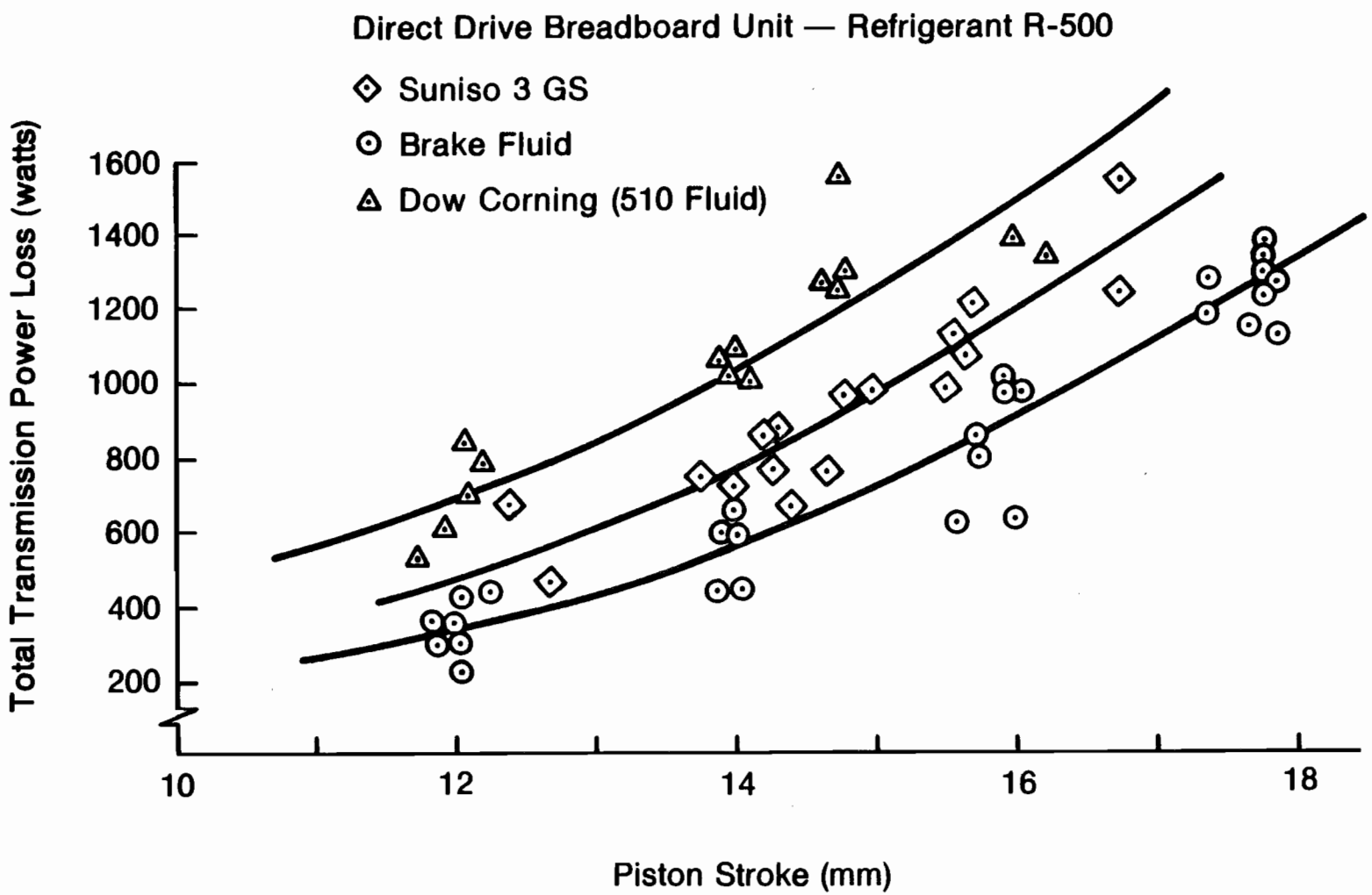

Figure 3-16 FPSE Diaphragm-Coupled Compressor Development
Total Hydraulic Transmission Loss

841926

Unfortunately, the brake fluid was found to be extremely corrosive and unacceptable for trouble-free operation, and continued operation with the brake fluid was impossible because of the damage that was done to the electronic displacement measuring probes. Subsequently, the breadboard engine was operated with a low-viscosity silicone oil that did not have the corrosive effects of the brake fluid. The fluid, Dow Corning 200 fluid, had a viscosity of 2 cs at 25°C and presented none of the problems encountered with the brake fluid. The results from tests conducted with the Dow Corning 200 fluid will also be presented in Section 3.3

3.1.5 Work Element 1E - Compressor Seal Loss:

This loss was not specifically identified in the contractual work statement since it is off-the-shelf technology; however, during the course of planned compressor development, it was determined that the compression seal on the pistons was a major loss function. Consequently, a task effort was focused on improving the compressor ring seal.

It was expected that the compressor would produce the rated 3-ton capacity when operated with the low-viscosity fluid and at the design point operating condition. The full-stroke testing, however, produced only a 2-ton refrigeration effect. With the lower-end losses substantially reduced and capacity lower than expected, the development emphasis was shifted from transmission losses to compression efficiency.

A significant body of empirical evidence pointed to refrigerant leakage past the piston seal as the most likely cause of the capacity decrement. Figure 3-17 shows a measured PV diagram for one of the refrigerant cylinders. Superimposed on this diagram are the ideal adiabatic compression and expansion curves. As indicated, the measured data show that only part of the adiabatic compression rate was being achieved with the hardware. Leakage past the compression seal could readily account for the nonideal compression rate. To investigate this hypothesis, a new set of backer rings for the ring seals were fabricated to provide improved sealing capability. The backer rings provide the preloading on the ring seals and the sealing at zero pressure differentials.

Tests were performed to evaluate the new backer ring and ring seal on the direct-drive compressor. Several operating conditions were established, including the

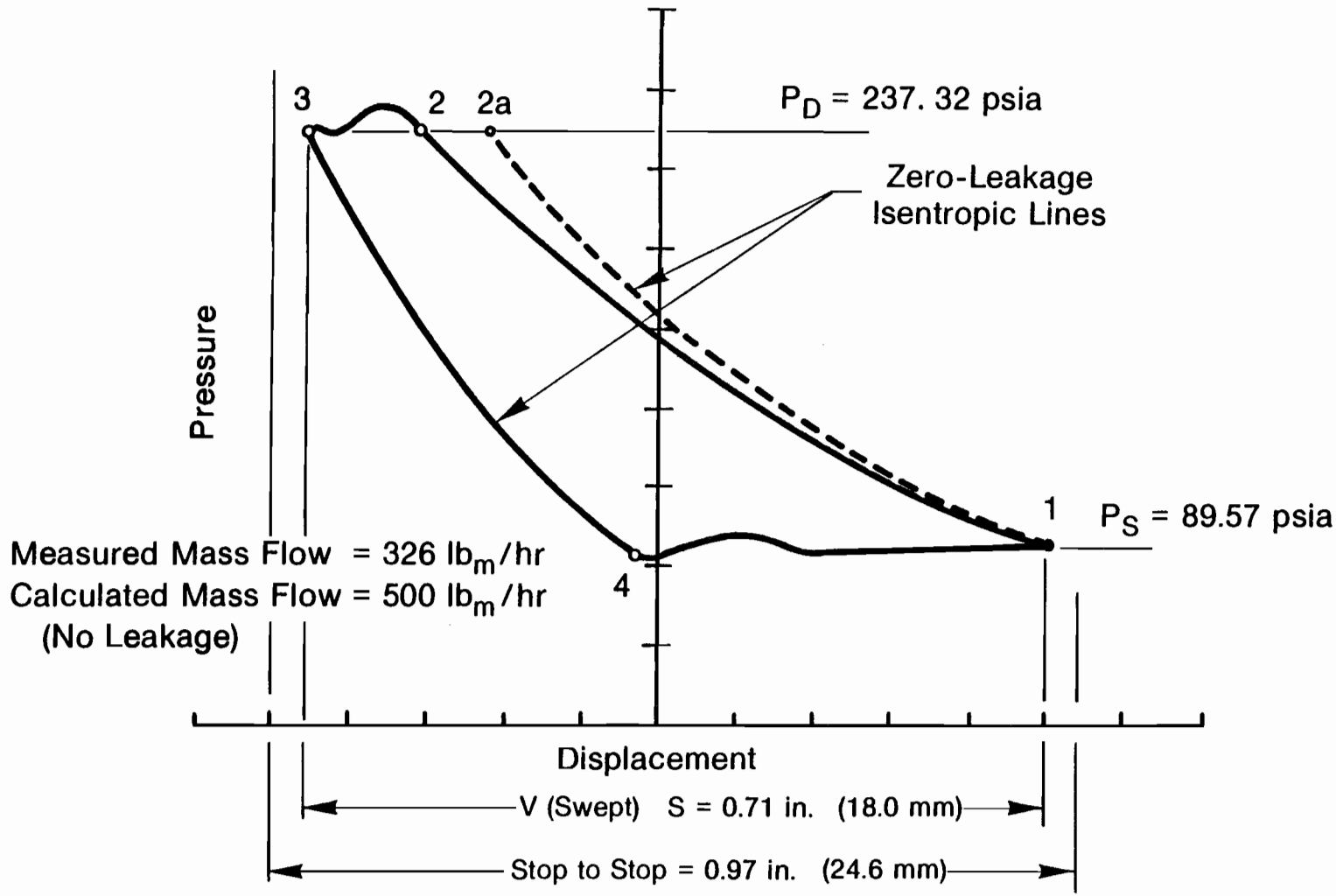

Figure 3-17 FPSE Diaphragm-Coupled Compressor Development

841930

95°F day temperature (≈90 psia suction, ≈270 psia discharge). Significant improvement in flow and efficiency were noted. The improved PV diagram obtained is shown in Figure 3-18, where the leakage was reduced from 40% of the calculated flow to a value that is less than the accuracy of the instrumentation. The calculated flow is computed from:

$$m \text{ (calculated per cylinder)} = f \cdot V(\text{suction}) \cdot \rho_s$$

where: f = frequency

$V(\text{suction})$ = the suction volume ($V_1 - V_4$)

ρ_s = the refrigerant density at point 1.

3.1.6 Work Element 1F - Porting Loss:

The work statement specified that the centerporting arrangement for both piston and counterweight will be reexamined to determine the restoring force provided and the losses associated with the ports. Based on this examination, new porting geometry will be implemented and tested to demonstrate reduction of losses and improved centering.

The restoring flow capability and associated flow losses of the outboard counterweight centerports have been examined. A simple computer code was developed to model the seal/port flows over a complete cycle, based on seal/port geometries and operating conditions.

The original seal/port configuration as shown in Figure 3-19 was comprised of two clearance seal/port pairs in series. The effective seal/port side clearance [(port width - seal width)/2] was small (<0.020 in.), giving very small port restoring flow capability and port loss.

Figure 3-20 shows the loss and flow characteristics for a range of port widths that can be accommodated in the modified counterweight configuration. The power and flow increase sharply with increasing seal/port side clearance; however, a reasonable restoring flow can be achieved at a 0.145-in. port width without excessive power loss. At first, the counterweight will be tested with no ports to determine empirically the stiffness (restoring force) of the counterweight ports. If required, the 0.145-in. port will be cut into the cylinder housing to establish

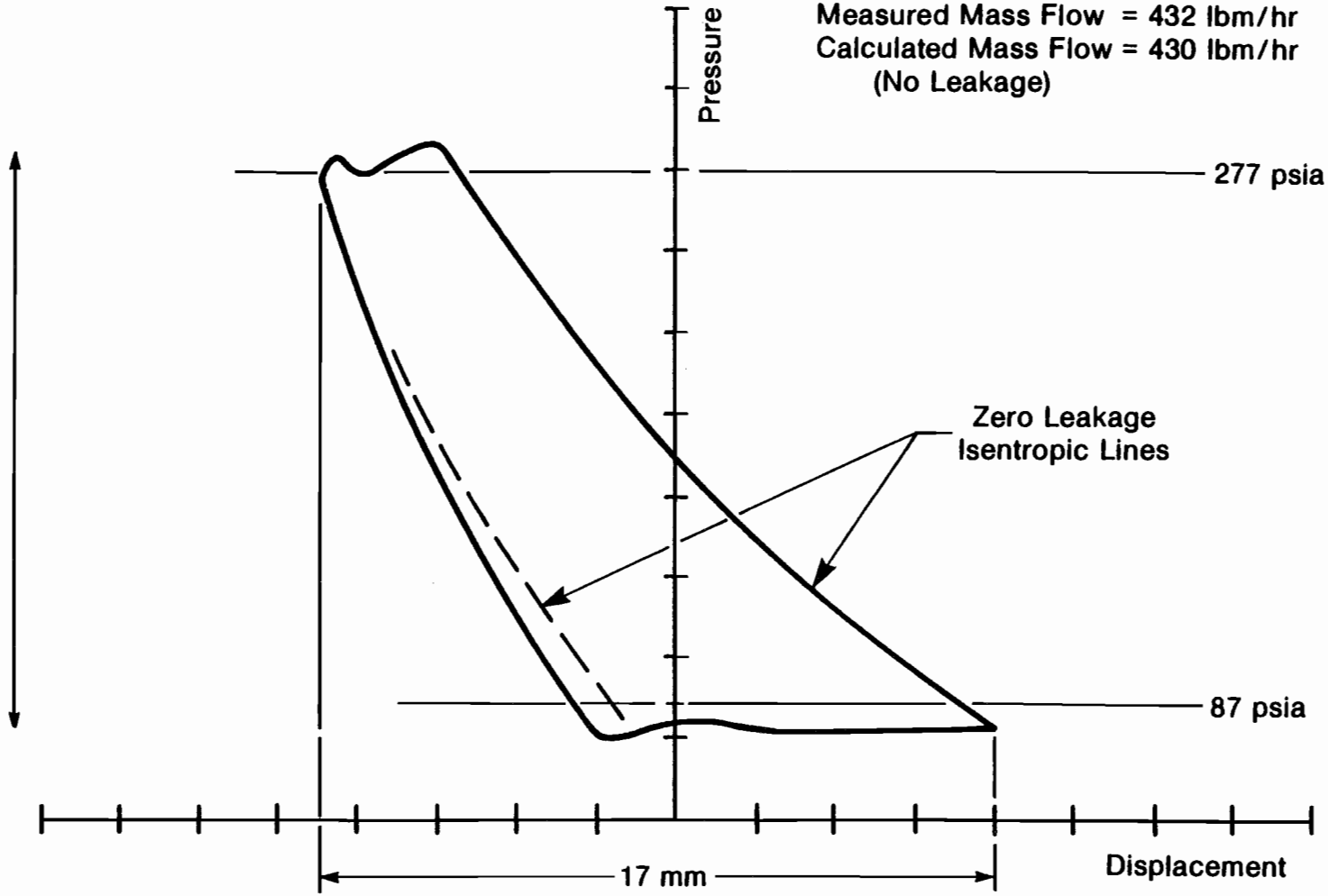

Figure 3-18 Refrigerant Compressor Cylinder PV Diagram with New Backer Ring

852438

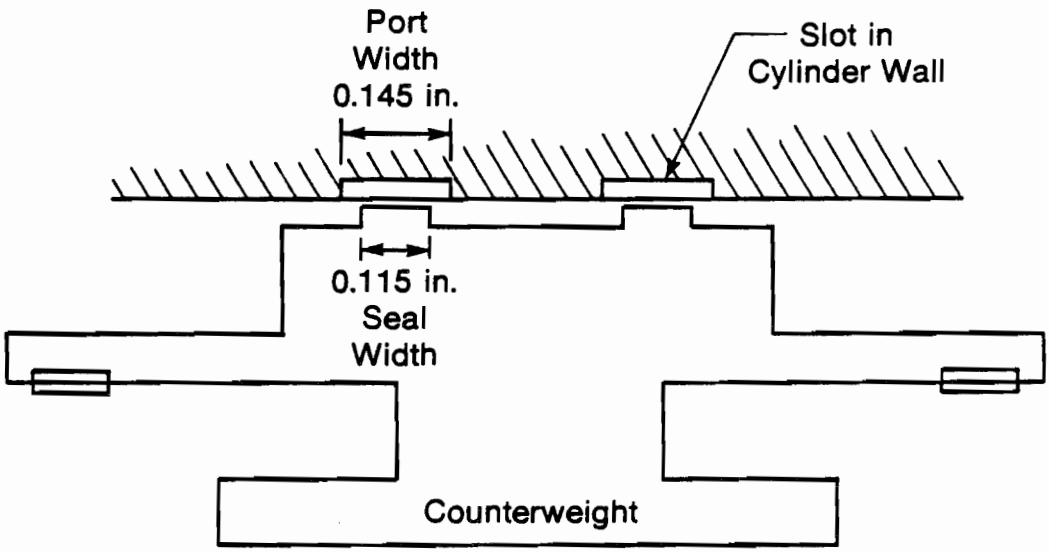

Figure 3-19 Outboard Counterweight Centerport Geometry

86151

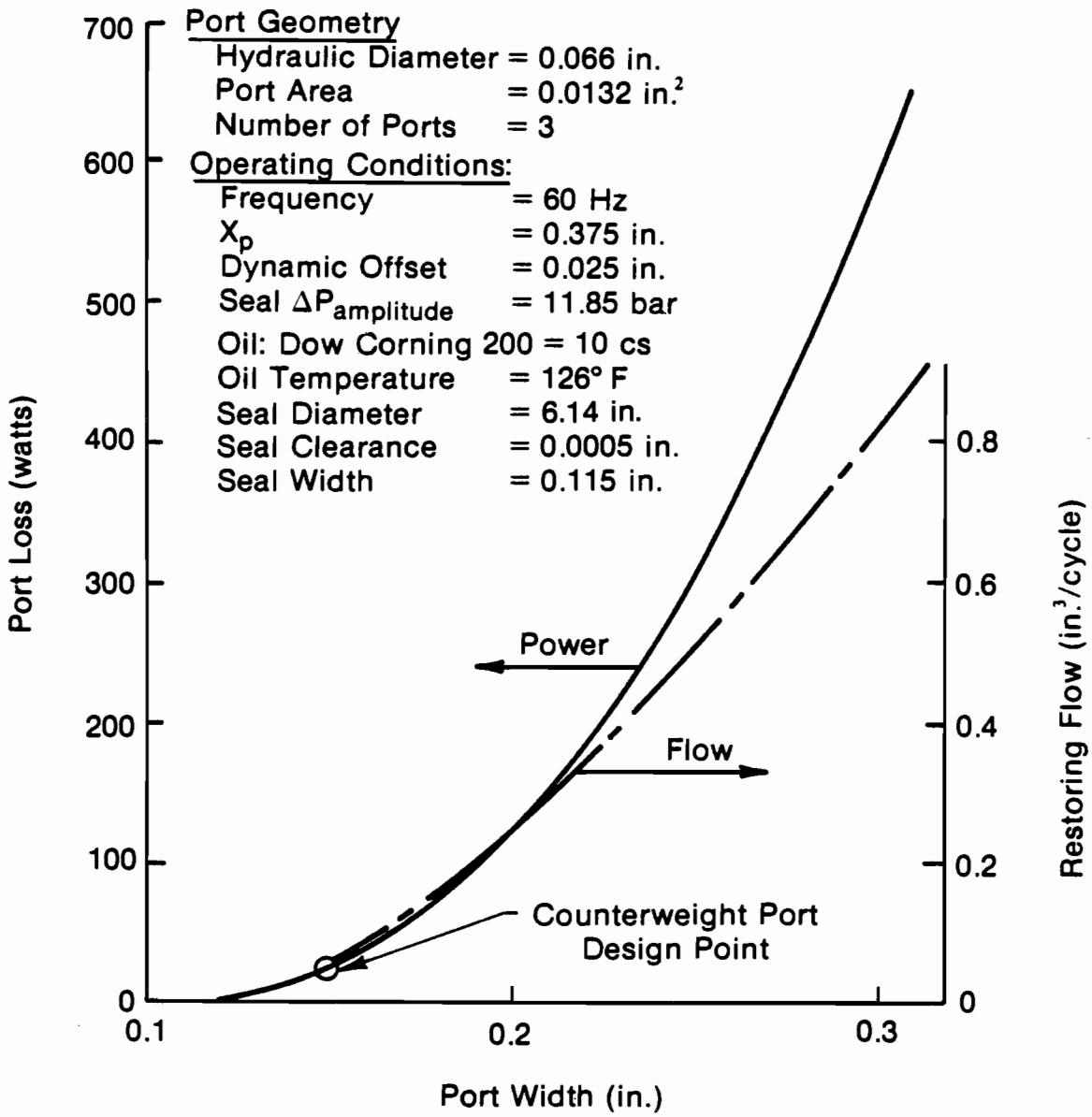

Figure 3-20 Counterweight Centerport Characteristics

851651

a centerport on the counterweight. Additional information about the centerports is contained in Section 3.2.2.

3.2 Milestone No. 2 - Improvement of Mechanical Operating Characteristics

3.2.1 Work Element 2A - Counterweight (Balancer)

The work plan stated that the counterweight design will be reviewed and alternative concepts will be evaluated. Based on this evaluation, a redesigned counterweight or balancer assembly will be fabricated and tested on the compressor.

Much of the work associated with modification of the counterweight is addressed in Milestone No. 1, Work Elements 1B and 1C. In addition to the improvements described therein, one further improvement has been made to the counterweight element; the mass of the counterweight has been reduced so that a better momentum balance can be achieved with the compressor piston. It was determined that the original counterweight was approximately 2 lb heavier than the compressor piston, yielding imperfect momentum balance. The new counterweight, shown in Figure 3-15, is 1.5 lb lighter than the original design and contains fairings to reduce viscous losses. The new design was tested during December 1984 and showed no significant improvement in heat pump performance as compared with the original counterweight, indicating that perhaps viscous losses dominate the overall transmission in efficiency.

3.2.2 Work Element 2B - Piston Centering and Centerporting

The objective of this task was 1) more accurately define the mechanisms which tend to produce offset in the counterweight and compressor piston; 2) review the mechanisms by which centerporting with oil can provide restoring force; and 3) implement and test an improved design of the centerporting.

The HAHP hydraulic transmission employs a counterweight moving in opposition to the compressor piston assembly to minimize transverse vibrations of the engine/compressor system. Both the counterweight and the piston assembly are free-piston members, with mechanical springs providing limited centering forces. Excessive offsets can occur, however, if destabilizing forces exceed the spring

forces. Offsets are undesirable since the mechanical stroke limit is reduced, resulting in mass flow reductions.

Centerports can provide stabilizing forces by pumping oil between volumes to counteract displacement offsets. Figure 3-21 shows the original HAHP porting layout. The four transmission oil volumes (A,B,C,D) operate with pressures PUOC, PLOC, PLHO, and PRHO, respectively. Three centerports (1,2,3) interconnect the volumes at the counterweight geometric midstroke.

Negative Stability - The original ports shown in Figure 3-21 were determined to provide a destabilizing (negative stability) effect on the centering of the counterweight as described in the following arguments.

In operation, the counterweight and piston midstroke positions are determined by their force equilibrium position. Midstroke offsets can result from unbalanced mechanical springs, oil leakage from oil volumes, and the compressor destabilizing force (a characteristic of a double-acting Rankine cycle compressor). During initial operation of the breadboard system with the counterweight transmission (September 1983), extremely large offsets of both the counterweight and piston occurred, limiting strokes to less than 0.27 in. (6.9 mm) out of a design stroke of 0.75 in. (19 mm). The cause of the problem was determined to be the destabilizing effect of the two counterweight sleeve ports (ports 2 and 3) as explained below.

The amplitude and phase of each of the transmission oil cavity pressures is a function of the 'external' transmission forces (compression load, engine pressure, and gas spring pressure) and the transmission inertias, mechanical spring forces, and internal losses. The action of a port is dependent on the pressures of the two volumes it connects and the counterweight position during engagement. A phaser diagram for a characteristic operating point is shown in Figure 3-22. Figures 3-23 through 3-25 show pressure displacement diagrams for the three ports, all designed to open at counterweight geometric midstroke. Referring to Figure 3-23, if the counterweight oscillates symmetrically about the port (X_{CW} = 0.0), then port flow from volume A to B during the down-stroke port crossing, returns from B to A during the up-stroke port crossing, and the net port flow over the cycle is zero (neglecting oil compressibility). The centering capability of port 1 is illustrated by assuming a 4-mm counterweight offset into volume A. The port will then engage at the position shown by the vertical dotted line at X_{CW} = -4 mm.

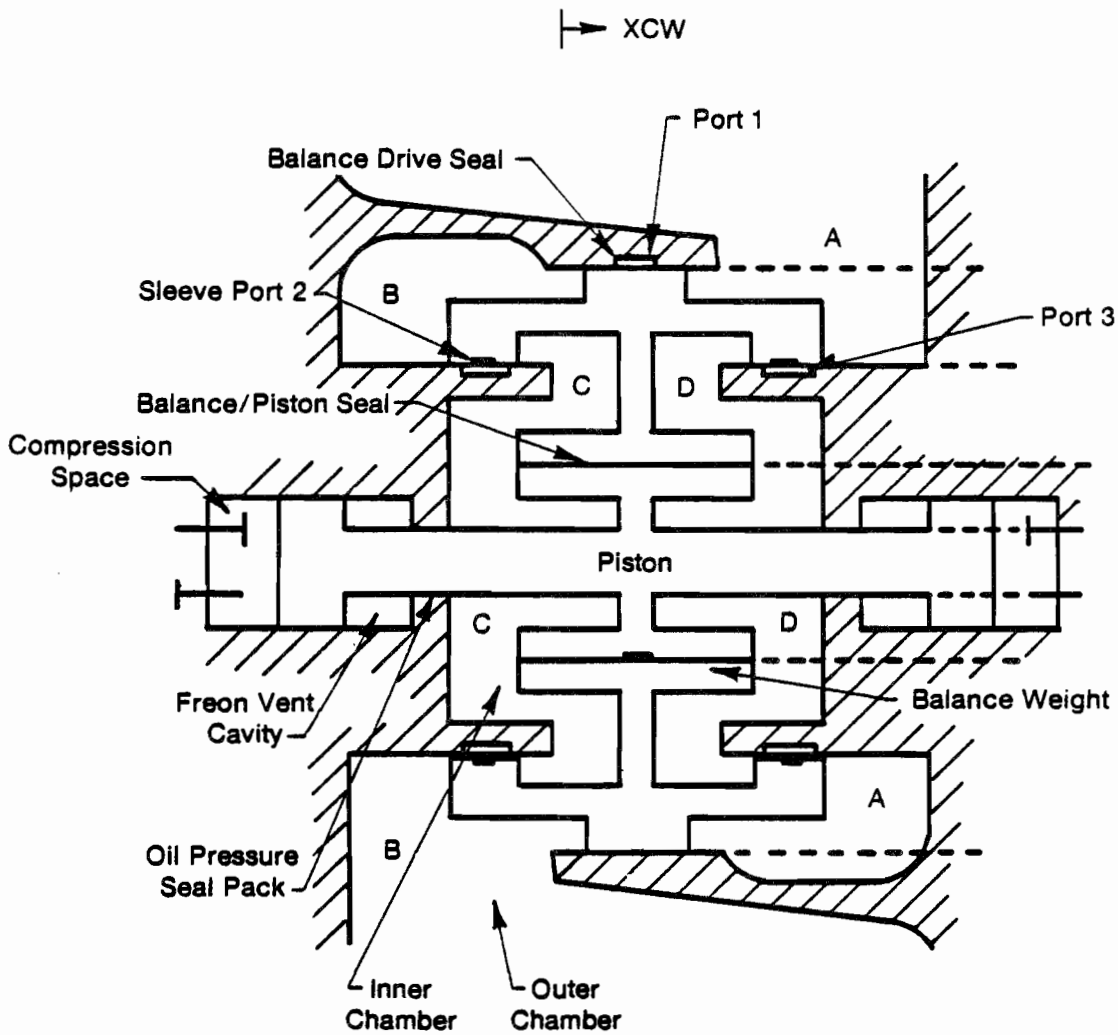

Figure 3-21 HAHP Transmission with Original Oil Centerporting Layout

852061-1

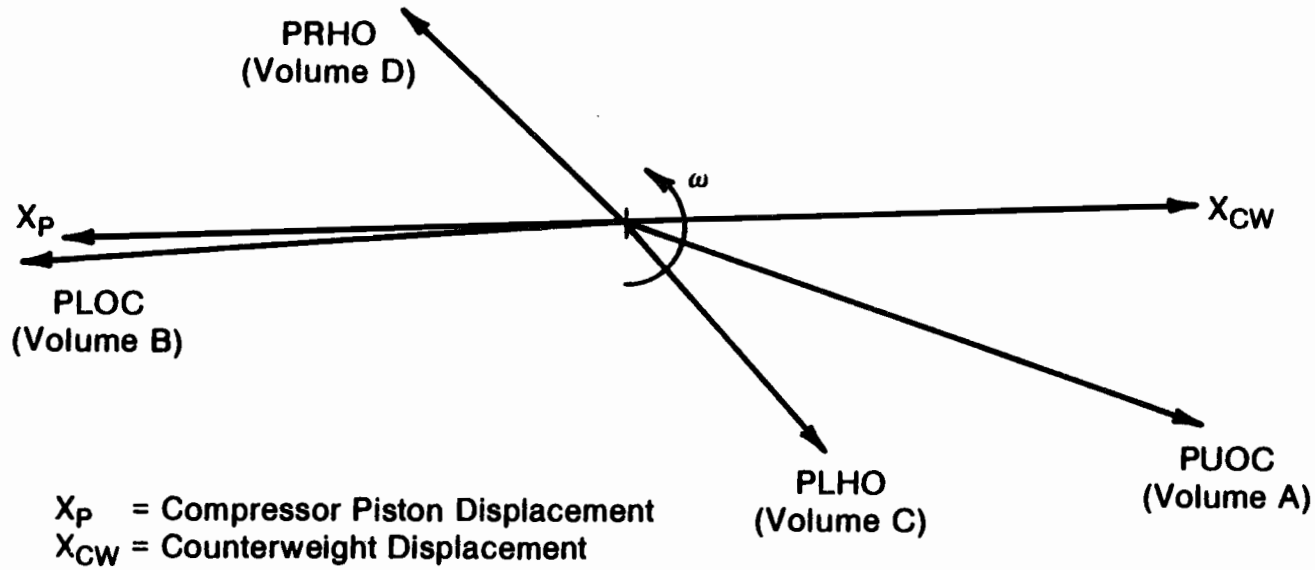

Figure 3-22 Transmission Phasor Diagram for Pressures and Displacements

851652

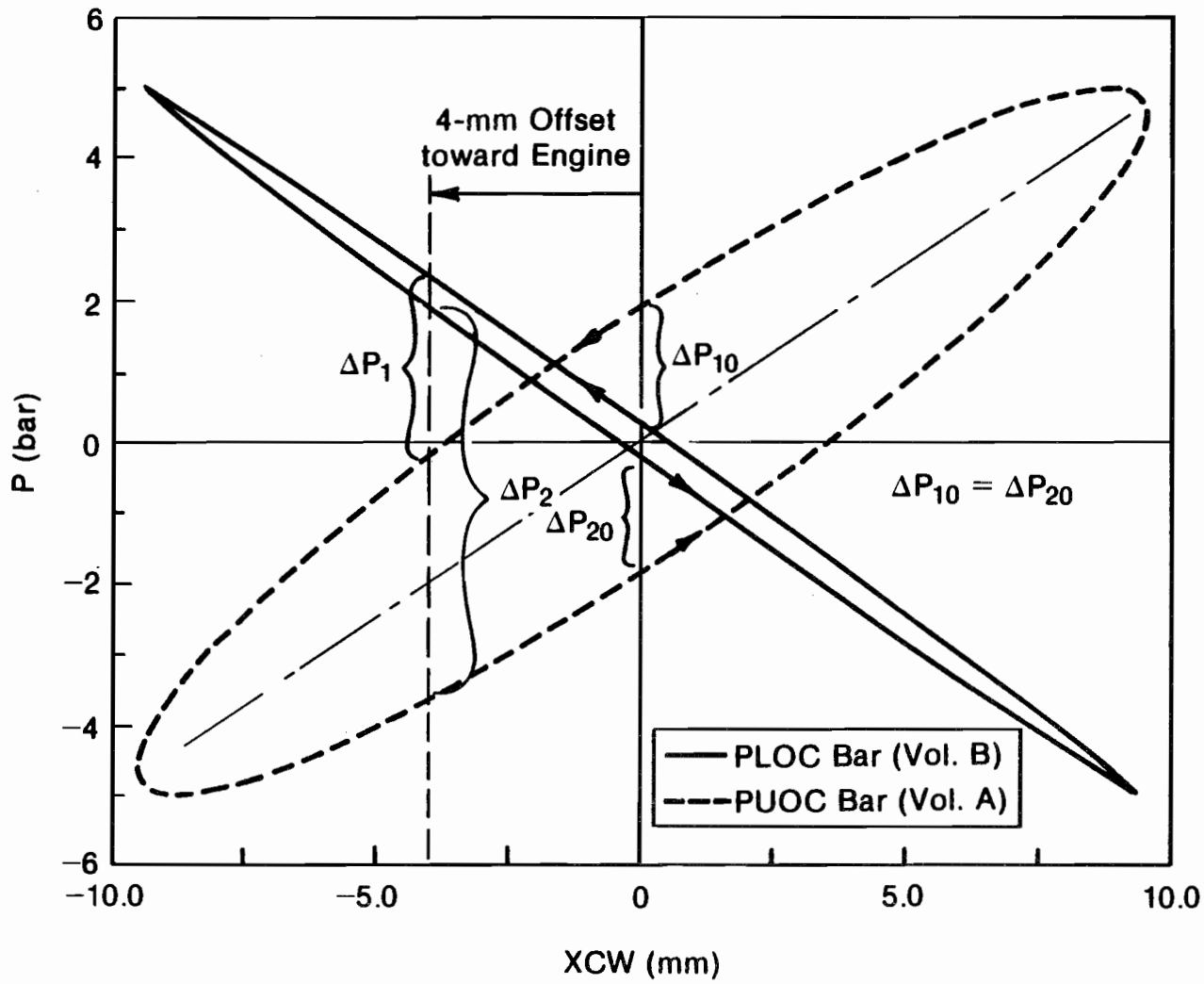

Figure 3-23 Port 1: Port Between Upper and Lower Oil Cavities Provides Stabilizing Force Resulting from Net Flow from Volume B to Volume A

851653

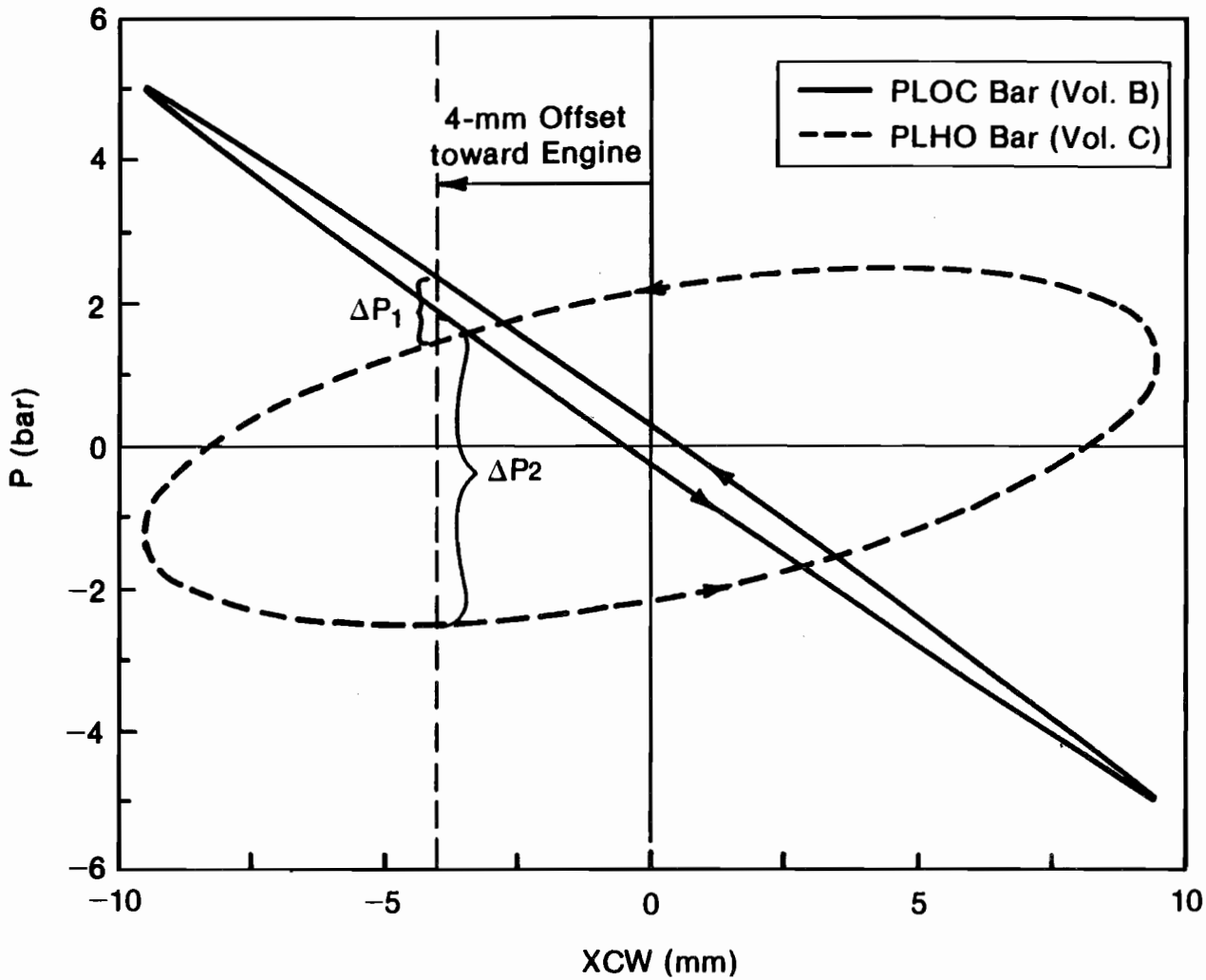

Figure 3-24 Port 2: Port between Lt.H. Oil and Lower Oil Cavities Results in Net Flow from Volume B to Volume C

851654

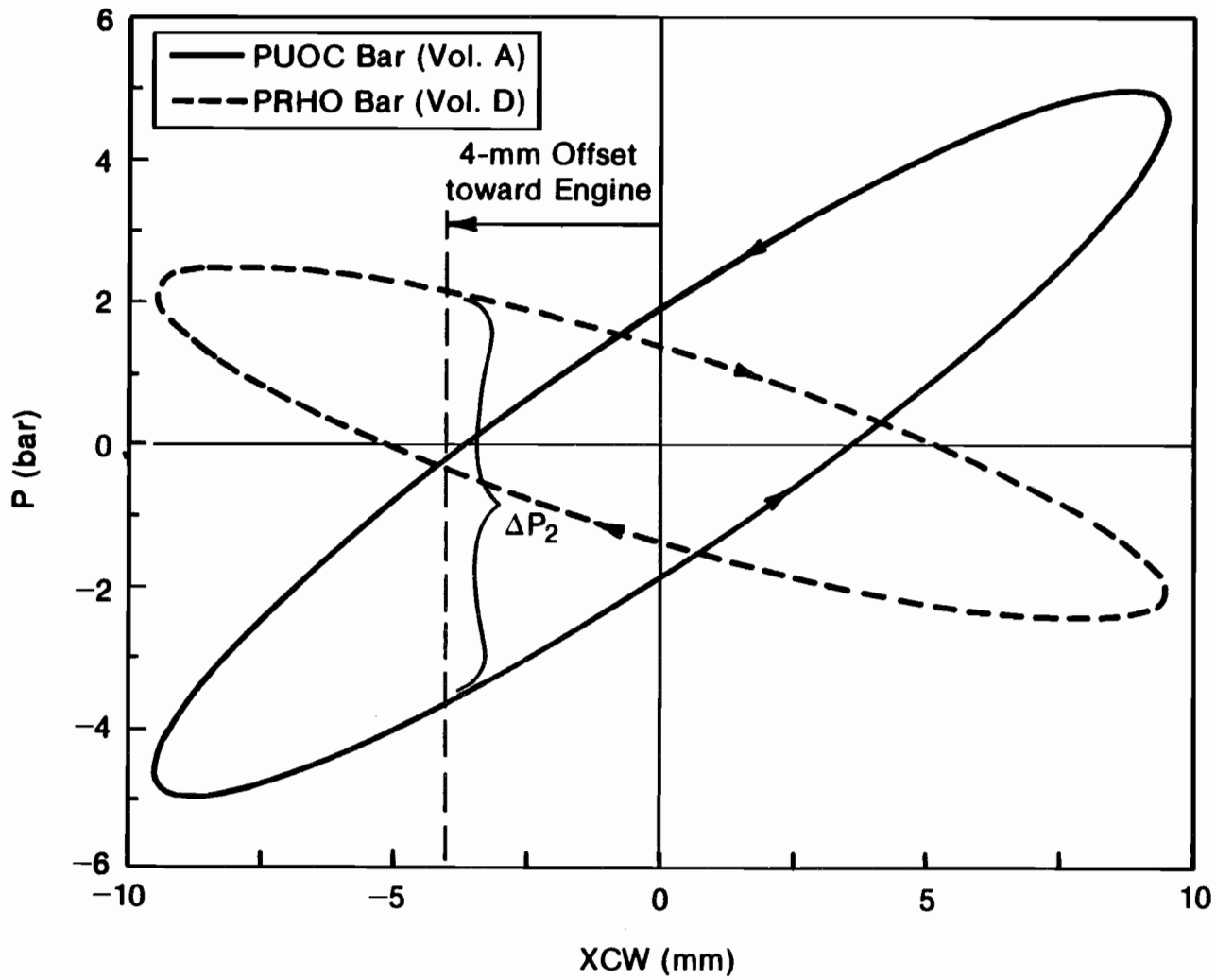

Figure 3-25 Port 3: Port Between Upper Oil and Rt.H. Oil Cavities Results in Net Flow from Volume D to Volume A

851655

During both up-stroke and down-stroke port openings, the port flow is from volume B to A, thus driving the counterweight back toward center.

Ports 2 and 3 also show zero net port flow over the cycle for centered (zero offset) counterweight operation (see Figures 3-24 and 3-25). The destabilizing action of these ports is illustrated by, again, assuming a 4-mm counterweight offset into volume A. Port 2 has a net flow from volume B to volume C, and port 3 has a net flow from volume D to volume A; both actions tending to drive the piston assembly into volume D. By a similar argument, this destabilizing effect of the ports is also observed for a counterweight offset in the negative direction.

Neutral Stability - Following the problem identification, ports 2 and 3 were effectively removed by filling with metal epoxy. Stable operation was observed over full-stroke range, but only at low (<3.0:1) compressor pressure ratios. At higher pressure ratios, the destabilizing effects of the compressor exceed the net piston assembly positive stiffness (mechanical springs and port 1), and, once perturbed, the piston tends to remain off center.

Positive Centering Means - To proceed with short-term development testing, new piston springs have been designed for maximum stiffness to help overcome the destabilizing forces at high-pressure ratios. For the longer term, a cross-porting scheme has been designed which connects volume C to volume A (port 4), and volume B to volume D (port 5); see Figure 3-26. This arrangement positively ports the inner oil volumes, which affect both the counterweight and the piston and should result in positive stability. Figure 3-27 combines the pressure-displacement diagrams for all four volumes to illustrate the cross-porting effect. For an assumed 4-mm counterweight offset into volume A and D, port 1, as before, has a net flow from volume B to volume A. Port 4 net flow is from volume C to volume A, and port 5 net flow is from B to D. All flows tend to drive both the piston and the counterweight back to center.

It should be noted that external plumbing lines with check valves have been used to connect volumes A to C and B to D. Although this is not a true 'porting' arrangement, it, nonetheless, can be used to validate the porting theory previously described. When incorporated on the test stand, these lines did provide restoring forces to the counterweight and piston, forcing them toward a centered

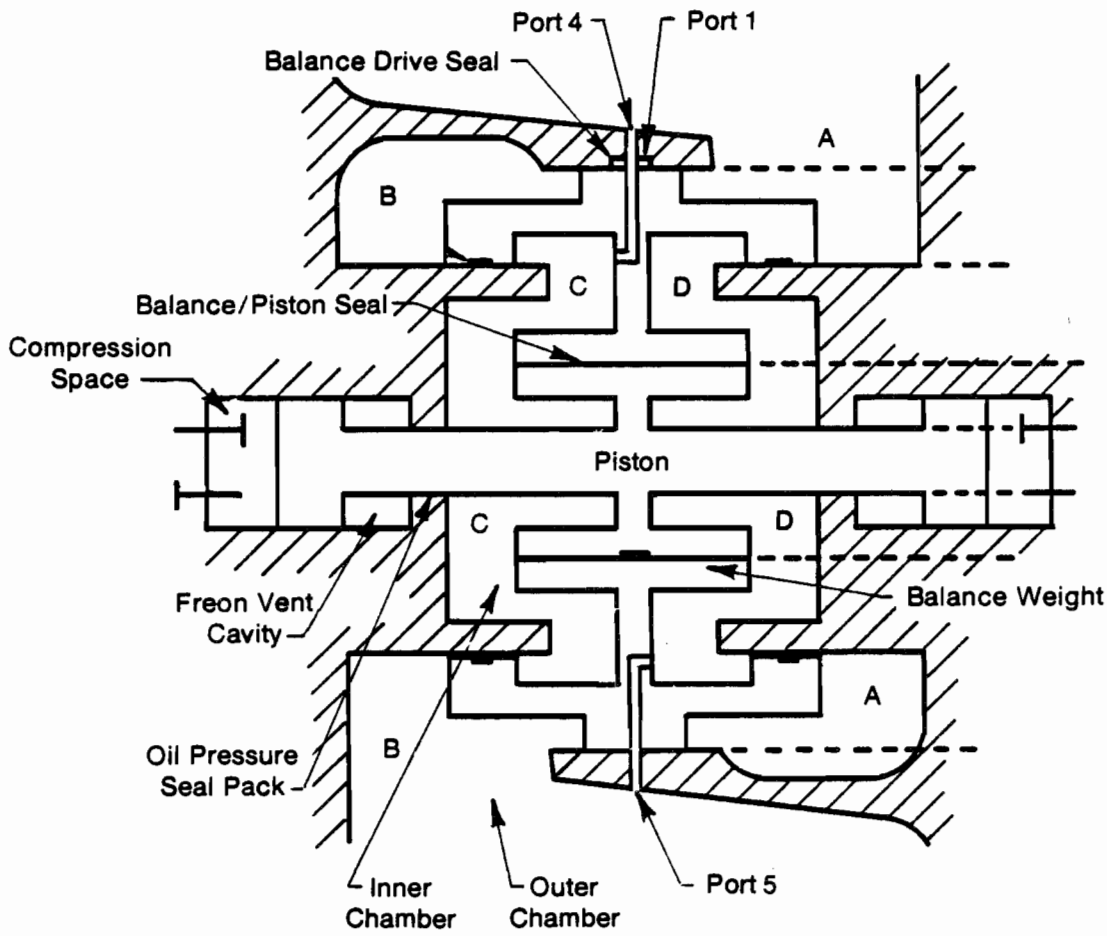

Figure 3-26 HAHP Transmission Cross-Porting Layout

852061

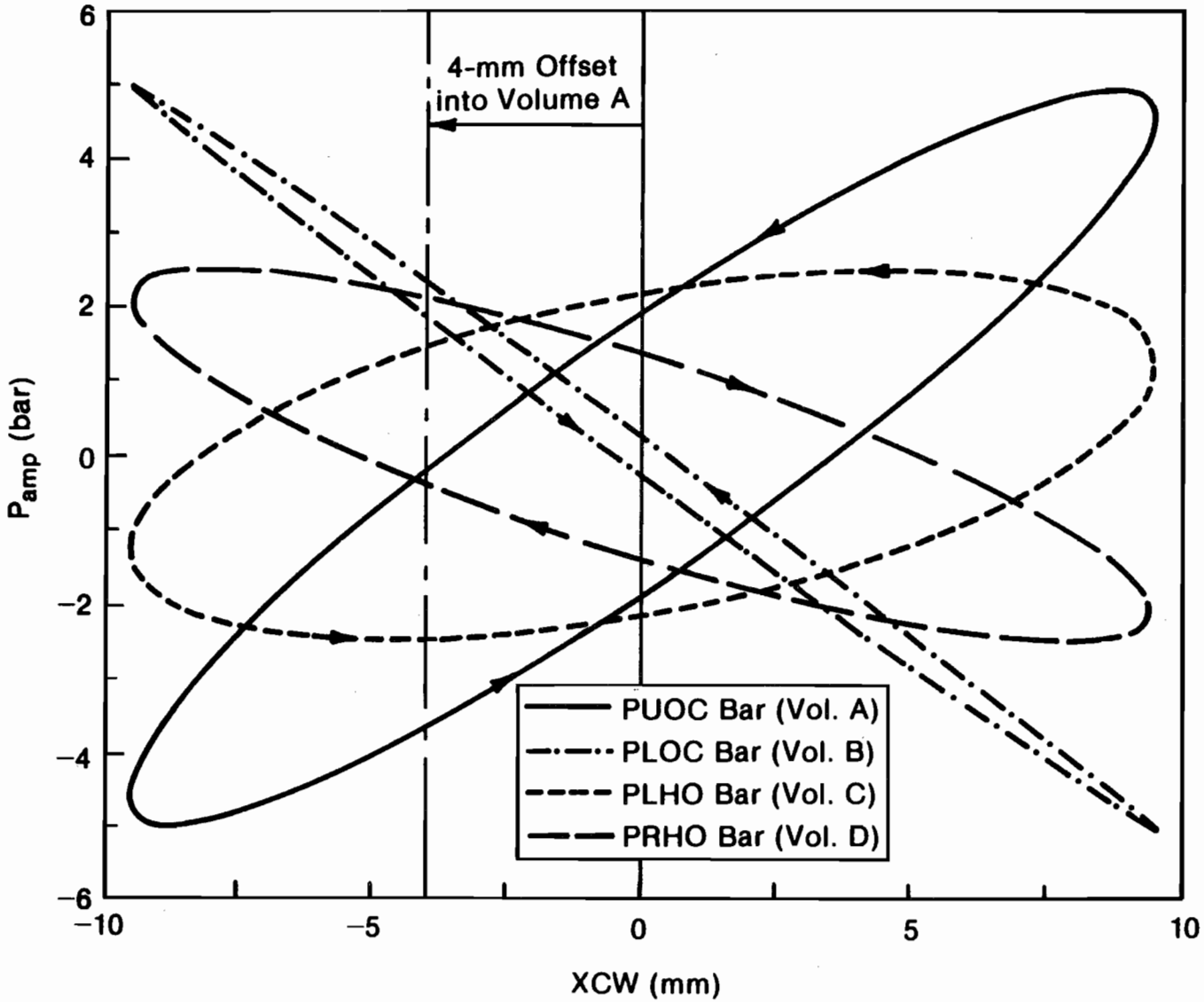

Figure 3-27 HAHP Counterweight Compressor Oil Pressure Interactions

851656

position. It is planned that ports 4 and 5 will be incorporated into the next hardware configuration.

3.2.3 Work Element 2C - Gas Spring

The work statement specifies that new compressor gas spring designs will be evaluated in which the gas spring losses due to hysteresis can be reduced. Pending evaluation, a modified gas spring will be designed, fabricated, and tested.

Alternative gas spring designs have been evaluated with the objective of reducing internal wetted area and associated thermal hysteresis loss. The existing gas spring, shown in Figure 3-28, incorporates a hydraulically backed metal bellows and a stack of volume stuffer rings which allow adjustments to be made in the spring rate. Also included is a diaphragm backing plate intended to support the diaphragm and prevent its rupture in case of sudden pressure loss in the gas spring; a condition very unlikely to occur. The total internal surface area of this design is approximately 732 square inches.

In order to improve gas spring efficiency, it was decided to eliminate the volume stuffer rings and adjust the bellows and diaphragm backing plate on the breadboard compressor. The design that resulted is shown in Figure 3-29. Spring rate adjustments are still possible by varying the heights of the volume stuffer plates which are o-ring sealed on their perimeters and sealed under the heads of each screw. The gas spring wetted area for this design is 205 square inches, and the predicted reduction in thermal hysteresis loss is 72%.

The equation developed at MTI to evaluate gas spring hysteresis loss is:

$$W_{GS} = K/4 \sqrt{\frac{\omega}{2\alpha_{ow}}}\ T_w\ \gamma\ (\gamma-1)\ A_o\ \left(\frac{\Delta V}{Vo}\right)^2\ F_{GS}$$

where:

K = gas thermal conductivity = 0.0278 W/m °k (nitrogen)

ω = angular frequency = 377 rad/s

α_{ow} = gas thermal diffusivity at wall temperature = 4.27×10^{-7} m^2/s

T_w = wall temperature = 50°C (323°K)

γ = ratio of specific heats = 1.40

A_o = wetted area = 732 in.^{2} (0.47 m^2)

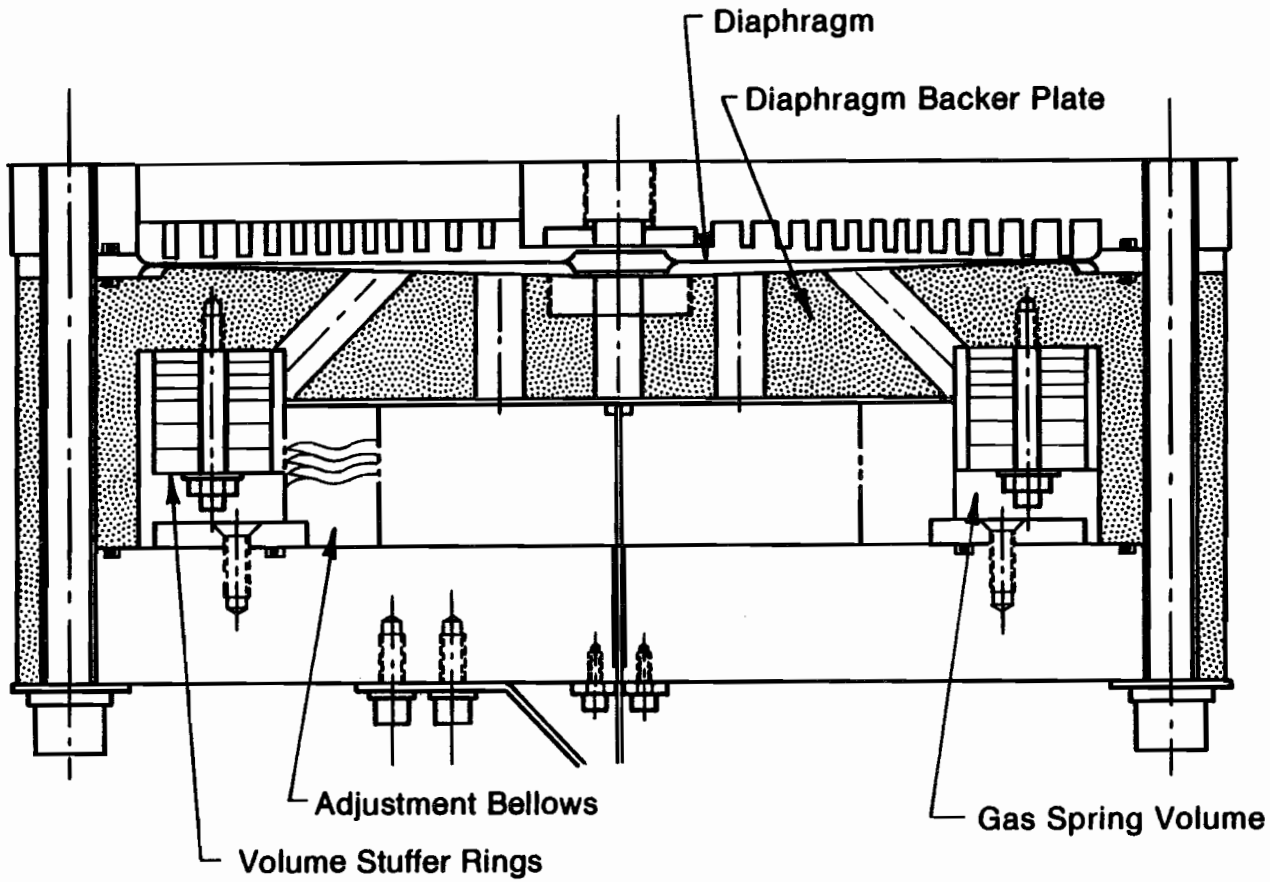

Figure 3-28 Original Gas Spring Assembly

852059

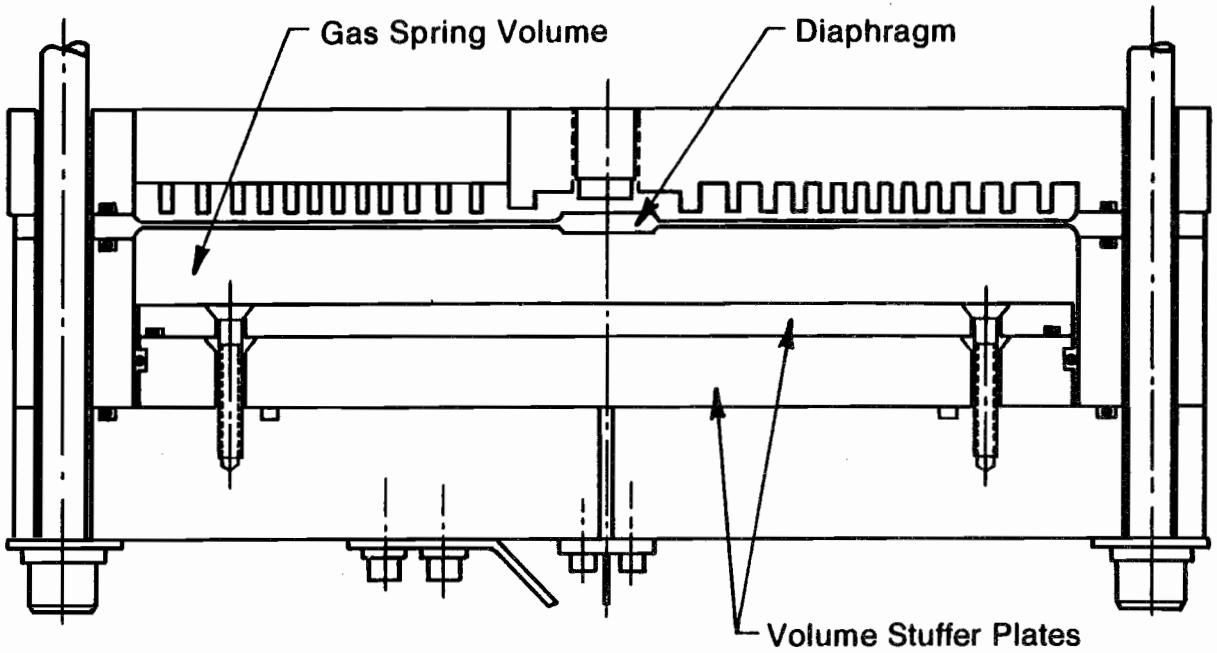

Figure 3-29 Improved Gas Spring Assembly

852058

$\Delta V/Vo$ = 0.061 at 0.75 in. piston amplitude, 4 in.^{3} diaphragm displacement

F_{GS} = enhancement factor - between 2 and 3

This equation predicts 138.5 W hysteresis loss for the original configuration using an enhancement factor of 3. Test results, however, when scaled up to full-stroke conditions indicate ~250 W loss, which is much larger than expected. One explanation may be that significant gas flow occurs at 60 Hz in the gaps between volume stuffer rings. These rings are clamped together with mounting screws but not sealed.

Assuming that 111 W are due to lack of sealing between components and that 72% of the hysteresis loss will be saved by reduction of wetted area, the total savings in gas spring loss for the new design is 210 W. The new gas spring was tested on the breadboard system during November 1984. Overall, there was no noticeable change in lower end losses. It should be pointed out, however, that at the time of the testing, there was a high degree of uncertainty in the piston stroke measurement, thereby making a thorough assessment of improvements due to the new simplified gas spring impossible. Further testing will be performed in future phases of the program.

3.2.4 Work Element 2D - Mechanical Springs

The work plan states that the function of the mechanical coil springs will be evaluated to determine their benefit to the system in view of revised centerporting designs. Tests will be conducted with and without the springs in place to provide data for evaluation.

As discussed in Work Element 2B, the mechanical springs produce important centering forces on the dynamic components. This is especially true during start-up when the porting system exerts the least influence. Additionally, at large refrigerant pressure ratios, port 1 alone is not sufficient to center the compressor piston. Analysis confirms that even stiffer mechanical springs are required to compensate for offsetting forces at high refrigerant compression ratios. A mechanical spring design has been identified which will provide 64% more spring stiffness than the original springs. The new springs were tested without any centerporting in order to evaluate the effectiveness of centering with mechanical springs alone. The results showed that the compressor could not be centered, even

at low refrigerant pressure ratios. Therefore, it was determined that effective centerporting is essential to achieving centered operation of the compressor and that mechanical springs play a secondary role in the centering process.

3.2.5 Work Element 2E - Refrigerant Shuttling

The work statement specified that test data will be reviewed to quantify the shuttling loss in the refrigerant transfer line in the present system. Buffer volumes to replace the transfer line will be fabricated and installed, and tests on the new system will be performed.

Referring to Figure 3-11, the refrigerant transfer line referred to here is an external flow line that connects the refrigerant vent cavities existing behind each of the compressor pistons. The function of this line is to shuttle the refrigerant vapor between the two vent cavities to prevent these cavities from acting as gas springs. Because the piston is reciprocating at 60 Hz, any pressure drop in the transfer line will quickly lead to a large power parasitic. An alternative to the transfer line is the use of buffer volumes connected to the exhaust of each vent cavity. The buffer volumes would reduce the loss by minimizing the pressure excursions in the vent volumes.

During the initial tests conducted on the breadboard unit during Phase IA of this program, refrigerant shuttle lines and fittings were changed to provide larger flow passages for shuttled gas. This was due to the calculation of the major flow restrictions in the plumbing line rather than in the compressor internal passages. Nonetheless, the initial baseline tests indicated no significant performance improvement over data taken with the previous configurations.

During the effort detailed under Work Element 1E, it was determined that it was beneficial from a reliability aspect to maintain the spaces behind the compressor pistons unbuffered and free to shuttle refrigerant from one side to another. This arrangement assures that the compressor seal 'sees' a pressure difference which is unidirectional, enhancing piston ring life and maintaining a positive sealing pressure on the piston ring seal at all times. For this reason, it was decided not to construct buffer volumes in place of the shuttling arrangement as proposed in the initial work statement.

The refrigerant shuttling tests were repeated on the hydraulic simulator, whereby the refrigerant shuttle port flow area was doubled, yet no performance change was evident. The result of measured transmission losses for the opened lines are shown in Figure 3-30. By comparing these losses to the data points labeled "Double Chevron" in Figure 3-6 (where the shuttle flow lines had one half as much cross-sectional area) it can be seen that the shuttling effect does not play a dominant role in the overall transmission loss function.

3.2.6 Work Element 2F - Life Tests

With the approval of the ORNL TM, the work plan states that life and reliability test conditions will be established and tests performed on selected components. These components may include diaphragms, rod bearings, rod seals, piston seals, and valve-plate assemblies. The hydraulic simulator test rig will be used for all life tests. The goal is to achieve the maximum possible operating hours experienced within the specified Phase IB program period of performance up to submission of Milestone No. 2.

With concurrence from the ORNL TM, the hydraulic simulator was not used to conduct durability testing; rather, it was employed to perform additional seal performance tests on the direct drive compressor configuration as reported under Work Element 1A and 1B.

3.3 Summary of Breadboard Heat Pump Performance Improvements for Phase 1B

As described in Section 3.1, several modifications were made to the breadboard heat pump lower end (hydraulic transmission and compressor) to improve its performance over the results that had been obtained in Phase I. The modifications that proved the most important were:

1. Removing the internal counterweight. This enabled the compressor stroke to be increased and hydraulic transmission loss data to be obtained over a much broader operating range.

2. Substituting refrigerant R-500 for R-22. This reduced the required compressor PV power for the same evaporator and condenser temperatures and also enabled larger piston strokes to be achieved.

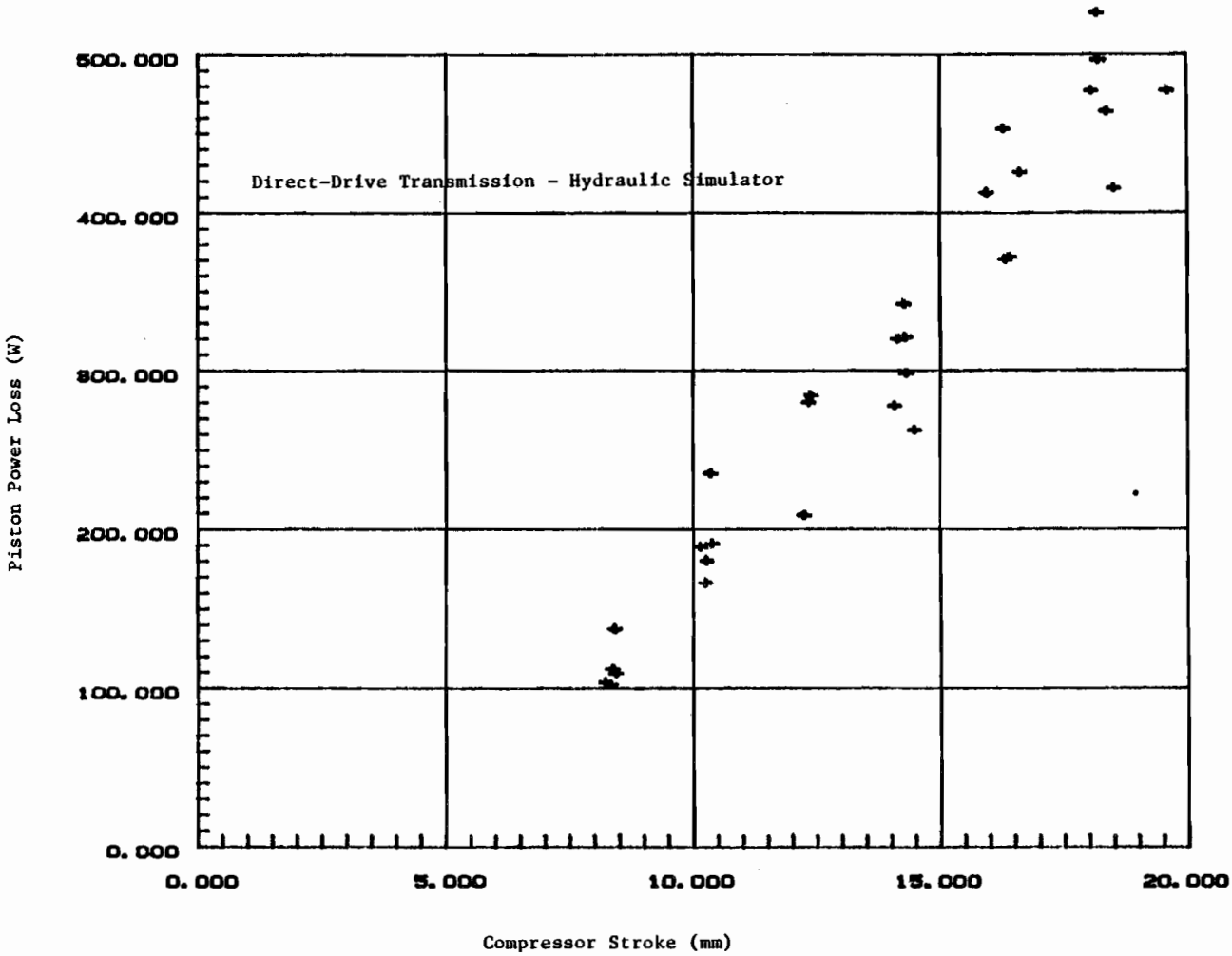

Figure 3-30 Shuttle Loss Test (1/8/85)

86699

3. Modifying the compressor piston seal backer ring. This modification produced a better seal and reduced the refrigerant leakage.

4. Using brake fluid in the hydraulic transmission. Brake fluid has a lower viscosity than the Suniso refrigerant oil previously used. The lower viscosity reduced the hydraulic transmission losses which produced a large increase in the refrigerant mass flow. Unfortunately, brake fluid is corrosive and it damaged the hardware.

5. Replacing the brake fluid with Dow Corning 200 fluid. Dow Corning 200 fluid has a low viscosity and is not corrosive like brake fluid.

The results of these tests are summarized in Tables 3-2 through 3-4. In Table 3-2, the comparison is presented for running with and without the counterweight. This one modification had the positive effect of increasing the piston stroke from 10.68 mm to 16.66 mm and increasing the capacity by 50%. Table 3-3 presents the results after the transmission fluid and refrigerant had been changed to brake fluid and R-500 and the new piston seal backer ring was installed. These changes increased the piston stroke from 16.7 mm to 17.8 mm.

The final performance test run was to replace the brake fluid with Dow Corning 200 fluid and again running with refrigerant R-22. The Dow Corning 200 fluid is a silicone-based oil with a room temperature viscosity of 2 cs. Comparing these results to the test results with Suniso 3GS shows that the improvements made due to a lower viscosity fluid and the new backer ring were an increase of 26% in flow and an increase in cooling capacity at the 95°F ambient conditions to 28,227 Btu/hr. Table 3-5 shows the advances that were made through these tests in reducing the lower end loss and increasing the lower end efficiency, which is defined in Appendix A.

Unfortunately these tests without the counterweight did not give good steady state data because long runs at high strokes could not be made without damaging the system. Primarily, the damage occurred in the combustor and a loss in head temperature would occur. Therefore, to continue the development of the heat pump, it was necessary to reinstall the counterweight. Following phases of the program will be directed at improving performance of a balanced unit.

Table 3-2

HAHP Breadboard Performance Comparison

Date	9/1/83[1]	3/13/84[2]
Refrigerant	R-22	R-22
Transmission Fluid	Suniso 3GS	Suniso 3GS
X_d (mm)	19.51	23.04
X_p (mm)	10.68	16.66
$\Theta_{d,p}$ (°)	56.71	67.60
P(mean) (bar)	56.3	62.2
Frequency (Hz)	57.1	59.8
P(Suction) (psia)	91.7	86.3
T(Suction) (°F)	104.4	87.3
P(Discharge) (psia)	279.9	288.7
T(Discharge) (°F)	203.5	190.2
Refrigerant Flow (lb_m/hr)	216.8	317.8
Capacity (Btu/hr)	16,238	22,000
P(Motor) (W)	527.1	1,818.2
Engine PV (W)	1,191.0	2,909.5
Q(Head) (W)	7,072.0	9,864.0
Total Lower End Loss[3] (W)	598.1	1,576.9
Piston + CW Loss (W)	378.1	976.6
Gas Spring Loss (W)	77.2[4]	22.4[4]
Hydraulic Loss (W)	142.7	577.9

1 - Base run used to establish performance of internal counterweight at the end of the Phase I, HAHP Program, September 30, 1984

2 - Unbalanced direct-drive compressor; internal counterweight removed from transmission

3 - Terms defined in Table A-4

4 - Using nitrogen gas

Table 3-3

HAHP Breadboard Performance Comparison

Date	3/13/84[1]	3/30/84[1]
Refrigerant	R-22	R-500
Transmission Fluid	Suniso 3GS	Brake Fluid
X_d (mm)	23.04	21.19
X_p (mm)	16.66	17.80
$\Theta_{d,p}$ (°)	67.60	82.81
P(mean) (bar)	62.2	60.6
Frequency (Hz)	59.8	57.8
P(Suction) (psia)	86.3	85.1
T(Suction) (°F)	87.3	80.3
P(Discharge) (psia)	288.7	198.2
T(Discharge) (°F)	190.2	150.72
Refrigerant Flow (lb_m/hr)	317.8	448.8
Capacity (Btu/hr)	22,000	32,269
P(Motor) (W)	1,818.2	1,219.0
Engine PV (W)	2,909.5	2,596.3
Q(Head) (W)	9,864	10,802
Total Lower End Loss[2] (W)	1,576.9	1,204.0
Piston + CW Loss (W)	976.6	916.0
Gas Spring Loss (W)	22.4[3]	145.1[3]
Hydraulic Loss (W)	577.9	142.9

[1] - Unbalanced direct-drive compressor; internal counterweight removed from transmission
[2] - Terms defined in Table A-4
[3] - Using nitrogen gas

Table 3-4

HAHP Breadboard Performance Comparison

Date	3/13/84[1]	6/13/84[1]
Refrigerant	R-22	R-22
Transmission Fluid	Suniso 3GS	DOW Corning 200, 2CS
X_d (mm)	23.04	20.71
X_p (mm)	16.66	16.64
$\Theta_{d,p}$ (°)	67.60	69.84
P(mean) (bar)	62.2	61.07
Frequency (Hz)	59.8	59.24
P(Suction) (psia)	86.3	97.2
T(Suction) (°F)	87.3	74.22
P(Discharge) (psia)	288.7	296.44
T(Discharge) (°F)	190.2	175.80
Refrigerant Flow (lb_m/hr)	317.8	401.6
Capacity (Btu/hr)	22,000	28,227.0
P(Motor) (W)	1,818.2	1,842.0
Engine PV (W)	2,909.5	2,408.3
Q(Head) (W)	9,864	7,537.0
Total Lower End Loss[2] (W)	1,576.9	718.37
Piston + CW Loss (W)	976.6	377.3
Gas Spring Loss (W)	22.4[3]	70.87[3]
Hydraulic Loss (W)	577.9	270.2

[1] - Unbalanced direct-drive compressor; internal counterweight removed from transmission

[2] - Terms defined in Table A-4

[3] - Using nitrogen gas

Table 3-5

Compressor Efficiency and Capacity Development

Date	Design	9/1/83[1]	3/13/84[2]	6/13/84[2]
Displacer Stroke (mm)	20.8	19.5	23.0	20.7
Compressor Stroke (mm)	19.1	10.7	16.7	16.6
95°F Day Capacity (Btu/hr)	36,000	16,238	22,000	28,227
Lower End Loss (W)	502	598	1,577	718
Lower End Efficiency (%)	69	NA[3]	48	64

[1] - Internal counterweight compressor
[2] - Unbalanced direct-drive compressor; internal counterweight removed from transmission
[3] - Short stroke comparison not applicable

Definitions for the nomenclature of the terms used in this section are presented in Appendix A, and Appendix B describes the refrigerant test loop used to set the compressor suction and discharge conditions.

3.4 Milestone No. 3 - Oil Management System Development

The HAHP hydraulic transmission requires high pressure oil to transfer the engine PV power to the compressor drive. To prevent overstressing the diaphragms, the oil must be replenished as it leaks past the compressor rod seals, and the nitrogen inventory in the gas spring must be regulated to equalize engine charge pressure. An oil management control system has been designed, fabricated, and tested to perform this function. The control system developed uses two eddy current sensors to monitor the center position of the diaphragms and from this control function, maintain a constant oil inventory in the hydraulic transmission.

The oil management system was first installed on the breadboard system in May 1984 and has been operating flawlessly since. It has demonstrated its dependability in over 200 hours of testing and plans are to incorporate it into future heat pump designs. This section describes the functions of the oil management system and presents a description of the control circuitry developed.

3.4.1 Overall System Description

The compressor of the HAHP Power Module contains an upper and a lower diaphragm. The upper diaphragm is the mechanical interface between the engine and the compressor. The lower diaphragm is the interface between the compressor and the compressor gas spring. Oil is maintained between the upper and lower diaphragms by means of an oil supply system. Nitrogen is regulated beneath the lower diaphragm. During system operation the upper and lower diaphragms must be maintained on center. The function of the oil management system is to automate the centering of the diaphragms during engine operation. The automated system eliminates the necessity for operator monitoring and regulation of the oil and nitrogen supplies.

A block diagram defining the control elements of the oil management system is presented in Figure 3-31. As shown, upper and lower diaphragm positions are sensed by means of eddy current probes. The position signals are input to an

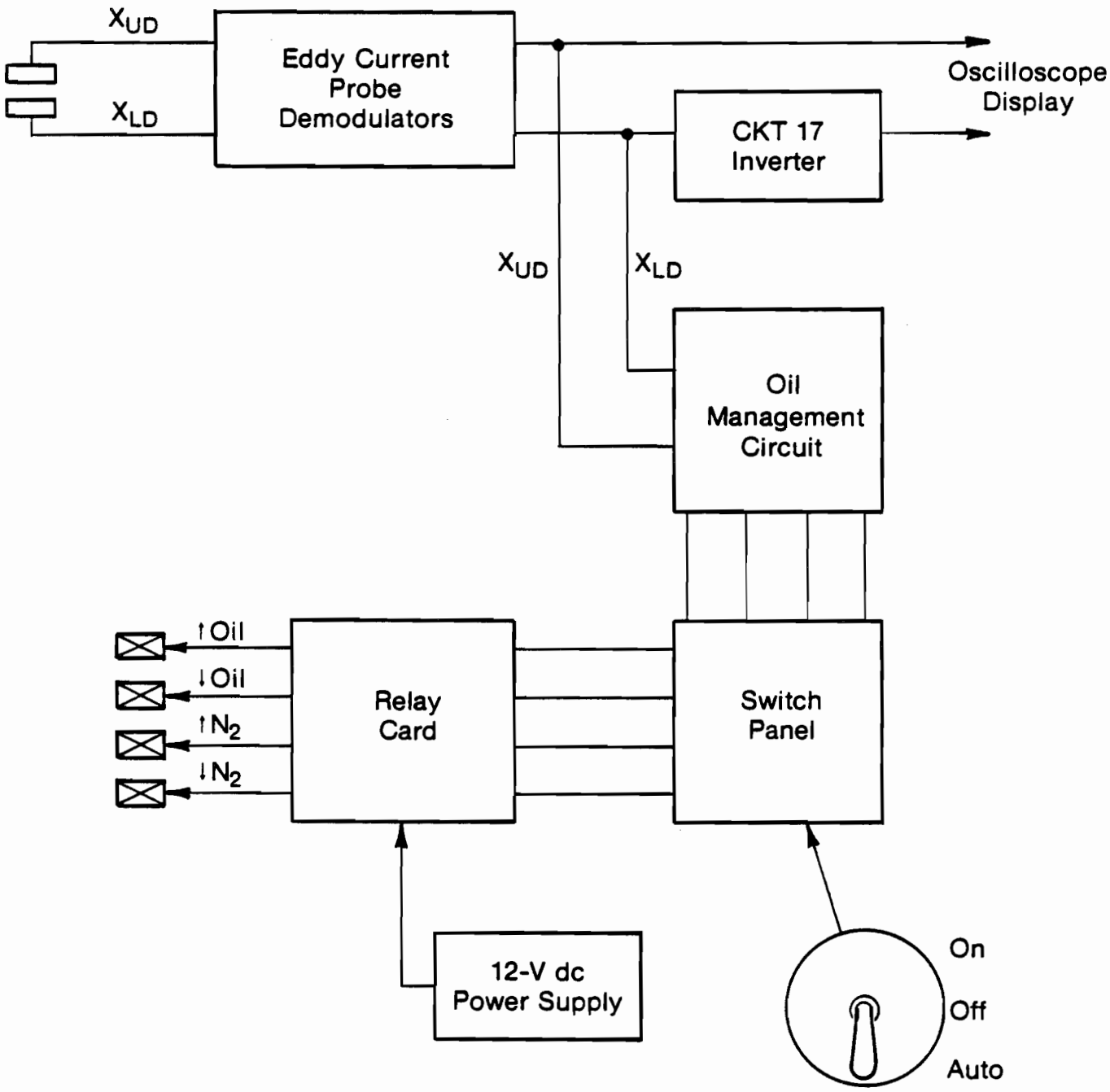

Figure 3-31 Oil Management System Block Diagram

852064

electronic circuit which extracts the low frequency components. The low frequency components of the position signals determine the mean position of the diaphgrams. The circuit determines what corrective action must be taken with the oil and nitrogen (charge or discharge) in order to center the diaphragms. The circuit outputs four signals (oil charge, oil discharge, nitrogen charge, nitrogen discharge) which are passed on to four relays. The relays activate solenoid valves which regulate the flow of oil and nitrogen. Additional regulation of oil and nitrogen flow is achieved with needle valves inserted in the oil and nitrogen, charge, and discharge lines. High pressure oil and nitrogen reservoirs supply oil and nitrogen to the charge solenoid valves. Oil is recirculated to an oil reservoir with the oil discharge solenoid valve; nitrogen is vented to the atmosphere with the nitrogen discharge solenoid valve. A layout of the piping arrangement for the oil management system is shown in Figure 3-32.

3.4.2 Control Logic

The control logic for the oil management system is shown in Figure 3-33. The essence of the logic is that it evaluates the mean position of the diaphragms and, depending on their offset, adjusts either the gas spring pressure or the volume of oil in the transmission to restore the diaphragms to their center position. The logic of this control approach may be seen by considering the following control scenarios.

1. If the gas pressuring in either the engine or gas spring changes, both diaphragms will move either up or down together because of the incompressibility of the oil. This offset can be corrected by either raising or lowering the gas spring pressure to return both diaphgrams to their center positions.

2. If oil leaks out of the transmission, the engine diaphragm will deflect down and the gas spring diaphragm will deflect up (toward the engine). The oil management system will correct this by adding oil until both diaphragms are returned to their center positions.

The lower diaphgram mean position is maintained by either charging or discharging nitrogen to the lower gas spring. If the lower diaphragm is above its center

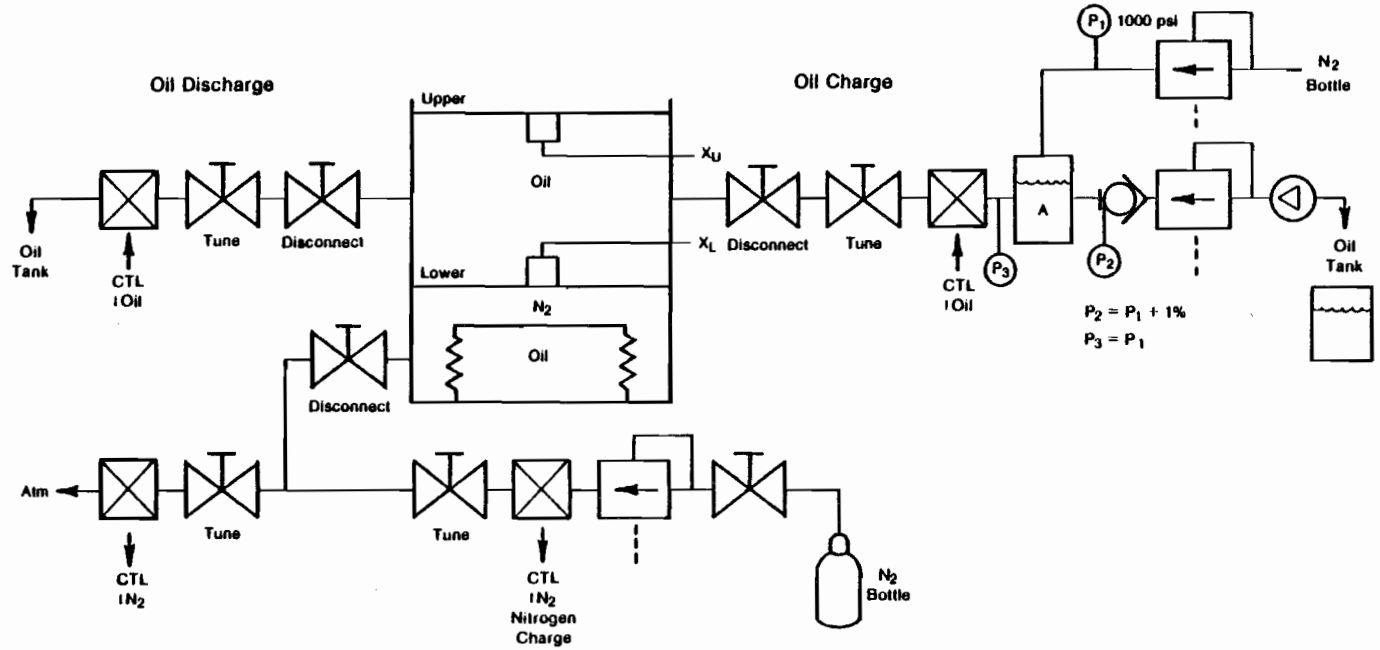

Figure 3-32 Oil Management System Piping Diagram

852065

dc Levels

X_U: Upper Diaphragm

X_L: Lower Diaphragm

$\bar{X}_L$: Inverted Lower Diaphragm (Cell 1 CKT)

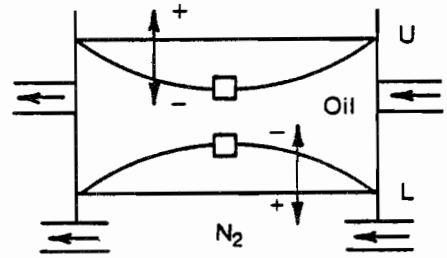

Condition	Sense	Action
	$X_L < 0;\ \bar{X}_L > 0$	↓ N_2
	$X_L > 0;\ \bar{X}_L < 0$	↑ N_2
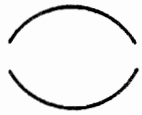	$X_U + X_L > 0;$ $X_U - \bar{X}_L > 0$	↓ Oil
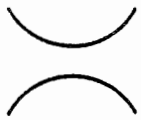	$X_U + X_L < 0;$ $X_U - \bar{X}_L < 0$	↑ Oil

Figure 3-33 Oil Management System Control Logic

852068

position, nitrogen is discharged from the lower gas spring. If the lower diaphragm is below its center position, nitrogen is added to the lower gas spring.

The upper diaphragm mean position is maintained, relative to the lower diaphragm mean position, by charging or discharging oil to the compressor. If the difference between the upper and lower diaphragm mean positions exceeds the difference in their center positions, oil is discharged from the compressor. If the difference between the upper and lower diaphragm mean positions is less than the difference in their center positions, oil is added to the compressor.

3.4.3 System Hardware

The hardware used on the oil management system consists of the electronic circuitry, relays, control panel console, and the solenoid control valves. The breadboard components for the system are shown in Figures 3-34 through 3-37. The components shown in these figures are installed in the breadboard system and have been running trouble free since May 1984. This same hardware will be incorporated into the Mark I heat pump system presently under development at MTI.

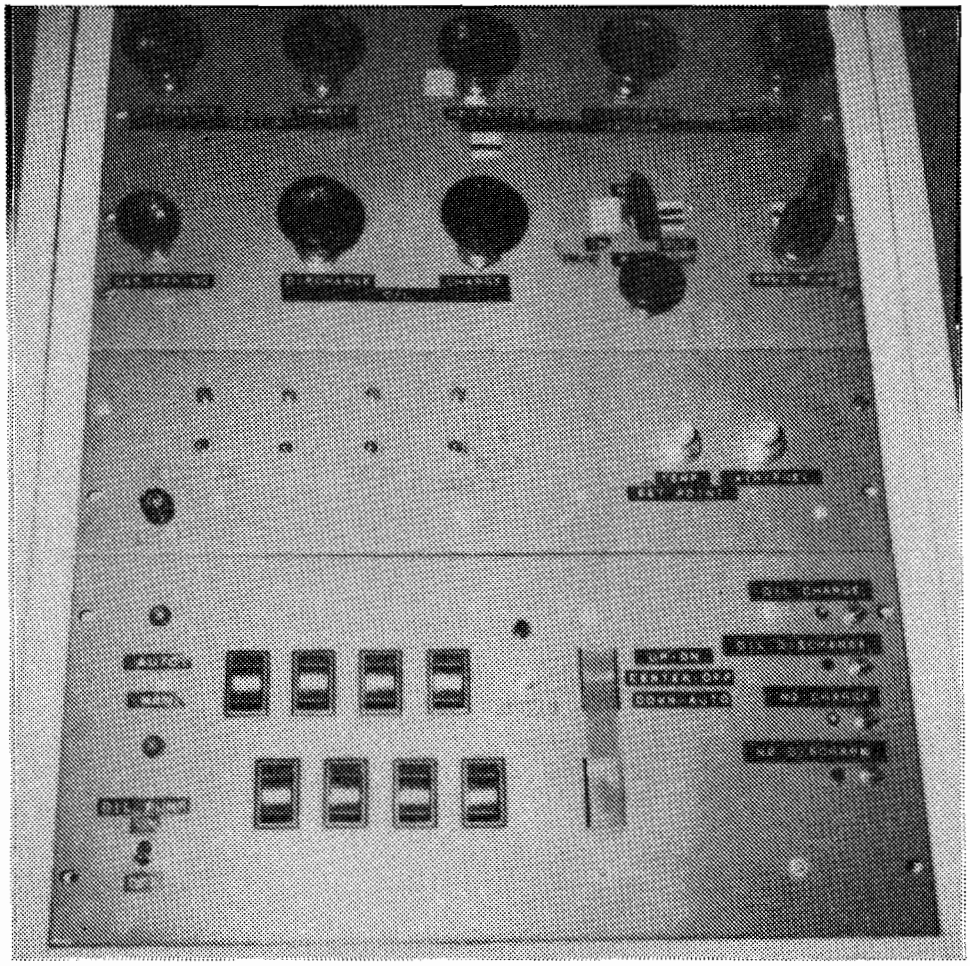

Figure 3-34 Oil Management System Control Panel

852072

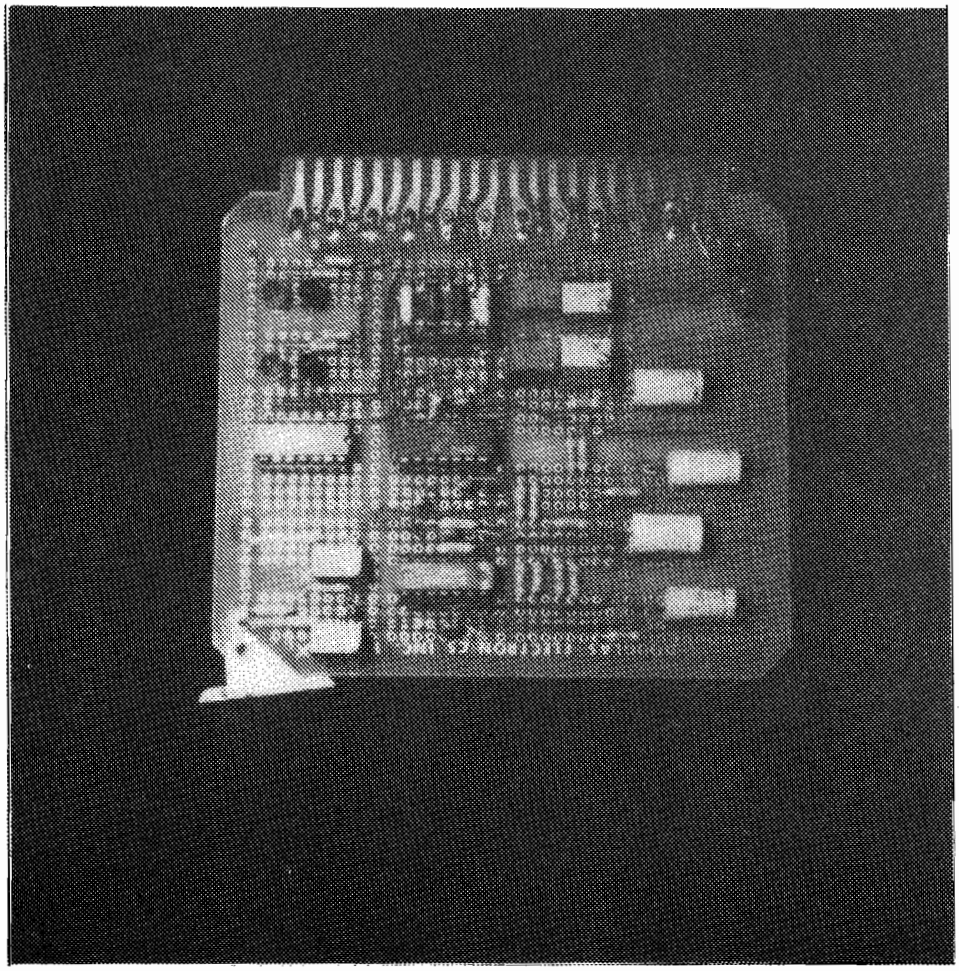

Figure 3-35 Oil Management System Logic Electric Circuit

852071

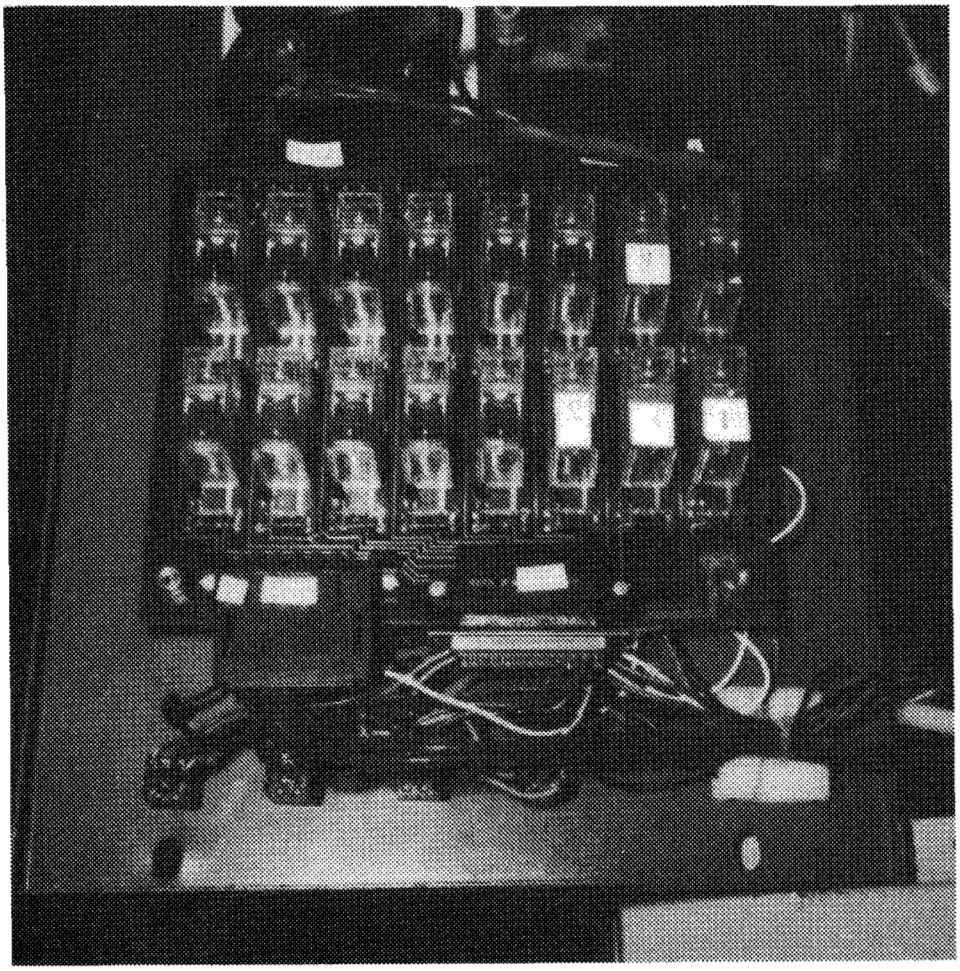

Figure 3-36 Oil Management System Relay Package

852069

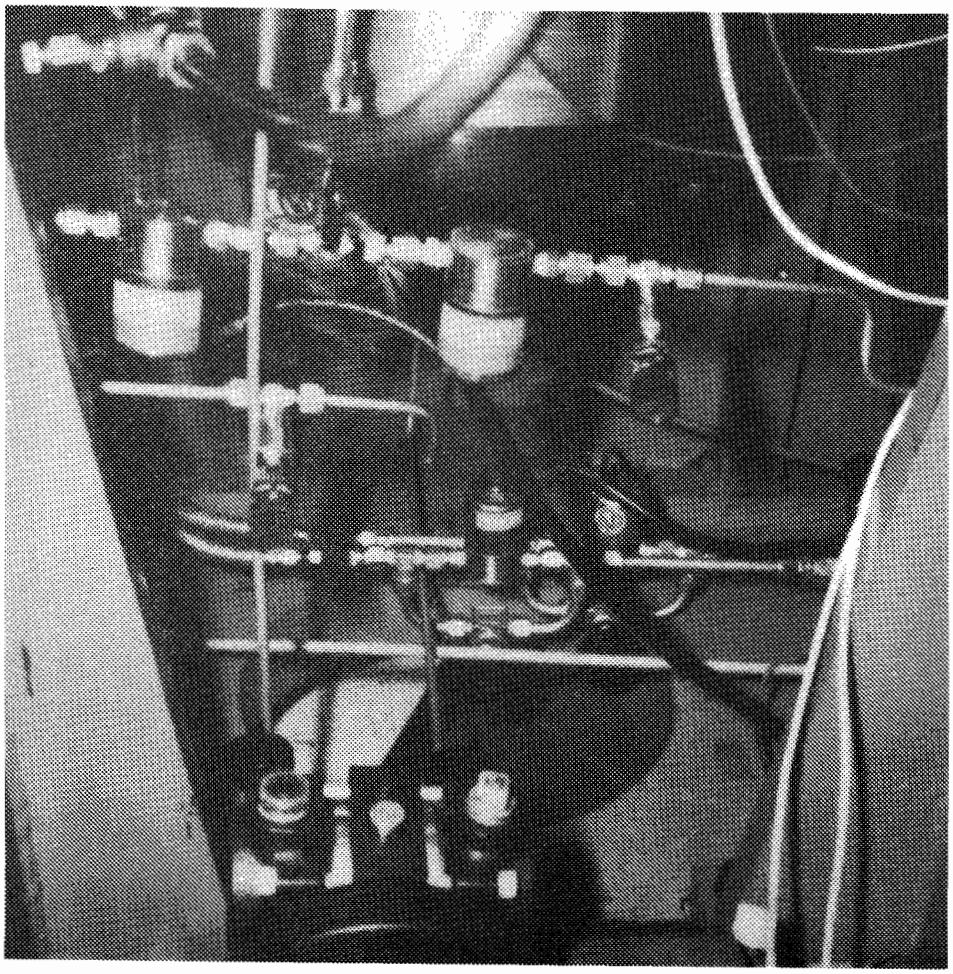

Figure 3-37 Oil and Nitrogen Control Solenoids

852070

4.0 EVALUATION OF NEW CONCEPTS

This task was to be performed only if the technical targets identified for compressor performance improvements could not be attained during the course of the program. The original expectations were that this task would not be executed. However, persistent difficulties with the internal balancer dictated the necessity for evaluating alternative compressor configurations.

The task of coupling a mechanical load to the FPSE while maintaining a hermetic seal (one of the inherent advantages of the FPSE) has a notorious history. During the early 1970s, programs at both General Electric's Space Division and at MTI were conducted in which attempts were made to couple the engine to a resonant refrigerant compressor using hollow spring tubes to carry the refrigerant flow.

Both of these programs fell substantially short of achieving their respective efficiency and operational targets.

In 1980, MTI proposed the diaphragm-coupled, hydraulically-driven compressor having only two independent dynamic bodies. This concept was seen as a way to overcome some of the technical drawbacks associated with the earlier programs, and demonstrate technical feasibility. At the end of Phase I, the technical feasibility of the diaphragm-coupled breadboard compressor was demonstrated in terms of operational stability and mechanical integrity. The performance goals, however, had not been accomplished. At that time, a series of internal meetings were held at MTI to evaluate the diaphragm concept relative to alternatives, including the resonant (inertial) compressor approach tried earlier. Two major conclusions were reached as a result of these meetings:

1. Despite its performance shortcomings to date, the diaphragm-coupled compressor design continued to show promise for further development progress and eventual commercialization. The possibility of using improved arrangements of the hydraulic transmission was considered attractive, e.g., an oil-driven vane with oscillating power shaft.

2. Due to technical difficulties and/or high costs associated with each of the nondiaphragm-coupled approaches considered, none of

these alternatives appeared to have reasonable chance for product success.

A detailed comparison was made between the diaphragm coupling and the resonant compressor configuration. A summary of this comparison is shown in Table 4-1. As can be seen from the table, two major issues put the potential for successful development of the resonant compressor in doubt: 1) predicted loss in efficiency due to significantly high preheating of the suction gas; and 2) uncertain life due to fatigue of the spring tube attachment points.

A more broadly scoped comparison of other alternatives is listed in Table 4-2. Of the six alternative concepts listed, none showed clear superiority over the diaphragm-coupled design.

Based on the above listed comparative assessment, Task 4.0 was conducted with the following constraints:

- Positive seal separation of the helium and refrigerant working fluids
- Hydraulic fluid transmission
- Dynamic balance of compressor momentums.

Based on these constraints, ten alternative transmission/compressor concepts were identified; the tenth concept calling for use of pressure balanced bellows instead of diaphragms. These concepts are outlined in the subsequent group of sketches, Figures 4-1a through 4-10b, and commentary on the advantages and disadvantages of each.

Table 4-3 summarizes the comparative assessment among the various concepts. Concepts No. 2, 4, and 5 offer high transmission efficiency and utilize an external, tuned vibration absorber so that no counterweight moving in oil is needed. Concept No. 5, in particular, is attractive because of only one compressor piston and head. The internal counterweight version (concept No. 1) suffers from oil viscous losses as well as seal blow-by losses. Much of the development pursued in this program has been to improve the design so as to minimize these losses. Concepts No. 1, 2, and 8 would be the easiest to build and test. However, concepts No. 2 and 3 appear to offer advantages in terms of high efficiency and attractive packaging. Certain arrangements of concept No. 3 offer an excellent combination

Table 4-1

Comparison Between the Diaphragm Coupled Compressor and Resonant Piston Compressor Design

Parameter	Diaphragm Coupled	Resonant Piston
Efficiency	Potential for high efficiency by reducing hydraulic losses	Concern for low efficiency due to preheat of suction gas
Capacity	Adequate	Adequate
Manufacturability	Requires value engineering	Requires value engineering
Cost	Potential to meet cost goals	Potential to meet cost goals
Reliability	Good with built in protection against diaphragm overstroke	Serious concern over spring tube fatigue life
Development Risk	Moderate	Moderate
Life	Good based on industry experience with diaphragm pumps	Serious concern over spring tube fatigue life

Table 4-2

Comparison of Alternative Design Concepts for Hermetic Coupling of Refrigerant Compressor to Free Piston Engine

Concept	Advantage	Disadvantage
Magnetic Coupling Across Pressure Shell	. Positive separation of working fluids	. Possible high magnet cost . Stroke limitation due to inertia force overpowering magnets . Potential for eddy current loss
Bellows	. Compact design with long stroke	. Limitation on allowable pressure across bellows
Resonant Compressor	. Maintains simplicity of free piston concept	. Possible spring tube fatigue . Suction gas preheating . Vibration . Dynamic control difficulty
Hydraulic Power Output to Drive Rotary Compressor	. More conventional compressor technology	. System complexity with accumulators, controls, and hydraulic motor . Additional working fluid . Modulation constraints
Oil-Driven Vane with Diaphragm Coupling	. Simple system design . High efficiency potential	. Oscillating shaft oil seal . Additional working fluid . New compressor design required (oscillating vane or linkage to piston)
Linear Oil-Driven Piston with Diaphragm Coupling	. High efficiency potential	. Numerous hydraulic seals if internal counterweight used . Additional working fliud

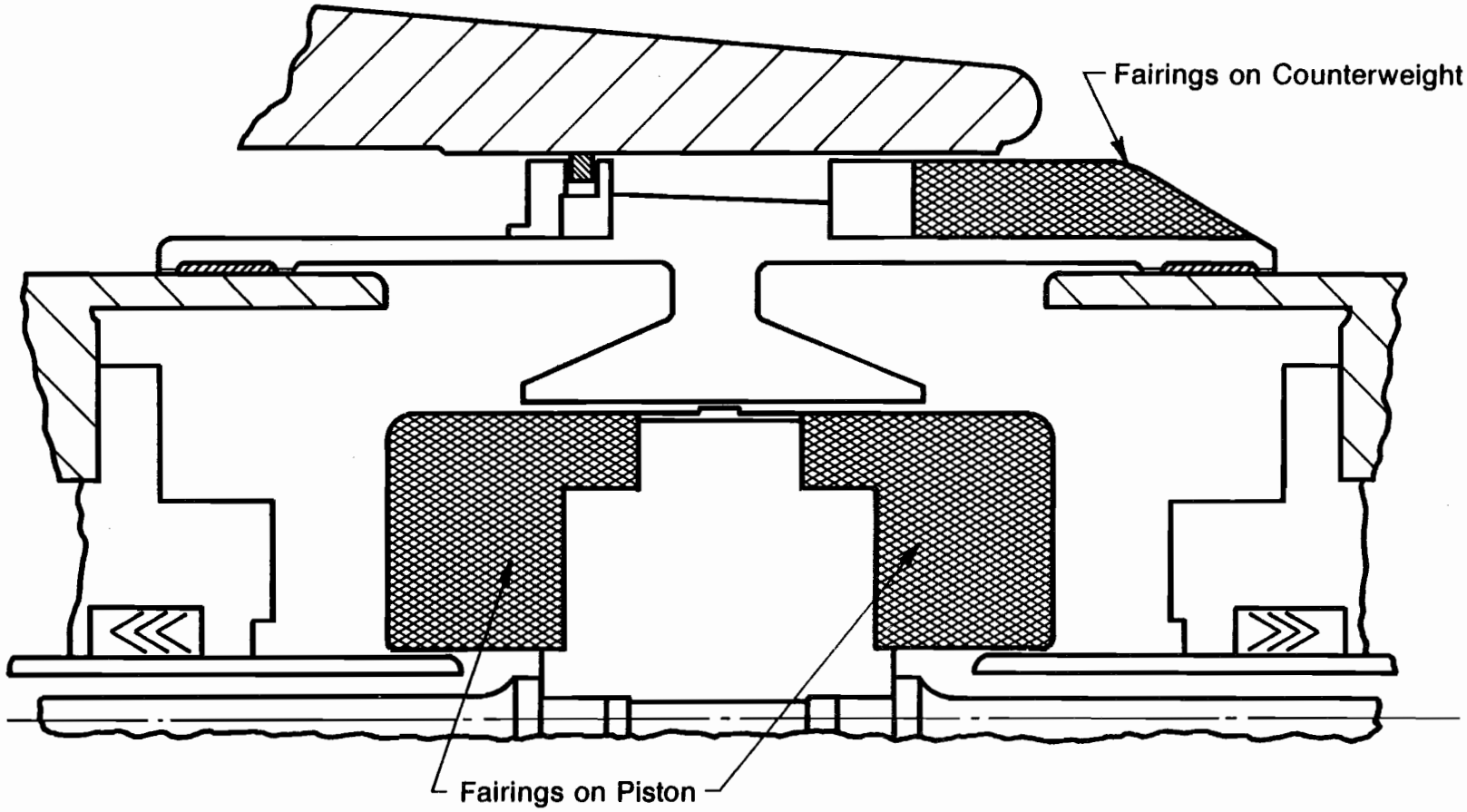

Figure 4-1a Improved Counterweight Version

852060

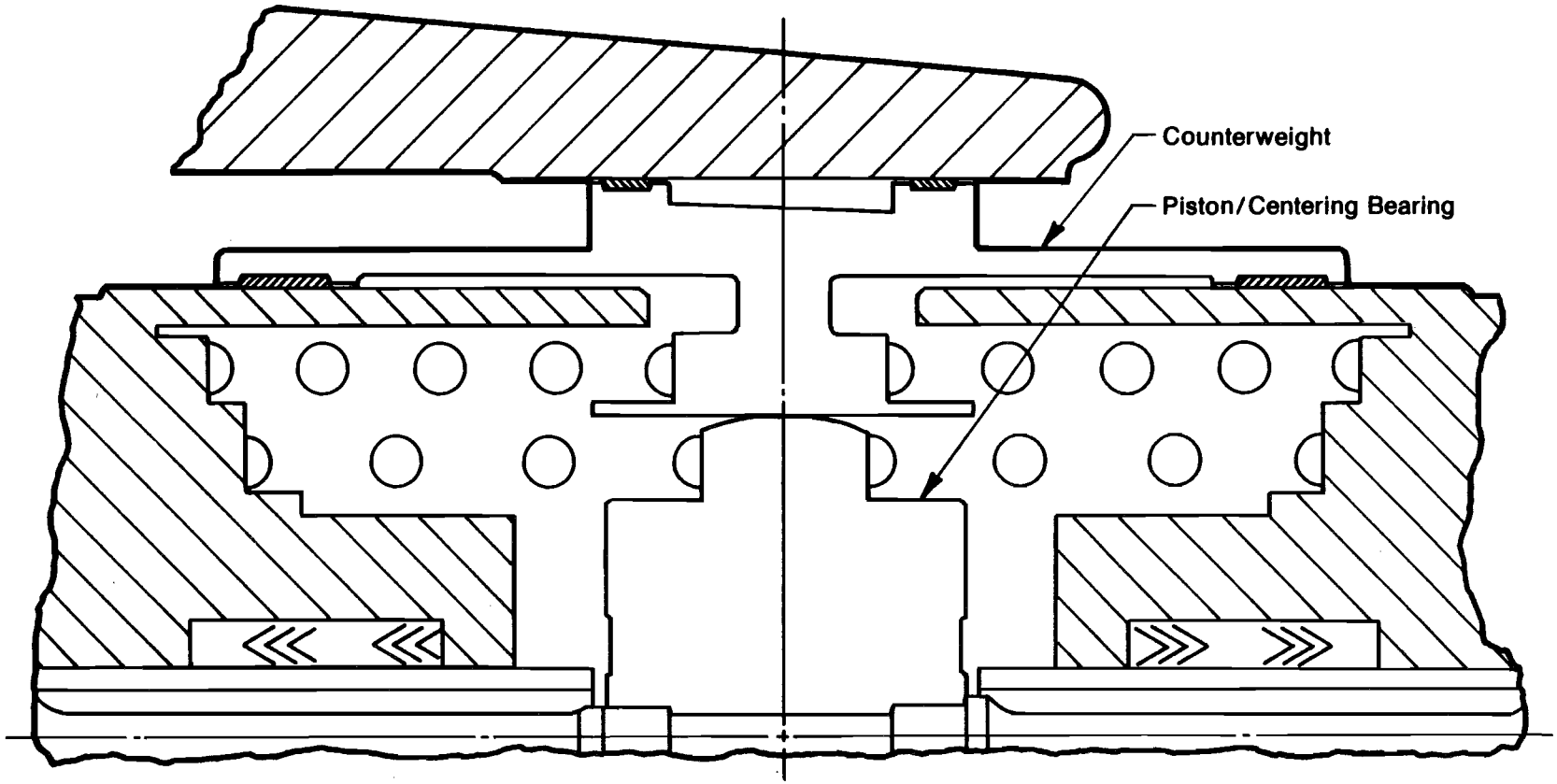

Figure 4-1b Existing Counterweight Version

85275

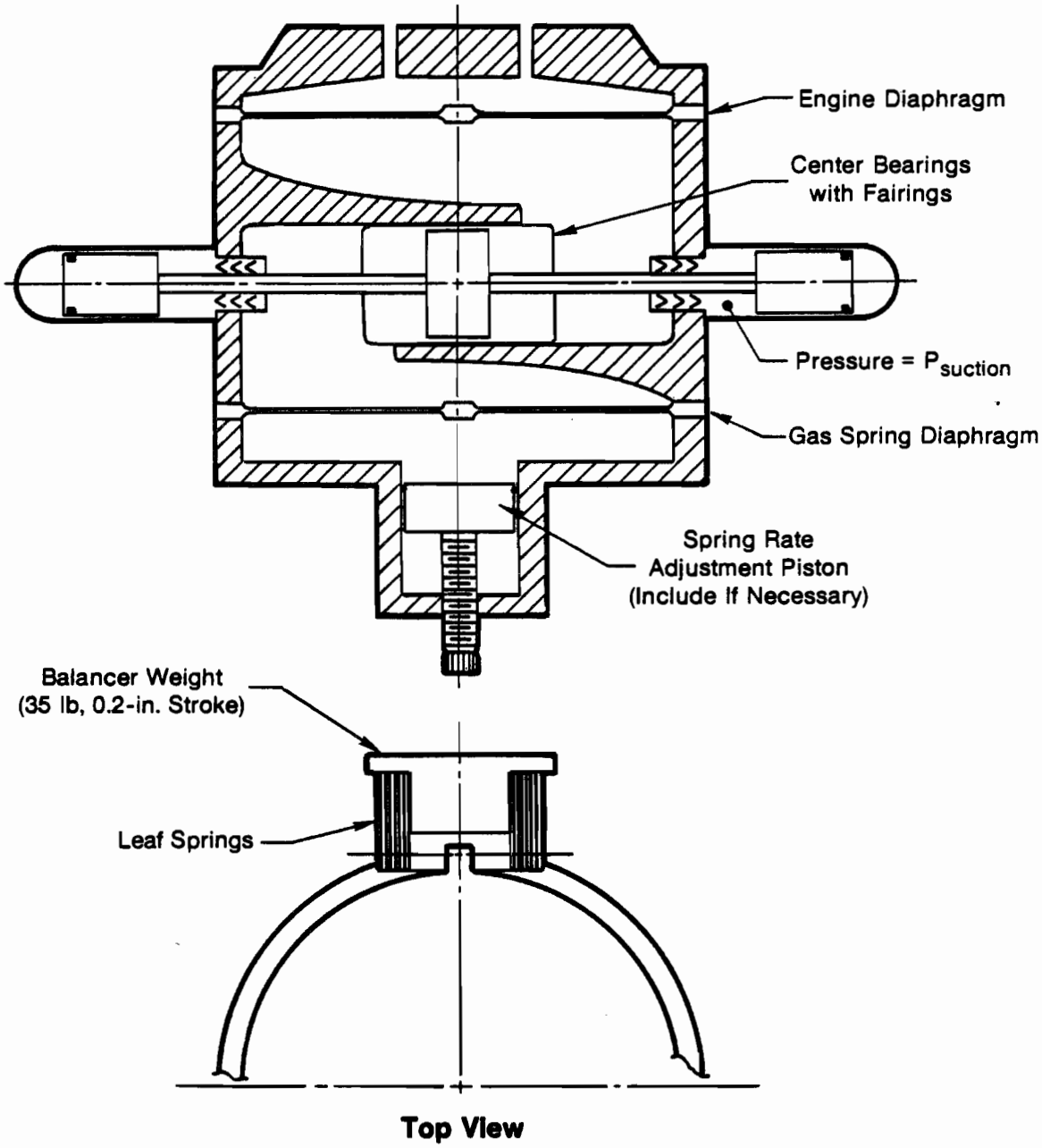

— Very Low Hydraulic Loss Is Possible.

— Improved Midstroke Porting Can Eliminate Need for Centering Springs.

— Two External Balancers Needed. Packaging of Balancers Somewhat Bulky. Shroud May Be Necessary to Reduce Noise.

Figure 4-2 Direct Acting with External Vibration Absorbers

85256

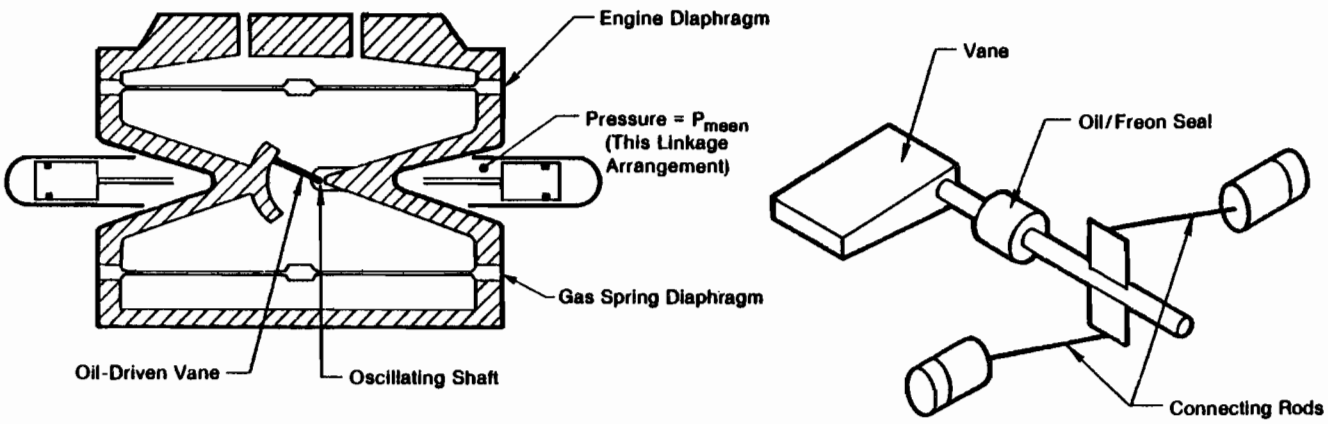

— Compressor Pistons Are Mounted Alongside Transmission. Small Motions of Components in Oil Leads to Very Low Transmission Loss.

— Shaking Moment Can Be Low. No Balancer Required.

— Drive Mechanism Requires Careful Design for Long Life. Oscillating Shaft Seal May Need Development.

— Alternative Linkage Arrangements and Center Drive Piston Instead of Vane May Prove Superior. Piston Backing Pressure Can Equal $P_{suction}$.

Figure 4-3 Linkage-Driven Oscillating Shaft

85257

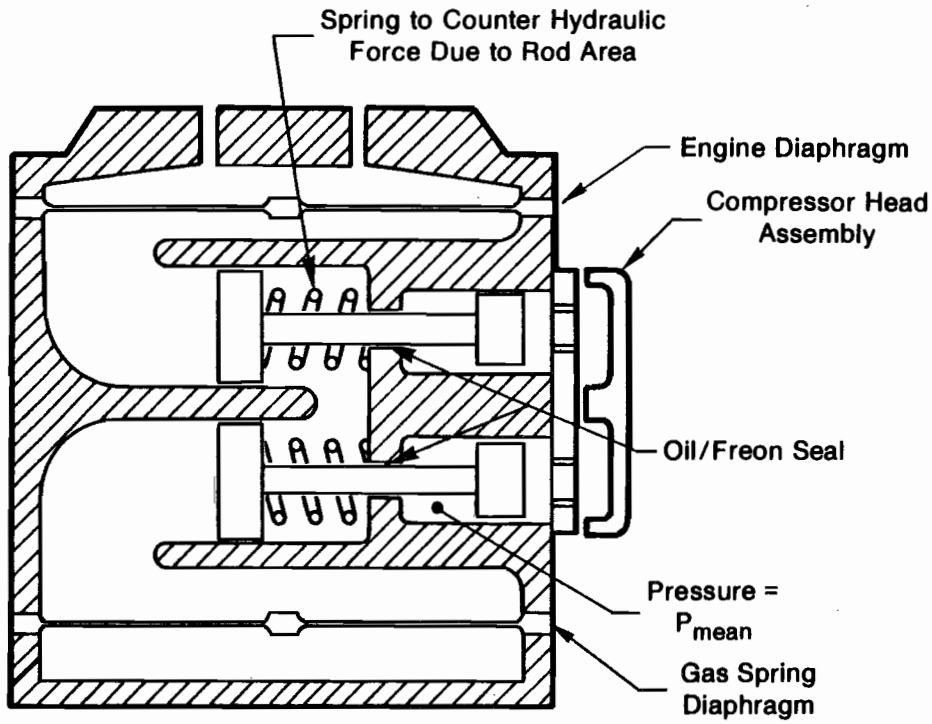

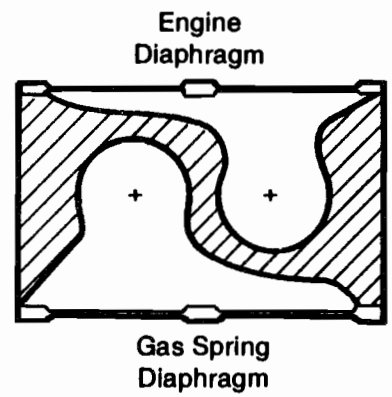

Side-by-Side Configuration (Preferred Arrangement)

— Use Side-by-Side Configuration. Shaking Moment Must Be Cancelled by External Balancer.

— Freon Centerports or Capillary Is Necessary to Maintain P_{mean} Freon Pressure at Back of Pistons. Midstroke Centering May Vary Slightly with Changing Freon Conditions.

— Low Hydraulic Loss Is Possible.

Figure 4-4 Hydraulically Driven Twin Pistons

85258

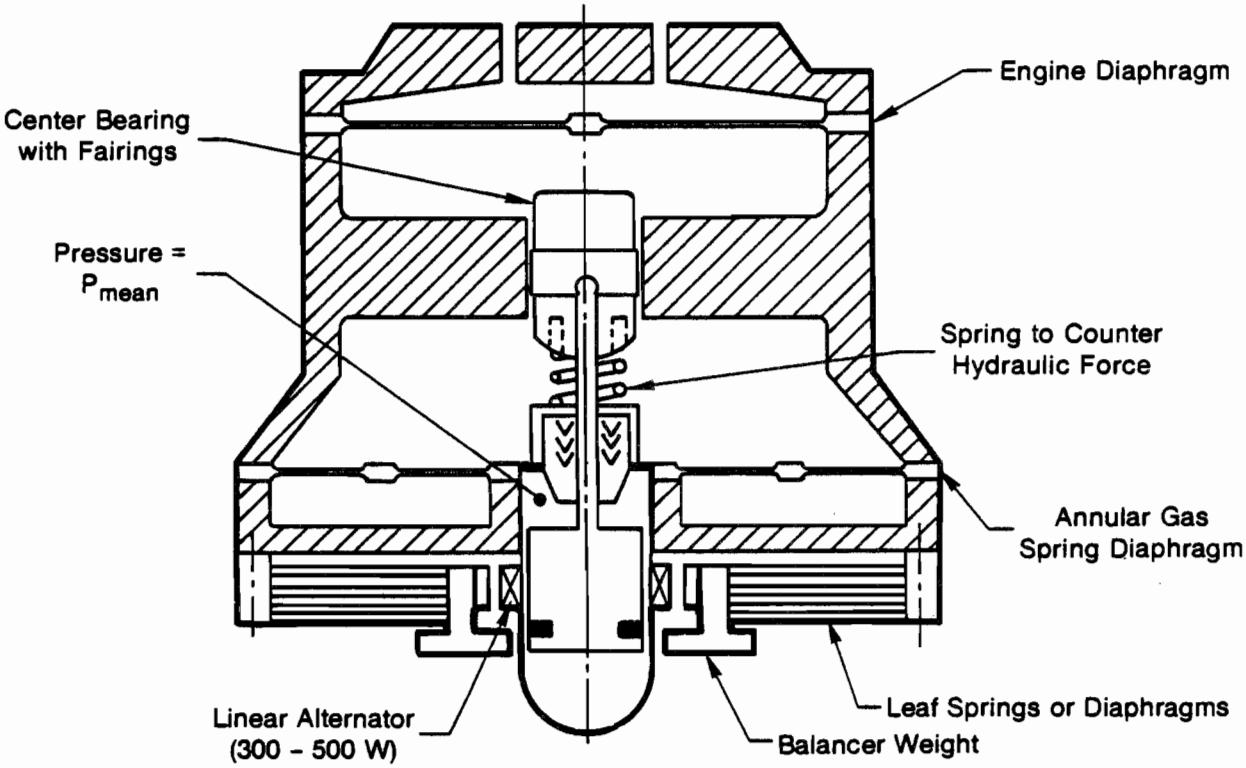

— Very Low Hydraulic Loss.

— Single Compressor Piston; Therefore, Clearance Volume and Midstroke Centering Are More Critical.

— Production Costs Lower with One Compressor Head.

Figure 4-5 Single Vertical Cylinder with External Absorber

85259

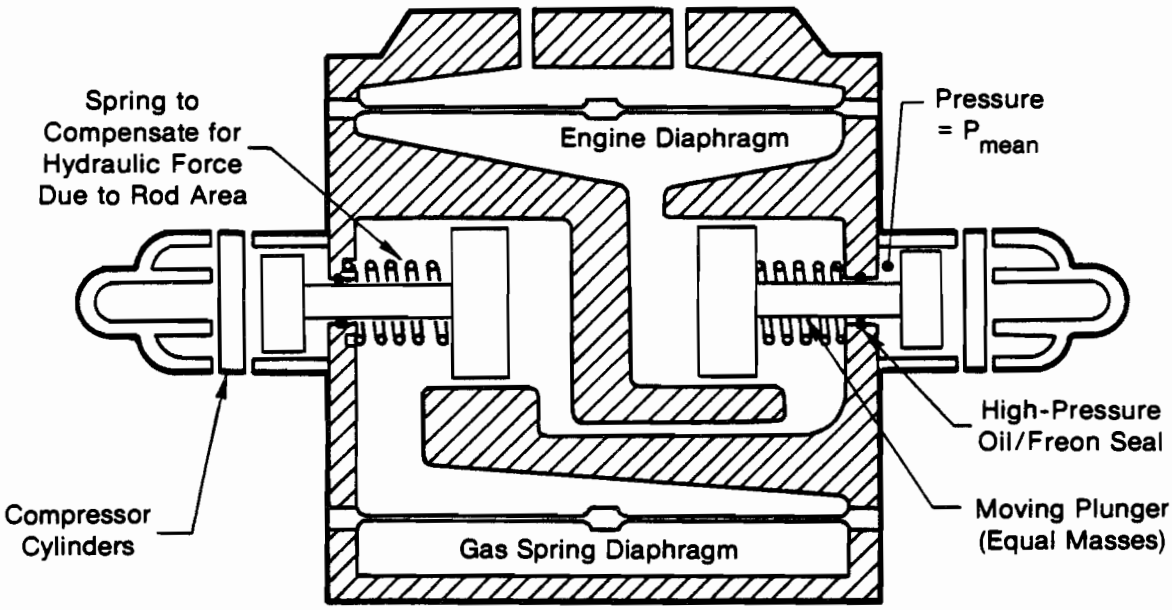

— Spread Between Faces of Compressor Pistons Increases by 5 or 6 in. Existing 14-in. Spread Becomes Approximately 20 in.

— High Viscous Loss Associated with Oil Flow to Drive Pistons.

— Complicated Transmission Case Design.

Figure 4-6 Opposed Pistons - Series Actuation

85273

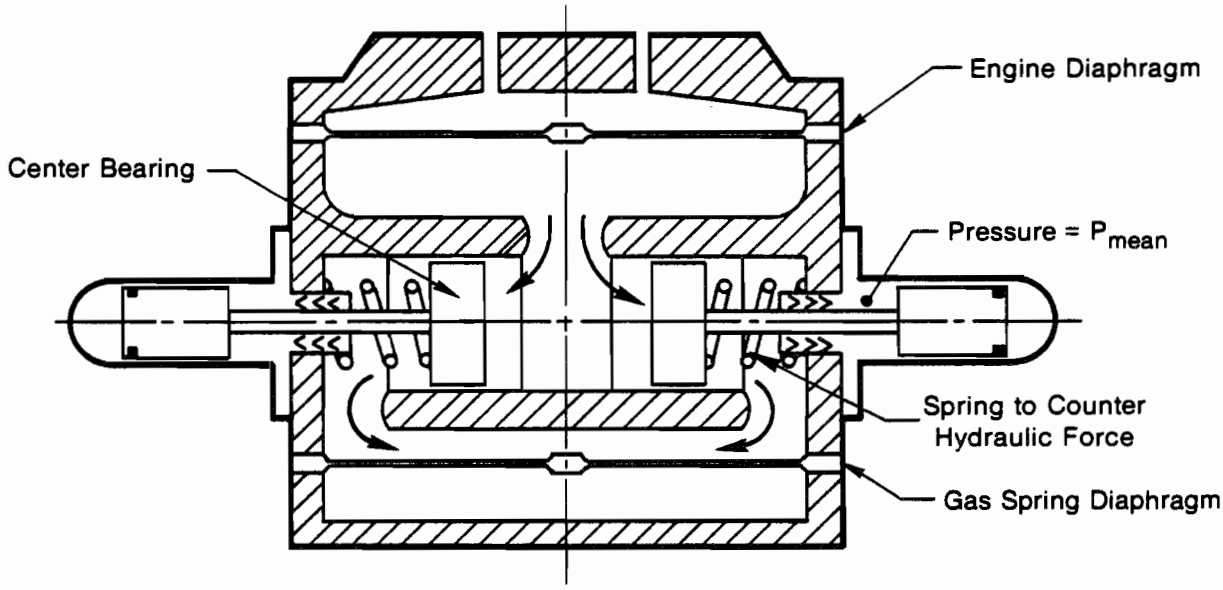

— Low Hydraulic Loss Is Possible.

— Inherent Horizontal Balance If Strokes are Equal. Equal Piston Strokes Difficult to Insure.

Figure 4-7 Opposed Pistons - Parallel Actuation

85272

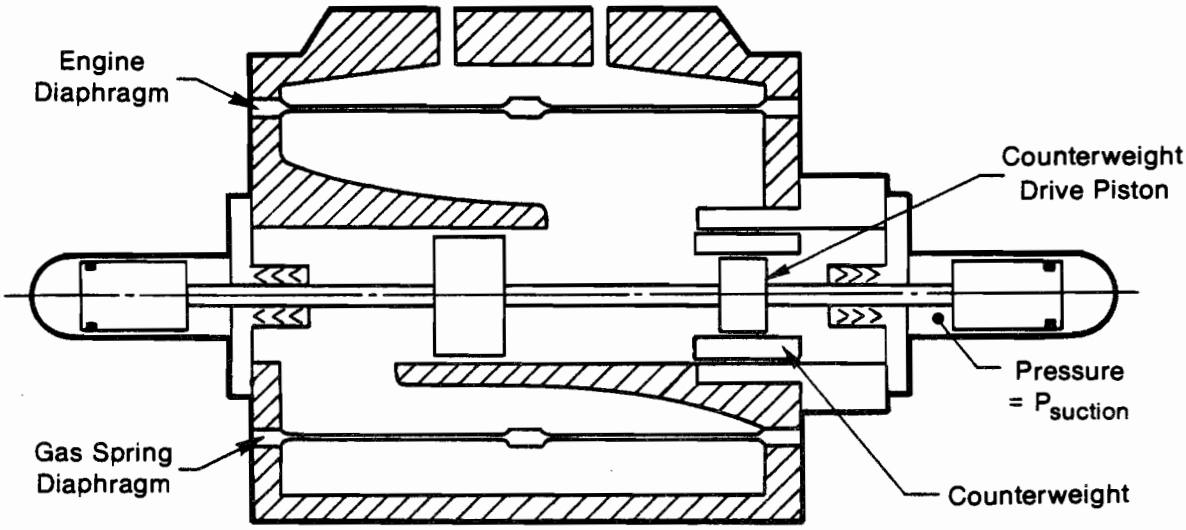

— Would Have Lower Viscous Loss Than Existing Counterweight Version.

— Centerporting Is Simplified. Use Centering Springs on Counterweight.

— Extra Length Between Pistons (~5 in.) Makes Packaging Difficult in Hermetic Shell.

— Modifications to Existing Hardware Can Be Made to Test Concept.

Figure 4-8 Direct Acting with Internal Parallel Counterweight

85261

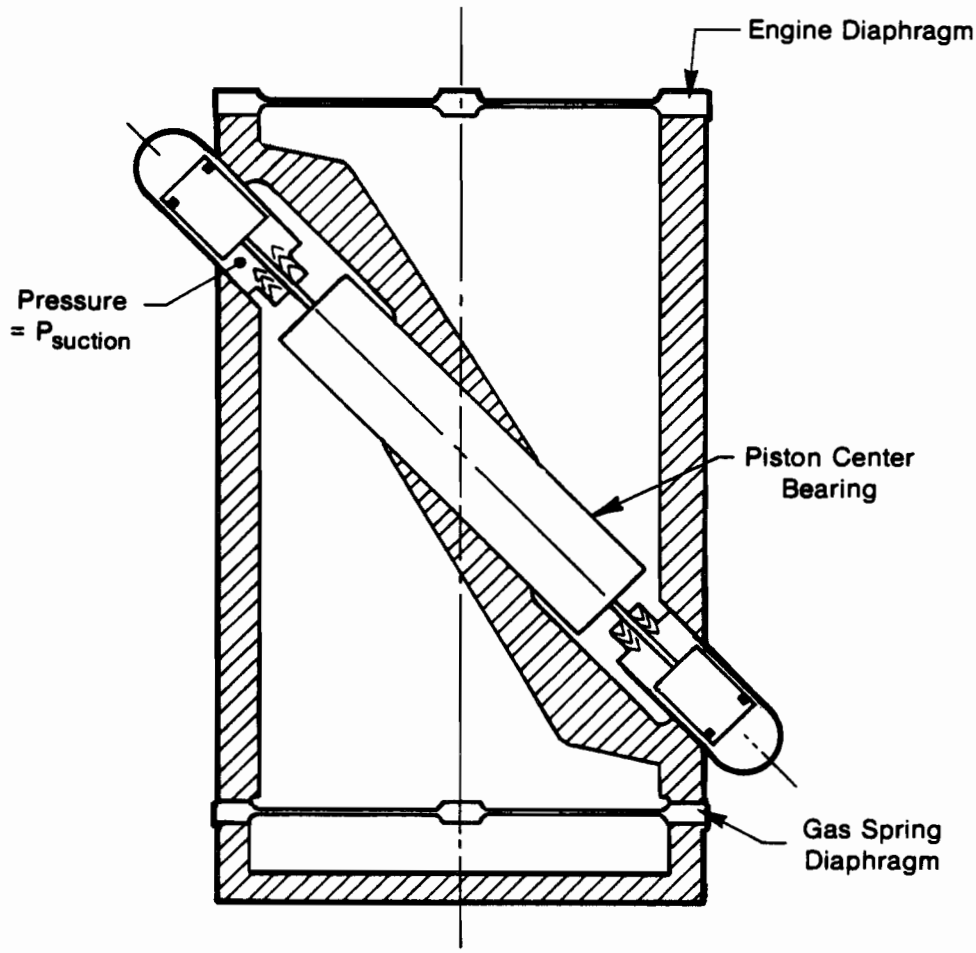

— Low Hydraulic Loss Is Possible

— Momentum of Displaced Oil Balances Momentum of Moving Piston. Horizontal and Vertical Balance Is Achieved by Proper Selection of Center Bearing Length, Angle of Motion, and Hydraulic Oil Having High Specific Gravity.

— Transmission Case Design and Packaging Are Very Awkward.

Figure 4-9 Direct Acting with Inherent Oil Balance

85279

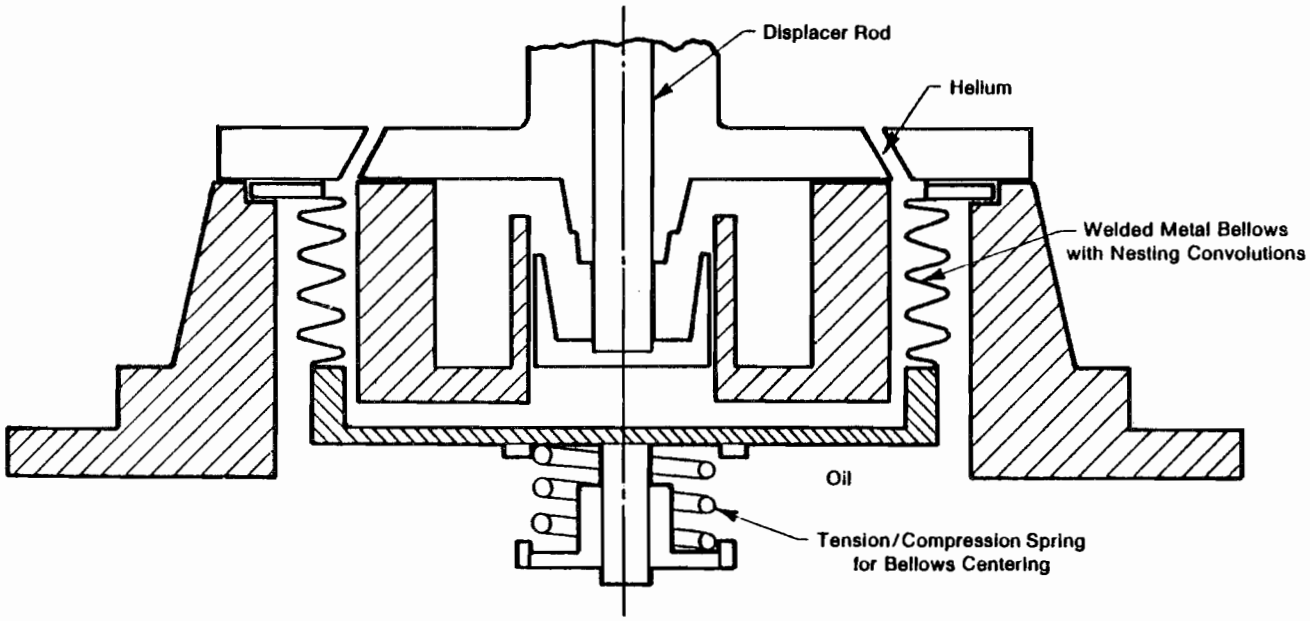

Figure 4-10a Metal Bellows Replacing Engine Diaphragm

85274

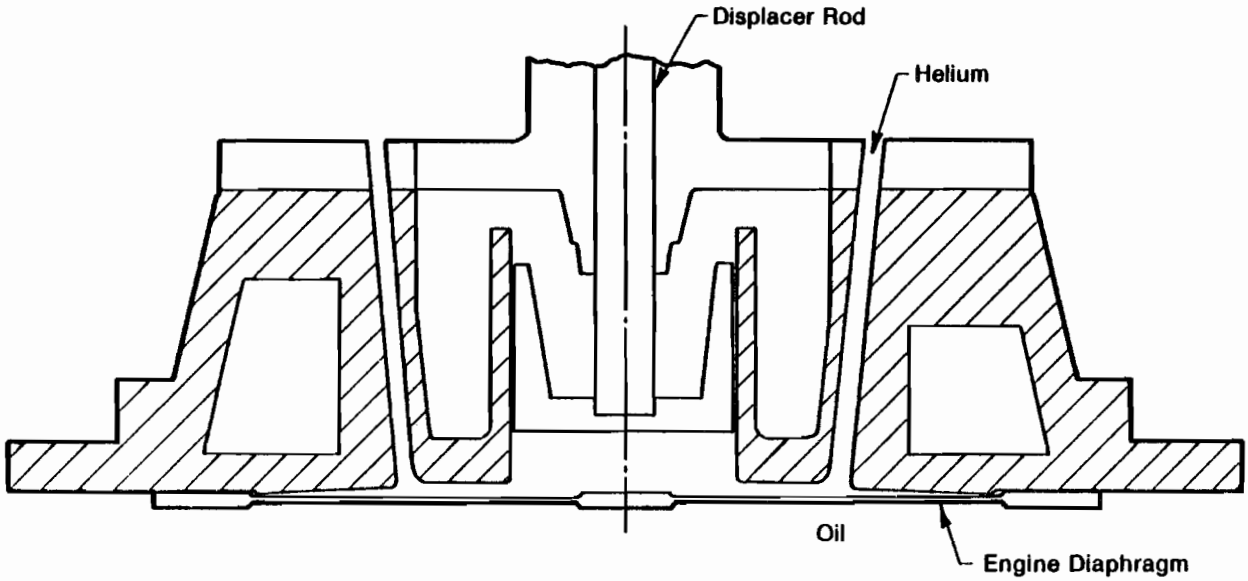

Figure 4-10b Existing Engine Diaphragm and Transition Plate

85278

Table 4-3

Advanced Concepts - HAHP Transmission/Compressor

Concept	No. of Seals	Pros	Cons	Development Required
1) Improved counterweight version with reduced hydraulic loss	(6)	Moderate efficiency potential. Excellent counterweight packaging with no external balancer required. $P_p = P_{suction}$.	Complicated power flow through various oil cavities; numerous seals. Separate compressor heads required. Improved oil centerports needed so springs can be removed.	Short-Mid term
2) Improved direct acting with external vibration absorber	(3)	Excellent efficiency. Simplified centerports; $P_p = P_{suction}$.	Absorber mounting can be bulky. Separate compressor heads required.	Short term
3) Linkage driven twin pistons; oscillating shaft and face seal.	(2)	Excellent efficiency, good packaging, dual compressor heads possible. No balancer required; $P_p = P_{suction}$.	Linkage required to drive compressor pistons. Face seal may require development.	Mid-long term
4) Twin pistons, hydraulically driven with external absorber.	(4)	Good efficiency. Low absorber mass/good packaging. Dual compressor head assembly.	$P_p = P_{mean}$; use Freon centerports or capillary tube; analysis becomes difficult.	Long term
5) Single vertical cylinder with concentric external absorber.	(2)	Excellent efficiency. Only one compressor head. Potentially lighter transmission case, but greater assembly height.	$P_p = P_{mean}$. Annualar gas spring diaphragm required for good packaging. Compressor clearance volume and midstroke centering more critical.	Long term
6) Opposed pistons - series actuation.	(4)	Inherent horizontal balance but potentially high hydraulic loss.	$P_p = P_{mean}$; separate compressor heads. Complicated transmission case design. Potentially low efficiency.	Long term
7) Opposed pistons - parallel actuation.	(4)	Inherent horizontal balance if strokes are equal. Very good efficiency.	$P_p = P_{mean}$; separate compressor heads. Equal piston strokes hard to achieve.	Mid-long term
8) Direct acting with oil-driven counterweight	(5)	Better efficiency than concentric counterweight. No external balancer. Possible to modify existing hardware. $P_p = P_{suction}$.	Separate compressor heads. Extra length needed between compressor pistons. More hydraulic loss than with external balancer.	Short-mid term
9) Direct acting with inherent hydraulic balance.	(3)	Very good efficiency. No mechanical balancer required. $P_p = P_{suction}$.	Separate compressor heads. Packaging is very difficult. Large volume of oil required.	Long term
10) Bellows coupling to oil instead of diaphragm; apply to all the above configurations.	N/A	Higher volume amplitude is possible with smaller diameter coupling. Reduced size and weight of compressor. Somewhat less expensive than contoured diaphragm.	Excess surface area in convolutions may decrease efficiency. More difficult to mount than a diaphragm. Bellows development required.	Mid term

of features. Concepts No. 6 and 7 are not considered to be attractive because of the complex flow paths. Concept No. 9 is interesting from a theoretical point of view; however, its construction would be very difficult.

One of the major concerns associated with concepts No. 4 through 7 is that the mean piston backing pressure, P_p, would have to be controlled via refrigerant centerports or with capillary tubes in order to provide pressure equalization with the refrigerant compression space. Otherwise, a large change in refrigerant pressure force across the piston would occur between the operational and the shutdown conditions, leading to a shift in the piston midstroke position which would limit compressor capacity. When opposed pistons are linked together on a common drive rod or through a linkage, P_p can equal the suction pressure, P_s, and refrigerant centerporting is obviated.

Another requirement in concepts No. 4 through 7 is the use of a compression spring on each piston to oppose the force generated by hydraulic pressure times rod area. The spring should not present significant design difficulties because the piston drive rod diameter can be kept small to minimize the force.

The following sections highlight the prime concepts considered. All of these concepts incorporate contoured diaphragms similar to the diaphragms used on the HAHP breadboard system. However, transmission size and weight could be reduced in all cases by substituting welded metal bellows which produce large volume displacement with reduced diameter. This concept is illustrated in Figure 4-10a while Figure 4-10b shows the existing engine diaphragm. At the time of this study, however, there remains a significant uncertainty regarding the substitution of bellows for the diaphgrams. Therefore, bellows were considered to be a part of an eventual value engineering and manufacturing development effort which would be pursued at a later time, after prototype performance feasibility has been fully demonstrated.

4.1 Concept Selection

Of the nine diaphragm-coupled compressor configurations identified, four were selected for final evaluation. The four were chosen on the basis of being the best representative configuration from each of the arrangement types considered, i.e., single-shaft, two-piston (concepts No. 1, 2, 8, and 9), kinematic linkage (concept

No. 3), dual-shaft, (concepts No. 4, 6, and 7) and single-piston (concept No. 5). The four concepts selected are existing internal counterweight with reduced hydraulic losses (concept No. 1); direct acting with external balance (concept No. 2); oscillating shaft, twin piston (concept No. 3 with arrangement improved over Figure 4-3); and, hydraulically-driven, twin piston with external torque balance (concept No. 4).

The four concepts were rated from best to worst in four categories: efficiency, package attractiveness, development risk, and reliability. Layout drawings were made for each of the four concepts, which are shown in Figures 4-11 through 4-14. The ranking of each concept was done on a qualitative rather than quantitative basis. To achieve some degree of objectivity, the ranking was determined by a concensus of the engineers working on this task. The results of that ranking are given in Table 4-4. The ranking was performed in a fashion such that the concept with the numerically lowest total score is considered to be the most attractive. As indicated in Table 4-4, concept No. 2, the direct acting with external vibration absorber, and concept No. 3, the oscillating shaft twin piston, were ranked as the most attractive. The oscillating shaft concept appears to have slightly better efficiency potential and packaging neatness than the direct acting concept. However, the latter has a significantly lower development risk and slightly higher reliability potential. Near term development success is much more certain with concept No. 2 than with concept No. 3, therefore, concept No. 2 is the recommended approach for future development.

It should be pointed out that concept No. 2 (minus the external balancer) has already been tested at MTI's laboratory during March through June 1984, and moderately attractive transmission efficiencies were measured (over 70%). It is estimated, with minor modifications, the transmission efficiency can be improved to 80% in the near term and to over 90% in the longer term. The near-term modifications envisioned include:

1. Changing the drive piston clearance to a compliant seal of the type that has been successfully tested on the internal counterweight.

2. Providing fairings to the drive piston to smooth the hydraulic flow path and reduce viscous loss.

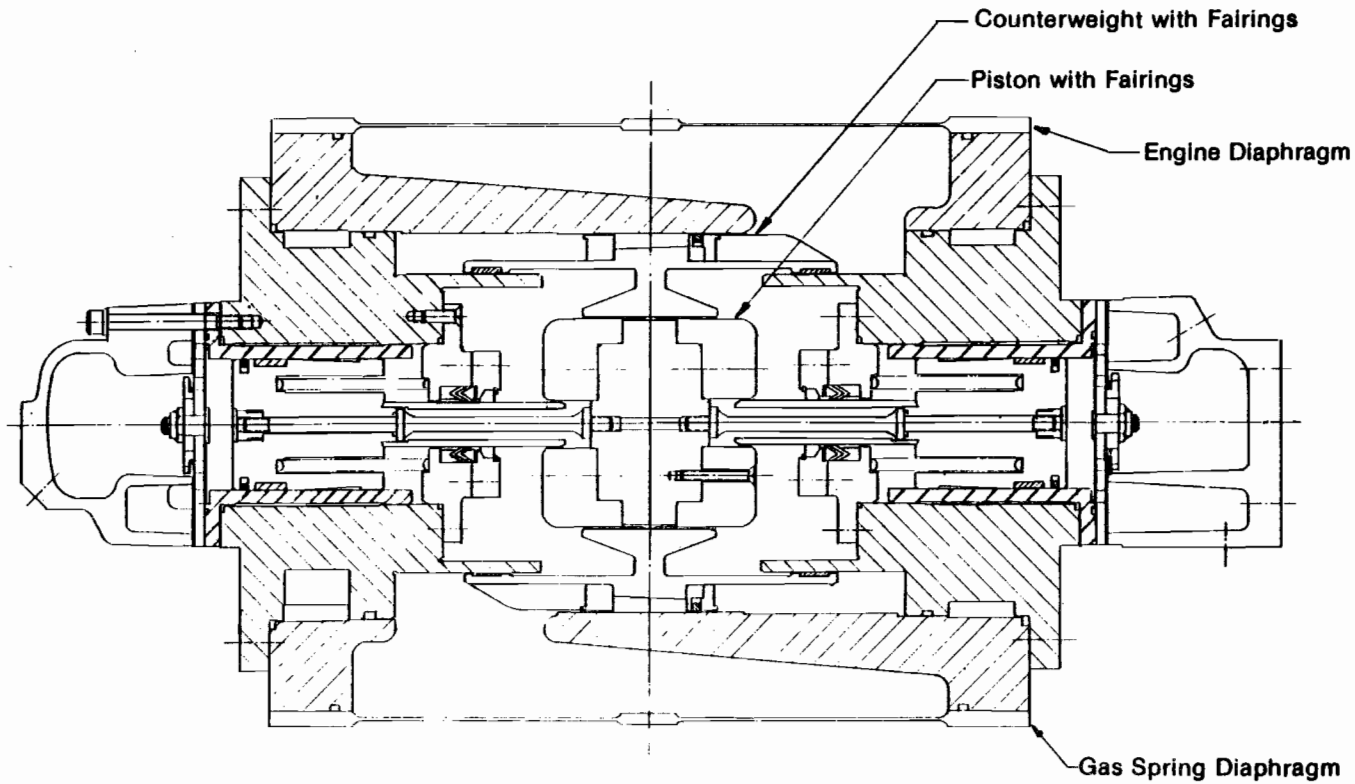

Figure 4-11 Improved Counterweight Version

861173

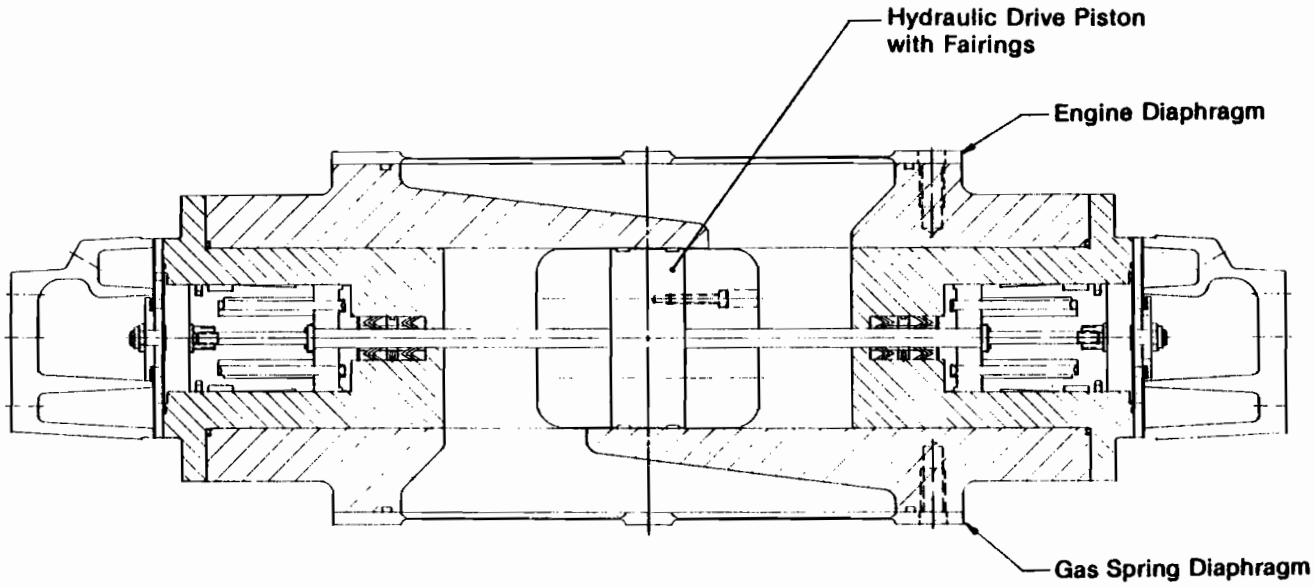

Side View

Figure 4-12a Direct Acting with External Vibration Absorbers

861174

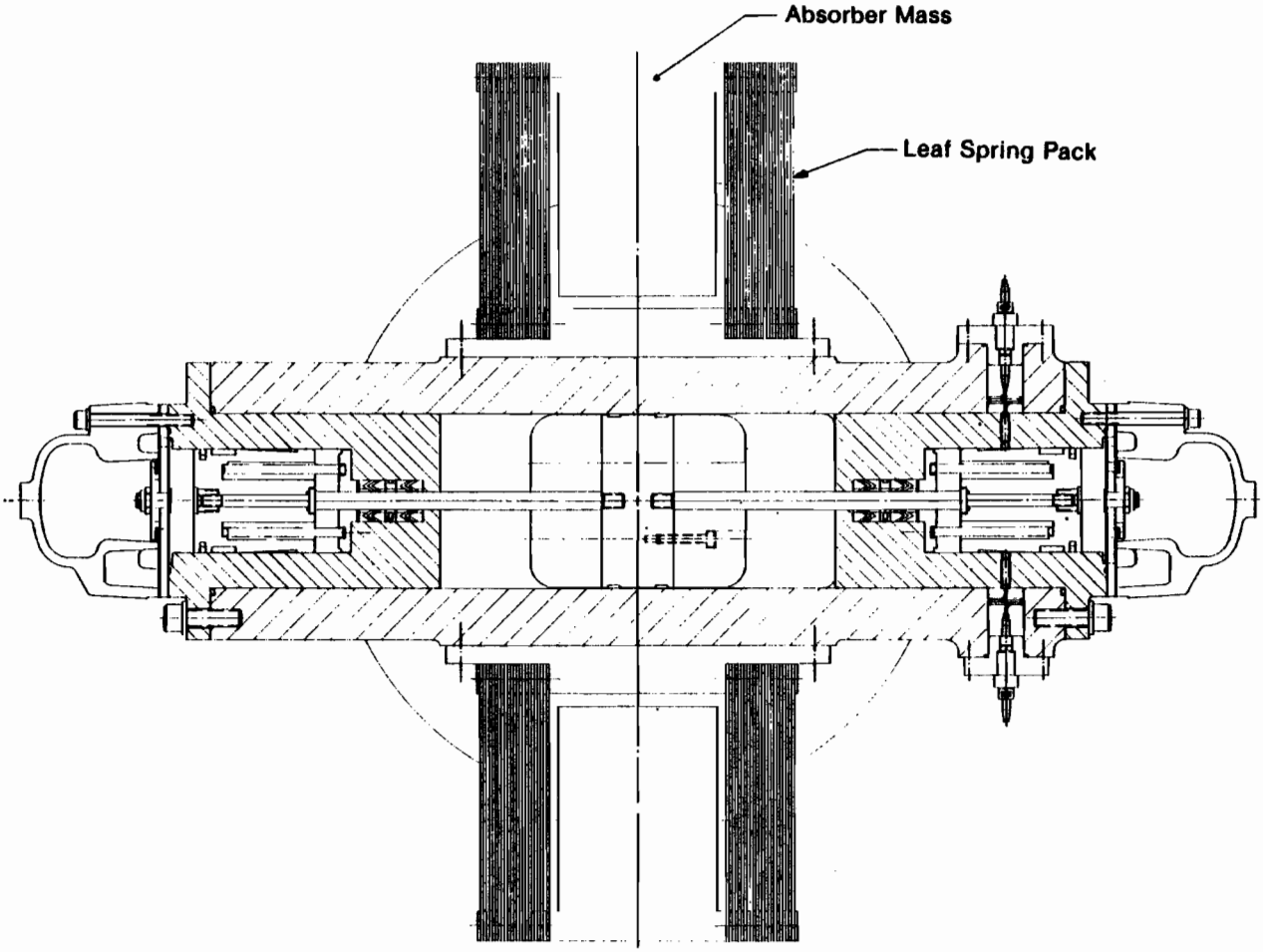

Figure 4-12b Top View

861175

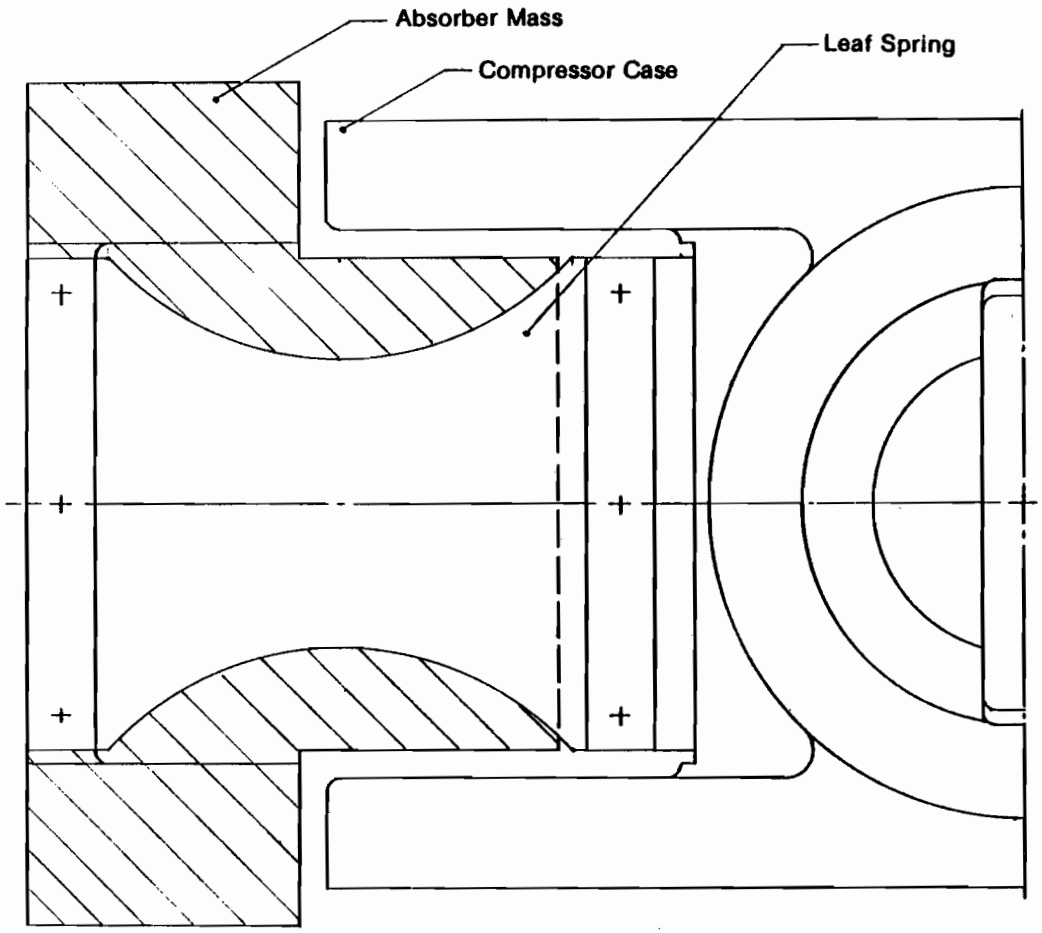

Figure 4-12c End View - Left Side Absorber

861176

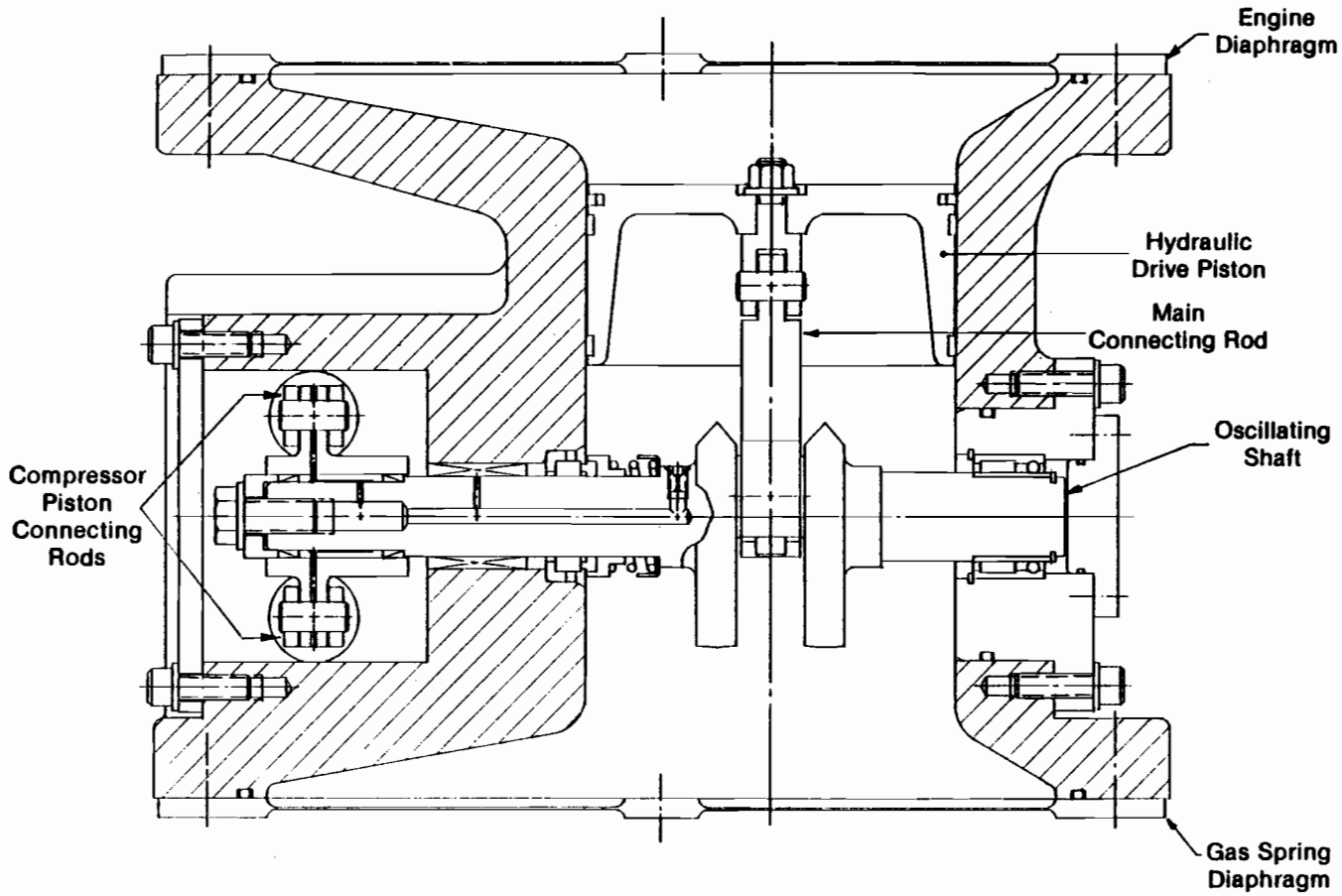

Rear View - Section Through Hydraulic Bore

Figure 4-13a Linkage Driven Twin Pistons; Oscillating Shaft

861177

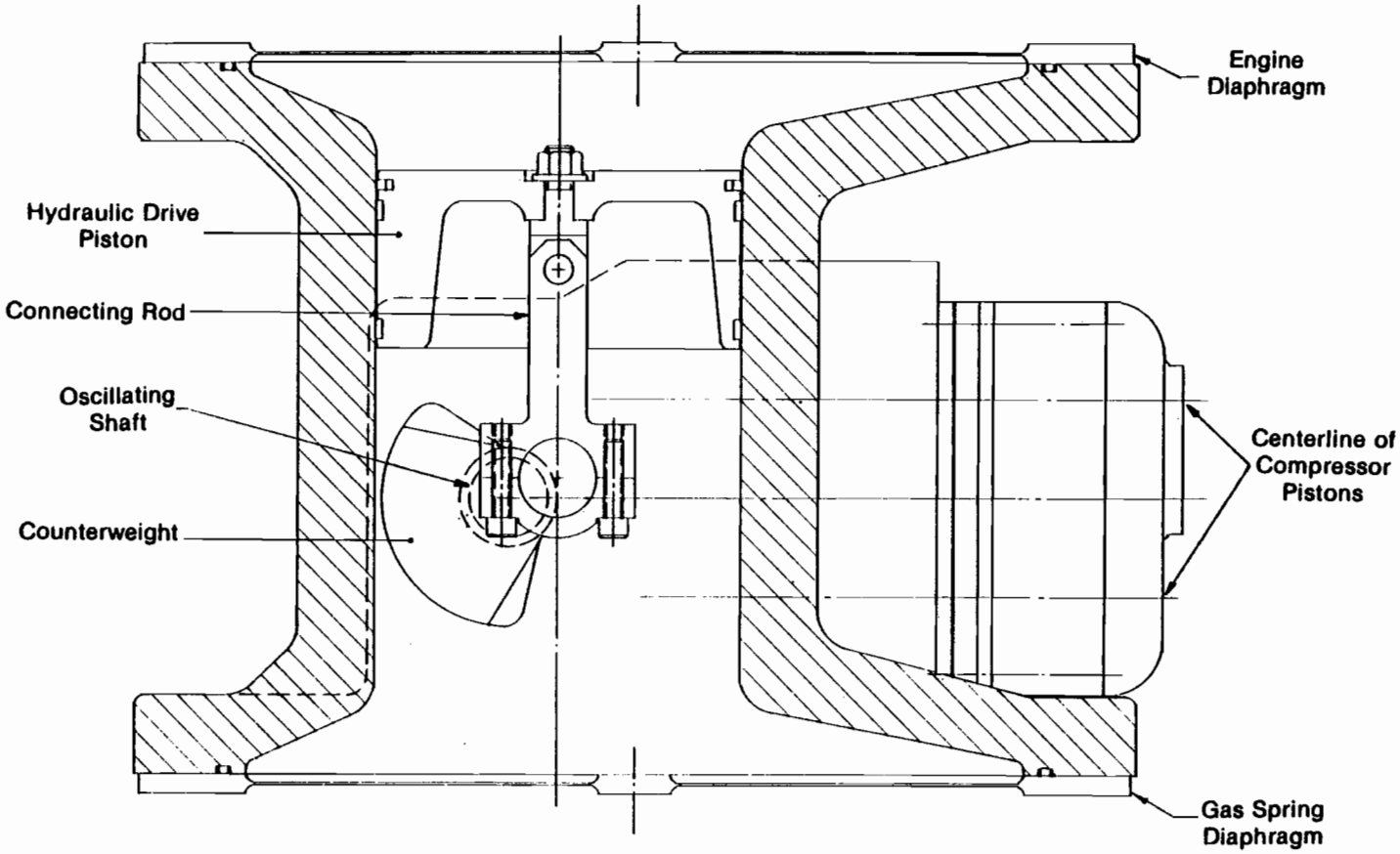

Figure 4-13b Side View - Section Through Hydraulic Bore

861178

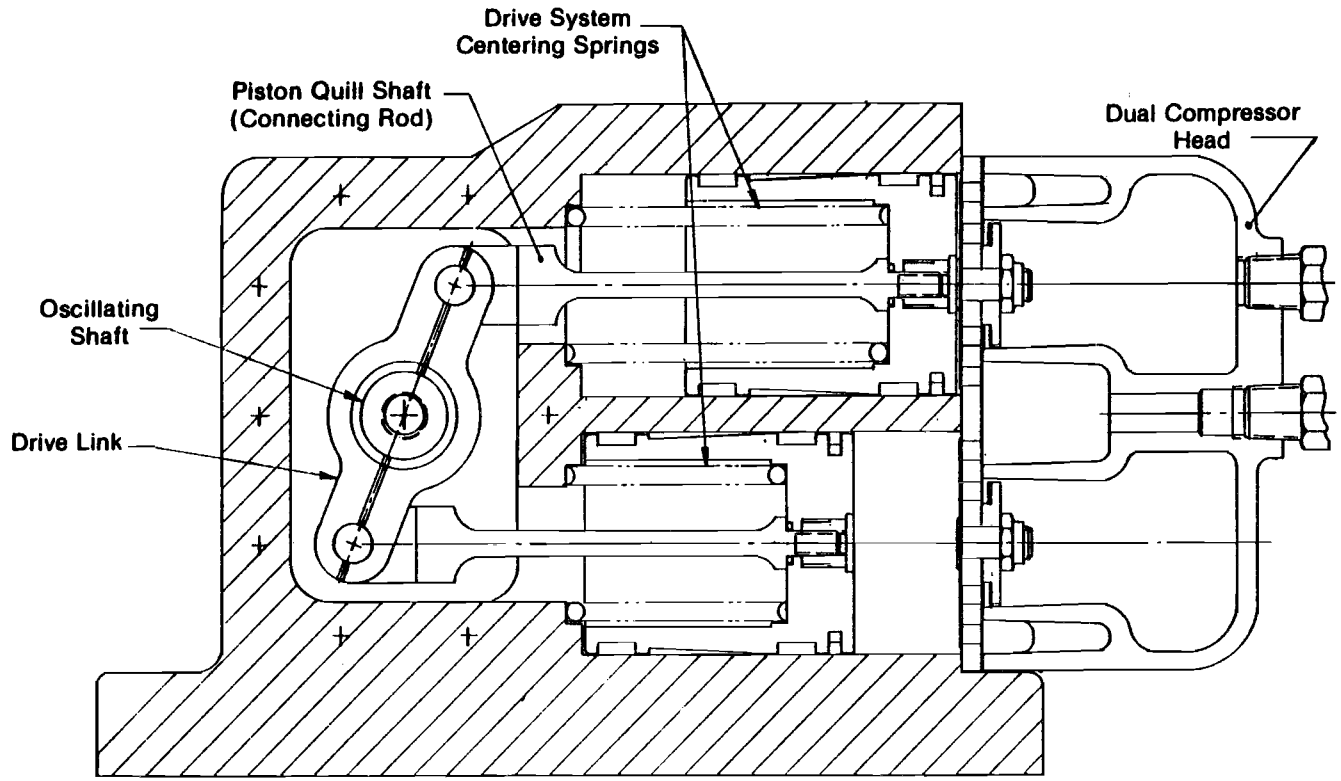

Figure 4-13c Section Through Compressor Pistons

861179

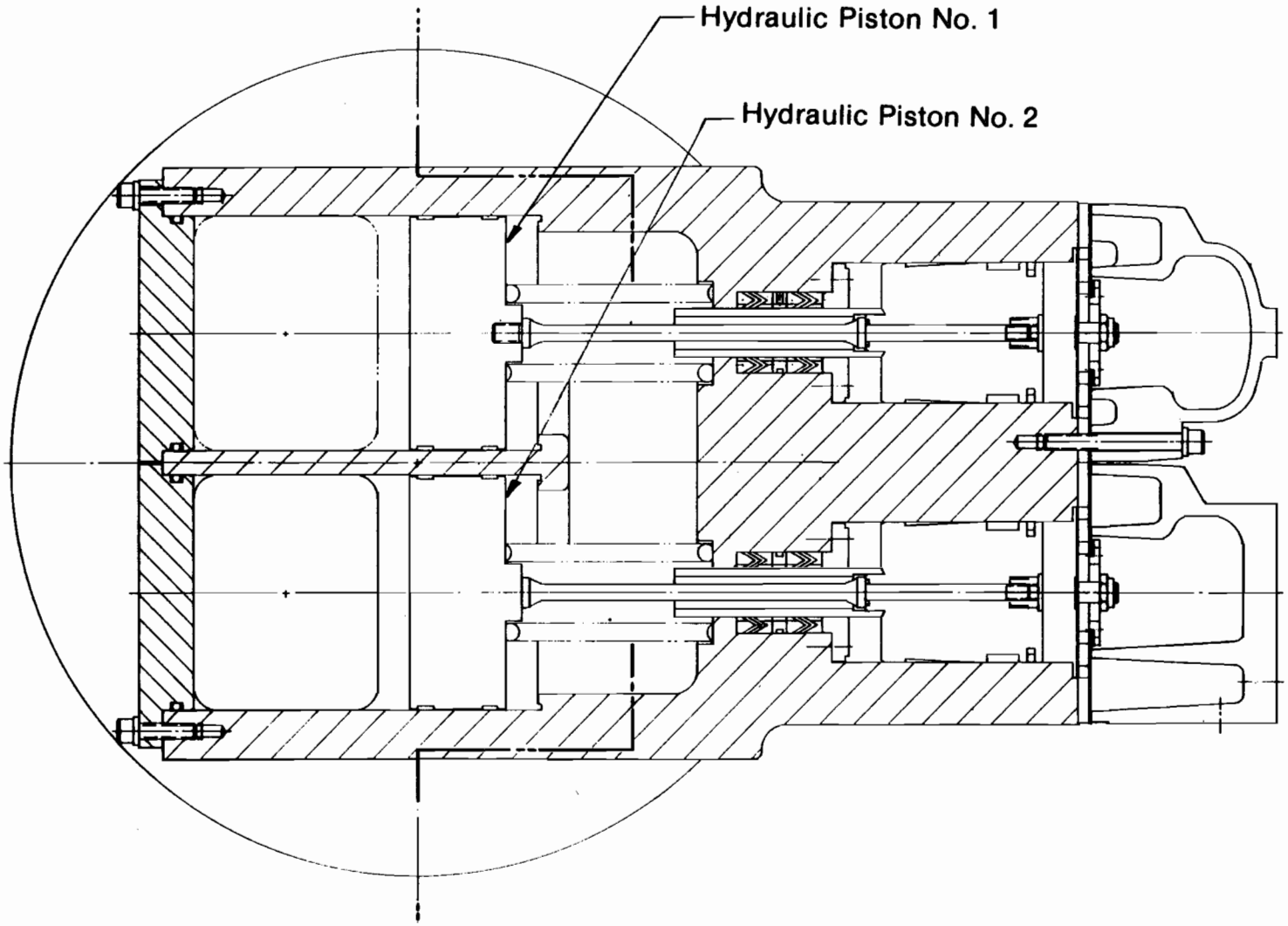

Top View

861180

Figure 4-14 Hydraulically Driven Twin Piston - Series Actuation

Table 4-4

Concept Ratings - HAHP Transmission/Compressor

Concept	Efficiency	Package Attractiveness	Development Risk	Reliability	Total Rating
1) Counterweight version with reduced hydraulic loss.	Lowest -4	Highest -1	Medium -2	Medium -3	-10
2) Direct acting version with external balancer.	High -2	Lowest -4	Lowest -1	Highest -1	-8
3) Oscillating shaft, twin piston compressor.	Highest -1	High -2	High -3	High -2	-8
4) Hydraulically driven, twin pistons, with external torque balancer.	Medium -3	Medium -3	Highest -4	Lowest -4	-14

3. Providing more open flow passages and rounding some of the sharp corners of the compressor housing so as to further reduce viscous loss.

The external balancer will be tuned for constant frequency operation and is expected to contribute an insignificant amount of additional loss to the transmission. Similar vibration absorbers have been built in the past by MTI for resonant piston machinery with good success and at Sunpower, Inc., specifically for balancing FPSEs.

Overall, it is anticipated that the externally balanced, direct-drive compressor can be developed to accomplish its design performance of 3-ton capacity at the 95°F day, with >75% transmission efficiency within a six- to eight-month period. It is recommended that this concept be funded for continued development of the FPSE diaphragm-coupled, heat-pump compressor so engineering prototype feasibility can be established as soon as possible.

APPENDIX A

HAHP BREADBOARD HEAT PUMP INSTRUMENTATION

The HAHP breadboard heat pump is instrumented to provide 17 time-dependent measurements that yield amplitude, phase, dc offset, and an optional Fourier harmonic analysis. In addition to time-dependent measurements, the system is instrumented to include 11 steady-state measurements and 52 channels of thermocouples. These measurements and probe types are defined in Tables A-1 and A-2 for time-dependent and steady-state measurements, respectively. The location of each of the probes is shown in Figure A-1.

For the Phase IB lower end loss measurements, the counterweight loss, piston loss, gas spring loss, and total lower end loss (hydraulic transmission and compressor) were calculated from the oil pressure measurements made in Volumes A, B, C, and D, as shown in Figure A-2, the refrigerant pressure measurement made in each of the compression volumes, the pressure measurement in the gas spring cavity, and the displacement measurements of the counterweight and compressor piston. The nomenclature used to record these measurements in the DAS is given in Table A-3. The power computation made in each volume was performed using the appropriate pressure and displacement measurements and the harmonic power relationship for sinisoidal functions:

$$\text{Power} = \pi\ f\ A_p\ X_o\ P_o\ \sin\Theta_p$$

where: f = Frequency

A_p = The frontal area of the moving element over which the pressure is acting

X_o = The fundamental amplitude of motion of the moving element

P_o = The fundamental amplitude of the pressure

Θ_p = The phase angle between the pressure and displacement phasors.

The nomenclature used to define the lower end losses, and the calculations performed to obtain the various losses

- Counterweight loss
- Compressor piston loss
- Hydraulic fluid loss
- Gas spring loss
- Total transmission loss
- Total lower end loss.

Table A-1

HAHP System Measurement Points

Time-Dependent Measurements*:

	Parameter	Probe Type
1.	Displacer Stroke	Eddy Current
2.	Counterweight Stroke	Eddy Current
3.	Piston Stroke	Eddy Current
4.	Compression-Space Pressure - Displacer Side	Strain Gage and Bridge
5.	Compression-Space Pressure - Diaphragm Gas Side	Strain Gage and Bridge
6.	Heater-Side Displacer Gas Spring Cavity Pressure	Strain Gage and Bridge
7.	Upper Virtual Rod Cavity Pressure	Strain Gage and Bridge
8.	Load Side Displacer Gas Spring Cavity Pressure	Strain Gage and Bridge
9.	Upper Oil Cavity Pressure	Piezoresistive
10.	Lower Oil Cavity Pressure	Piezoresistive
11.	Compressor LH Valve Plate Pressure	Strain Gage and Bridge
12.	Compressor RH Valve Plate Pressure	Strain Gage and Bridge
13.	Piston Gas Spring Pressure	Piezoresistive
14.	Upper Diaphragm Position	Eddy Current
15.	Lower Diaphragm Position	Eddy Current
16.	Inner LH Oil Cavity Pressure	Piezoresistive
17.	Inner RH Oil Cavity Pressure	Piezoresistive

Table A-2

HAHP System Measurement Points

Steady-State Measurements:

	Parameter	Probe Type
1.	Combustion Airflow	Laminar-Flow Element
2.	Fuel Flow	ΔP Transducer, ABS, Pressure Temperature
3.	Temperatures - Air, Gas, and Liquid other than noted below (52 channels)	Type-K Thermocouples
4.	Engine Cooling Water Flow	Bearingless Turbine
5.	Engine Coolant Temperature Difference	RTD
6.	Refrigerant Flow	Coriolis-Force, Mass Flow meter
7.	Compressor Suction Pressure	Piezoresistive
8.	Compressor Suction Temperature	Thermistor
9.	Compressor Discharge Pressure	Piezoresistive
10.	Compressor Discharge Temperature	Thermistor
11.	Piston Gas Spring Bellows Position	LVDT
12.	Engine Mean Pressure	Piezoresistive

*Amplitude, Phase, DC Offset, Optional Fourier Analysis

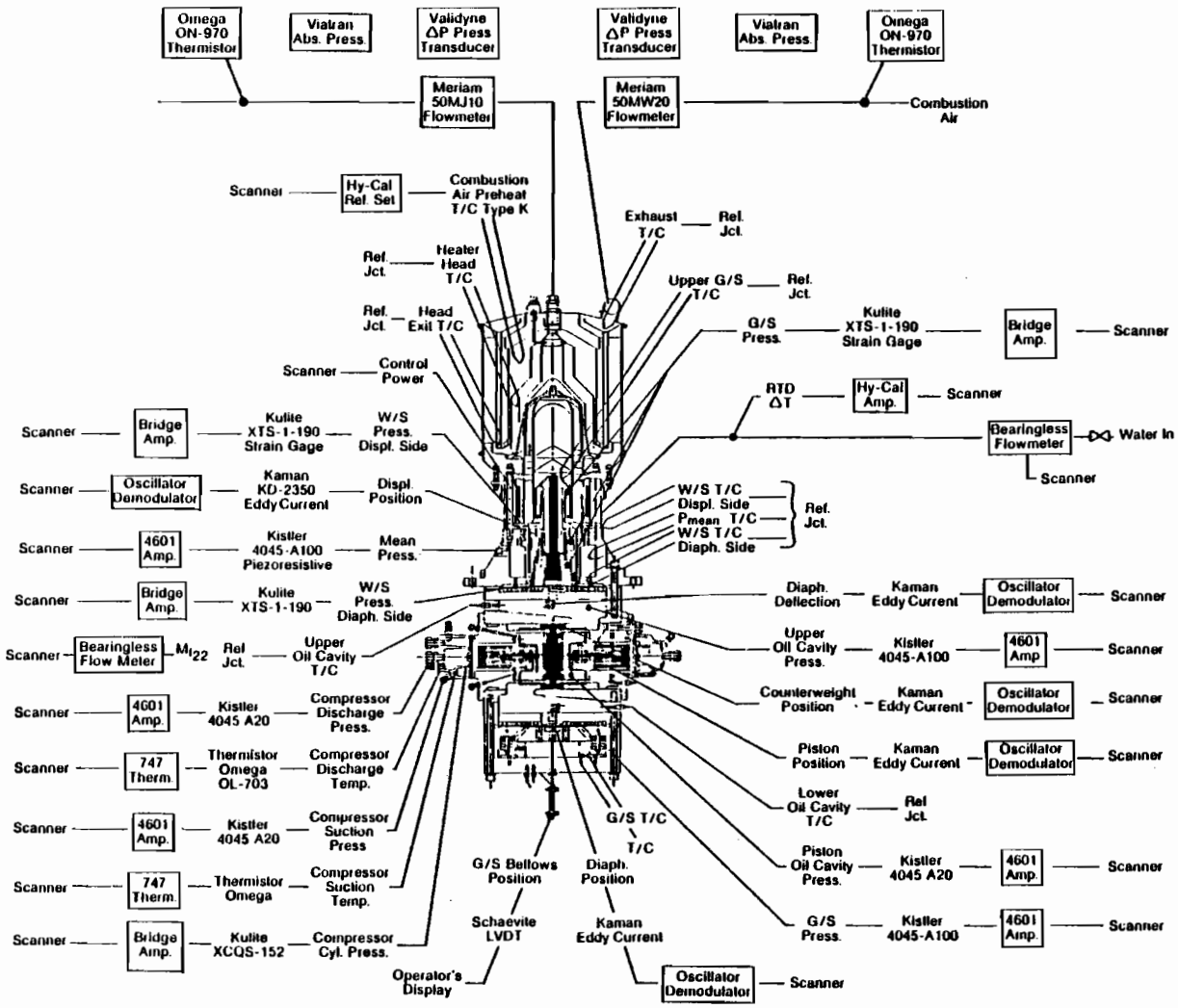

Figure A-1 HAHP Instrumentation Schematic

83470-1

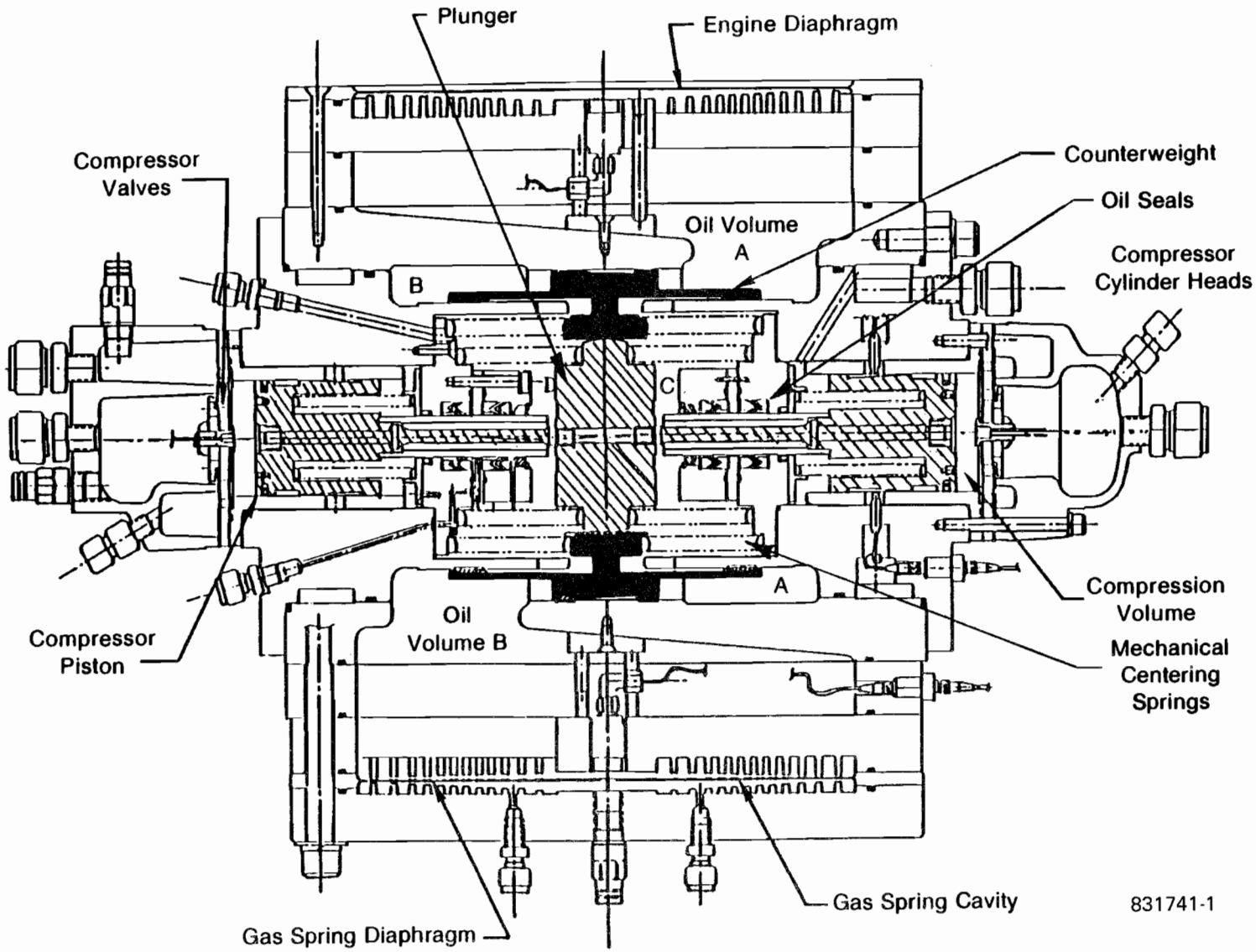

Figure A-2 Heat Pump Compressor and Hydraulic Transmission Layout

Table A-3

Hydraulic Transmission and Compressor Measurement Probes

Probe	Definition	Type
PUCS	Pressure upper compression space. This is the engine compression space pressure.	Strain Gage
PUOC	Pressure upper oil cavity. This is the oil pressure in Volume A	Piezoresistive
PLOC	Pressure lower oil cavity. This is the oil pressure in Volume B.	Piezoresistive
POPRH	Right hand oil pressure. This is the pressure in Volume C.	Piezoresistive
POPLH	Left hand oil pressure. This is the pressure in Volume D.	Piezoresistive
PPGS	Gas spring cavity pressure.	Piezoresistive
PRHVP	Right hand valve plate pressure. This measures the refrigerant pressure in the right hand compression volume.	Strain gage
PLHVP	Left hand valve plate pressure. This measures the refrigerant pressure in the left hand compression volume.	Strain gage
XCW	Counterweight displacement.	Eddy current
Xp	Compressor piston displacement.	Eddy current

are all given in Table A-4. These terms and their sign conventions are further described in Figure A-3. For the "direct acting" system shown in Figure A-4, the problem is simplified by the elimination of the two inner oil volumes C and D. An example of the results obtained at the end of Phase 1B, with and without the counterweight, are given in Table A-5.

Two efficiencies were also used to describe the performance of the lower end; these were:

- Hydraulic transmission efficiency
- Lower end efficiency.

The hydraulic transmission efficiency was calculated from:

$$\eta \text{ (hydraulic transmission)} = \frac{\text{PV (compressor)}}{\text{PV (engine}} = \frac{-(\text{PLHVP} + \text{PRHVP})}{\text{PVKUL}}$$

and the lower end efficiency was defined as:

$$\eta \text{ (lower end)} = \eta \text{ (hydraulic transmission)} \cdot \eta \text{ (compressor)}$$

where:

$$\eta \text{ (compressor)} = \frac{\text{Compressor Isentropic Power}}{\text{PV Compressor}}$$

The compressor isentropic power is defined as:

$$W(\text{isentropic}) = \dot{m}\,[n/(n-1)]\,P_b \nu_b [(P_c P_b)^{n-1/n} - 1]\eta_m;$$

where: P_b = compressor suction pressure
P_c = compressor discharge pressure
ν_b = specific volume at inlet
η_m = mechanical efficiency
n = polytropic gas constant (1.173)
$\dot{m}$ = measured refrigerant mass flow rate.

In testing that proceeded beyond the conclusion of Phase IB, performance results were obtained for the lower end containing the counterweight. A summary of the

Table A-4

Definition of Power and Efficiency Terms

PKUL	Helium compression space
PPGS	Gas spring
PVUOIL	Upper oil Volume (A) acting on CW
PVLOIL	Lower oil Volume (B) acting on CW
PCWLH	Left hand oil Volume (C) acting on CW
PCWRH	Right hand oil Volume (D) acting on CW
PPISLH	Left hand oil Volume (C) acting on piston
PPISRH	Right hand oil Volume (D) acting on piston
PLHVP	Left hand refrigerant cylinder acting on piston
PRHVP	Right hand refrigerant cylinder acting on piston
Counterweight Loss (PCWLOS)	PVUOIL + PVLOIL + PCWLH + PCWRH
Piston Loss (PISLOS)	PPISLH + PPISRH + PLHVP + PRHVP
Hydraulic Loss	PVKUL + PLHVP + PRHVP + PPGS - PCWLOS - PISLOS
Total Transmission Loss	PVKUL + PLHVP + PRHVP + PPGS
Total Lower End Loss	PVKUL + PLHVP + PRHVP

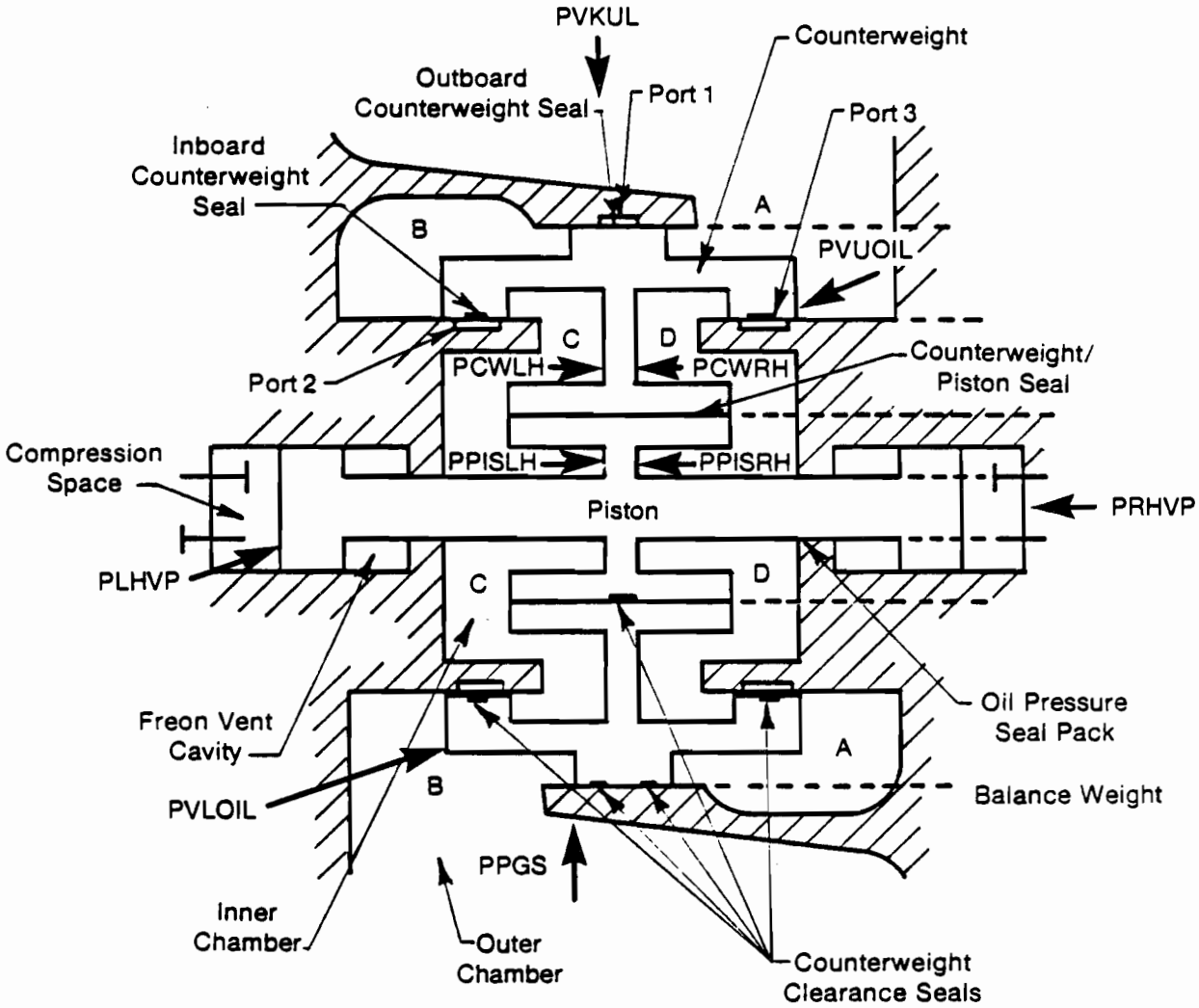

Figure A-3 Hydraulic Transmission Energy Flow Diagram

852062-1

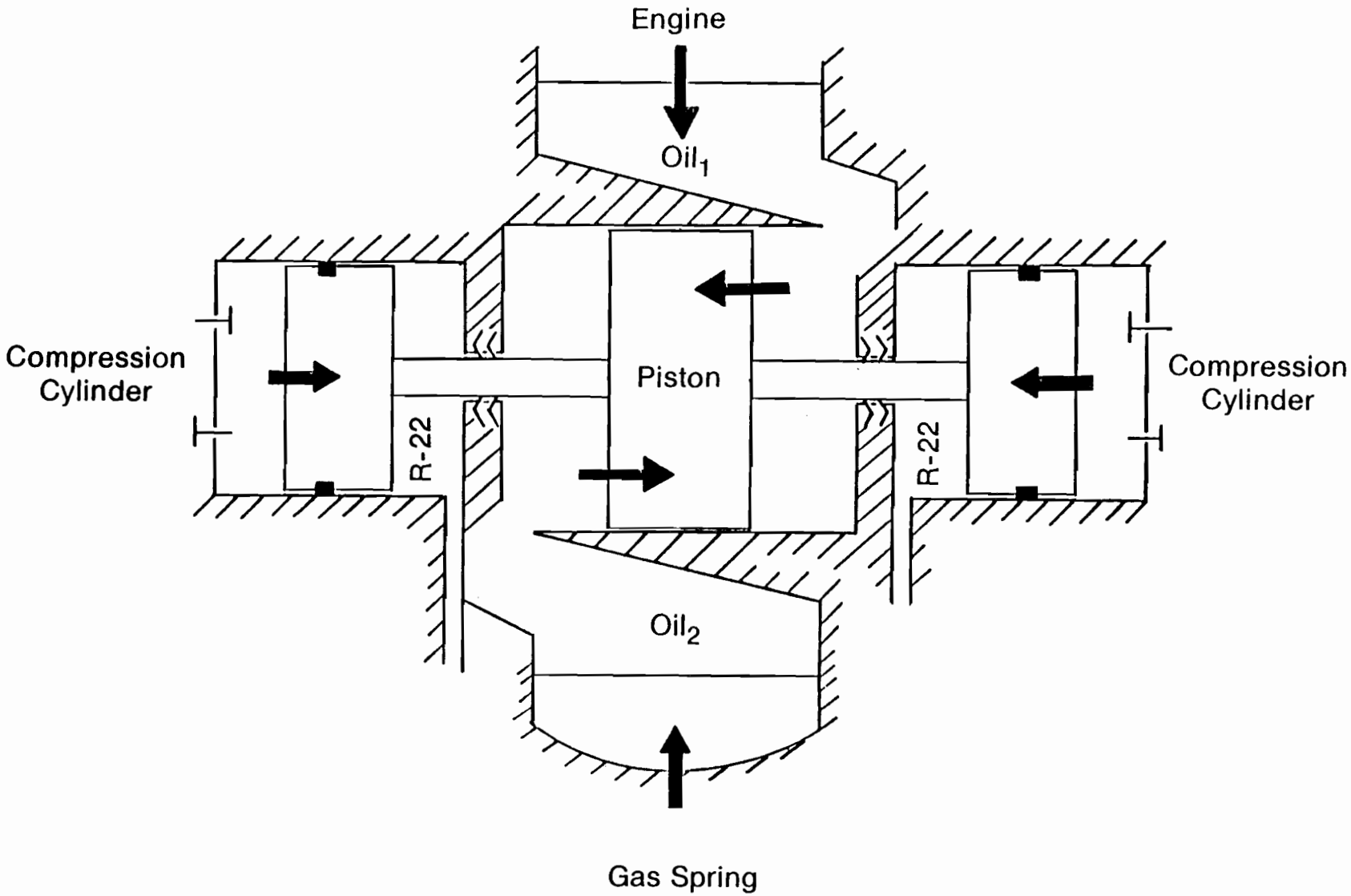

Figure A-4 "Direct Drive" Compressor Measured Energy Flow

841844

Table A-5

Comparison of Breadboard Heat Pump Performance Results with and without the Counterweight

Mode		No Counterweight	With Counterweight
Date		6/13/84	3/29/85[1]
Scan No.			34
Refrigerant		R-22	R-22
Hydraulic Oil		DC-200,2	DC-200,2 cs
Mean Pressure	(bar)	61.1	62.1
Frequency	(Hz)	59.2	58.0
Average Heater Head Temperature	(°C)	710	710
Counterweight Stroke	(mm)	NA	15.25
Piston Stroke	(mm)	16.6	15.25
Displacer Stroke	(mm)	20.7	21.73
$\Theta/_{d,p}$	(°)	69.8	89.8
Suction Pressure	(psia)	97.2	89.6
Discharge Pressure	(psia)	296.4	280.3
Suction Temperature	(°F)	74.2	46.6
Discharge Temperature	(°F)	175.8	144.5
Freon Flow	(lbm/hr)	401	342
Refrigerant Capacity	(Btu/hr)	28,227	23,000
Comp. Adiabatic Power	(W)	1,561.0	1,258.8
Compressor PV Power	(W)	1,689.9	1,576.3
Engine PV Power	(W)	2,408.3	2,511.6
Counterweight Loss	(W)	NA	612.8
Piston Loss	(W)	377.3	299.2
Gas Spring Loss	(W)	70.9	28.7
Hydraulic Loss	(W)	270.2	(5.4)
Overall Lower End Efficiency	(%)	64.8	50.1
Hydraulic Transmission Efficiency	(%)	70.2	62.8

[1]With 3 mm piston shim

best results obtained with and without the counterweight is given in Table A-5. Again, the addition of the counterweight significantly reduced the heat pump capacity, and it appears that nothing can be done to eliminate this problem except to eliminate the counterweight from the system.

APPENDIX B

REFRIGERANT TEST LOOP AND COMPRESSOR LOADING CONTROL

The refrigerant loop (see schematic in Figure B-1) consists of the following:

- Desuperheat heat exchanger (freon to water)
- Condenser-evaporator (freon-freon)
- Subcooler/liquid receiver (freon to water)
- Line filter
- Bearingless flow meter
- Vapor quality sight glass
- Main system expansion valve
- Thermostatistically/manually controlled desuperheat mixing valves.

Water flow is maintained by setting the manual adjustment at the water regulator (condenser pressure control valve, Figure B-1), which presets the spring tension and provides the force to balance with a sealed pressure force. The sealed pressure force is generated from a temperature bulb (fluid-filled line) referenced to the condenser inlet line downstream of the desuperheater. This arrangement of manual-course adjustment plus constant-temperature fine control will maintain a constant preselected condenser pressure.

The evaporator pressure (temperature) is maintained by the main system expansion valve by way of a through-flow regulator (Grove valve). The driving potential for the Grove valve is a refrigerant loop tap from the upstream liquid side of the valve being flashed to a vapor by a small heat exchanger at the compressor discharge line, venting finally to the low-pressure side of the main expansion valve passing through the Grove valve. The Grove valve is manually set to provide the required evaporator pressure for a given mass flow rate, and the interaction of the regulator and main system expansion valve provide a constant evaporator pressure for varying mass flows.

Compressor suction desuperheat is controlled by mixing wet vapor of low quality from the evaporator inlet to the dry gas at the compressor suction inlet line. Control of the desuperheat valves is accomplished by the action of three thermostatic valves of varying orifice size that can be selected from the control console. The thermal bulb reference to the thermostat controller is located in the suction line. As the suction temperature rises (rising superheat temperature), the thermostat opens the selected desuperheat valve to allow more wet vapor to mix with the superheat vapor cooling the vapor.

The operating range and control characteristics of the three basic controls as a function of mass flow rate for given condenser/evaporator pressures will have to be determined. It is assumed that the condenser-to-evaporator heat exchanger is of sufficient size so as not to be limiting. The compressor load (for controlled condenser/evaporator pressures) can then be made a function of mass flow rate and compressor mechanical efficiency:

$$W(\text{isentropic}) = \dot{m}\,[n/(n-1)]\,P_b \nu_b [(P_c P_b)^{n-1/n} - 1]\eta_m;$$

where: P_b = compressor suction pressure
P_c = compressor discharge pressure
ν_b = specific volume at inlet
η_m = mechanical efficiency
n = polytropic gas constant (1.173)
$\dot{m}$ = measured refrigerant mass flow rate.

The compressor mass flow rate for a given geometry and operating frequency is a function of the volumetric efficiency:

$$m = \eta_v\, VD/\nu_3;$$

where: η_v = volumetric efficiency
VD = total swept volume per time
ν_3 = compression volume inlet specific volume (valve pressure drop).

The volumetric efficiency is related to the clearance volume factor:

$$\eta_v = [1 + C = C\,(P_c/P_b)^{1/n}]\nu_3/\nu_b;$$

where: C = clearance volume factor.

Finally, the clearance volume factor can be related to stroke:

$$C = V_d/V_b - V_d;$$

where: $V_d = V_{cl} + X_{p-p}A_p - X_{pL}A_p$
$V_b = X_{p-p}A_p$

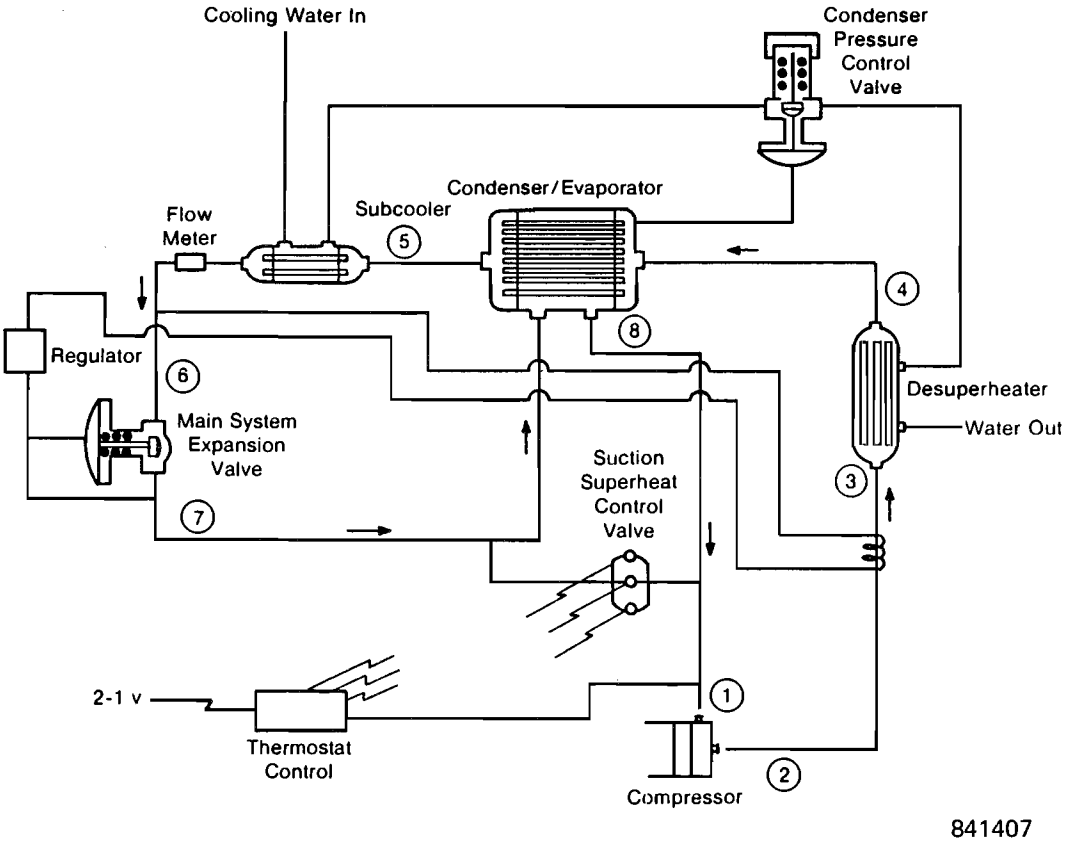

Figure B-1 HAHP Refrigerant Calorimeter

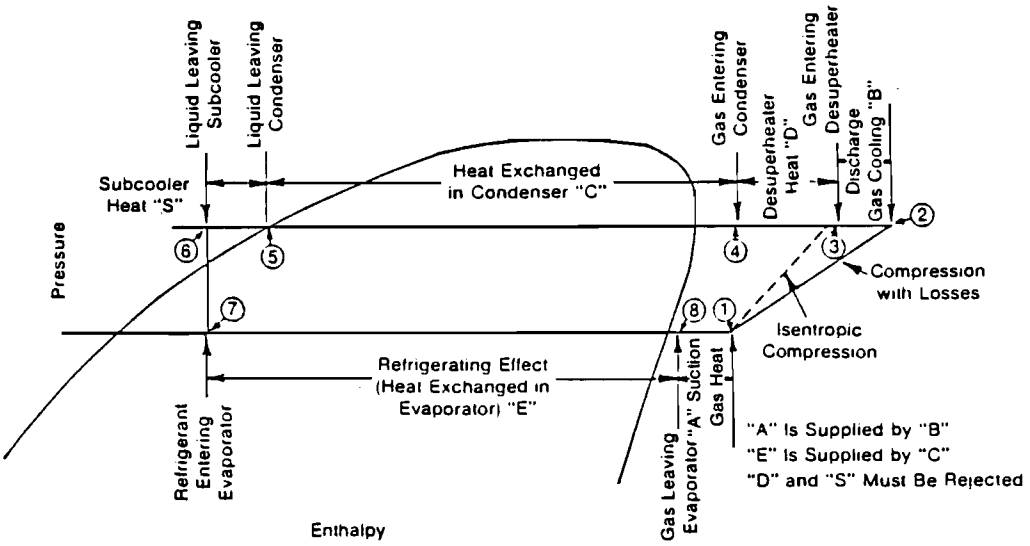

Figure B-2 Refrigerant Test Loop State Points

791879

A_p = piston area

X_{pL} = operating stroke

X_{p-p} = maximum stroke

V_{cl} = clearance volume.

In summary, within the limitations of the test loop controls, to maintain fixed condenser/evaporator pressures and suction superheat temperature, the compressor load and, hence, engine load can be maintained as a function of stroke once refrigerant flow is established.

The cooling capacity measured in Phase IB was found from the refrigerant state points given in Figure B-2. The cooling capacity is defined as:

$$Q \text{ (cooling capacity)} = m(h_1 - h_7)$$

where: m = refrigerant mass flow rate

h_1 = refrigerant vapor in the manifold heading to the compressor

h_7 = enthalpy of the refrigerant centering the evaporator.

ORNL/Sub/83-47985/1
Dist. Category UC-95d

INTERNAL DISTRIBUTION

1. F. C. Chen
2. F. A. Creswick
3. N. Domingo
4. P. D. Fairchild
5. S. K. Fischer
6. W. Fulkerson
7. F. P. Griffin
8. M. A. Kuliasha
9. F. C. Maienschein
10. S. H. McConathy
11. R. W. Murphy
12. G. T. Privon
13. C. D. West

14-33. Energy Conservation Distribution, Bldg. 9102-2, Room 218

34-35. Central Research Library

36. Document Reference Section
37. Laboratory Records-RC

38-39. Laboratory Records

40. ORNL Patent Section

EXTERNAL DISTRIBUTION

41. R. A. Ackermann, Mechanical Technology, Inc., 968 Albany-Shaker Road, Latham, NY 12110
42. William Beale, Sunpower, Inc., 6 Byard Street, Athens, OH 45701
43. Glendon M. Benson, Energy Research and Generation, Inc., Lowell and 57th Streets, Oakland, CA 94608
44. Don Beremand, NASA-Lewis Research Center, 21000 Brookpark Road, Cleveland, OH 44135
45. Dick Bloomquist, Code 2752, David W. Taylor Naval Ship R&D Center, Annapolis, MD 21402
46. T. A. Braun, Tectonics Research, Inc., 9556 West Bloomington Freeway, Minneapolis, MN 55431
47. J. P. Budliger, Battelle-Geneva, 7 route de Drize, 1227 Carouge (Geneva), Switzerland
48. J. M. Calm, Electric Power Research Institute, P.O. Box 10412, Palo Alto, CA 94303
49. J. G. Carbonell, Associate Professor of Computer Science, Carnegie-Mellon University, Pittsburgh, PA 15213
50. Stig C. Carlqvist, Societe ECA, Boite Postale 16, 92194 Meudon Cedex, France
51. Dick Cawley, Lennox Industries, Inc., 1600 Metrocrest Drive, Carrollton, TX 75006
52. W. S. Chiu, General Electric Company, P.O. Box 527, King of Prussia, PA 19406
53. M. Clinch, Gas Research Institute, 8600 West Bryn Mawr Avenue, Chicago, IL 60631
54. E. H. Cooke-Yarborough, Lincoln Lodge, Longworth Nr Abingdon, Oxfordshire, OX13, 5DU, England
55. J. G. Daley, Argonne National Laboratory, 9700 South Cass Avenue, Argonne, IL 60439

56. D. K. Darooka, General Electric Company, P.O. Box 527, King of Prussia, PA 19406
57. R. L. Demler, Foster-Miller Associates, Inc., 350 2nd Avenue, Waltham, MA 02254
58. G. R. Dochat, Mechanical Technology, Inc., 968 Albany-Shaker Road, Latham, NY 12110
59. J. E. Dudenhoefer, NASA-Lewis Research Center, 21000 Brookpark Road, Cleveland, OH 44135
60. T. Finkelstein, Stirling Associates International, P.O. Box 643, Beverly Hills, CA 90213
61. R. J. Fiskum, Energy Conversion Equipment Branch, CE-112, GF-217/FORS, Department of Energy, 1000 Independence Avenue SW, Washington, DC 20585
62. M. Foster, Homach Systems, Ltd., Hargreaves Road, Groundwell Industrial Estate, Swindon Wilts, SN2, 5AZ, England
63. A. A. Frank, Department of Electrical and Computer Engineering, University of Wisconsin-Madison, 1500 Johnson Drive, Madison, WI 53706
64. S. Freedman, Gas Research Institute, 8600 West Bryn Mawr Avenue, Chicago, IL 60631
65. M. Fukiwake, Agency of Industrial Science and Technology, Ministry of International Trade and Industry, 1-3-1 Kasumigaseki, Chiyoda-Ku, Tokyo, Japan
66. D. R. Gedeon, Gedeon Associates, Box 141 A, South Canaan Road, Athens, OH 45701
67. Ted Gilles, Lennox Industries, Inc., Promenade Towers, P.O. Box 400450, Dallas, TX 75240
68. S. M. Gillis, Dean, Graduate School, Duke University, 4875 Duke Station, Durham, NC 27706
69. L. Goldberg, University of Minnesota, Dept. of Civil and Mineral Engineering, 500 Pillsbury Drive SE, Minneapolis, MN 55455
70. B. S. Goldwater, Mechanical Technology, Inc., 968 Albany-Shaker Road, Latham, NY 12110
71. A. C. Harvey, Foster-Miller Associates, Inc., 350 2nd Avenue, Waltham, MA 02254
72. R. E. Hise, Consolidated Natural Gas Research Company, 11001 Cedar Avenue, Cleveland, OH 44106
73. Bob Holtz, Argonne National Laboratory, 9700 South Cass Avenue, Argonne, IL 60439
74. R. C. Hundt, Lennox Industries, Inc., 1600 Metrocrest Drive, Carrollton, TX 75006
75. P. Huntley, Borg-Warner Research, 1200 South Wolf Road, Des Plaines, IL 60018
76. B. C. Hwang, Code 2722, David W. Taylor Naval Ship R&D Center, Annapolis, MD 21402
77. H. S. Izawa, Northern Natural Gas Company, 2223 Dodge Street, Omaha, NE 68102
78. L. N. Johansson, Stirling Power Systems, 7101 Jackson Road, Ann Arbor, MI 48103
79. F. R. Kalhammer, Vice President, Electric Power Research Institute, P.O. Box 10412, Palo Alto, CA 94303

80. T. Kapus, Building Equipment Division, Department of Energy, CE-113, 1000 Independence Avenue SW, Washington, DC 20585
81. R. E. Kasperson, Professor of Government and Geography, Graduate School of Geography, Clark University, Worcester, MA 01610
82. K. P. Lee, Aspen Systems Inc., 275 Boston Post Road, Marlborough, MA 01752
83. M. Lesson, Consulting Engineer, 12 Country Club Drive, Rochester, NY 14618
84. Bengt Lundquist, Swedish Council for Building Research, Sankt Goransgatan, S-11233 Stokholm, Sweden
85. A. R. Maret, Gas Research Institute, 8600 West Bryn Mawr Avenue, Chicago, IL 60631
86. J. C. Mayor, Swiss Federal Institute for Reactor Research, CH-5303 Wurenlingen, Switzerland
87. R. C. Meier, General Electric Company, P.O. Box 527, King of Prussia, PA 19406
88. R. J. Meijer, Stirling Thermal Motors, Inc., 2841 Boardwalk, Ann Arbor, MI 48104
89. N. P. Nightingale, Mechanical Technology, Inc., 968 Albany-Shaker Road, Latham, NY 12110
90. Herbert Nilsson, United Stirling AB, P.O. Box 856, S-201 80 Malmo, Sweden
91. L. B. Penswick, Sunpower Inc., 6 Byard Street, Athens, OH 45701
92. W. H. Percival, United Stirling, Inc., 1800 Diagonal Road, Alexandria, VA 22314
93. B. Qvale, Laboratory for Energetics, The Technical University of Denmark, DTH Building 403, DK-2800 Lyngby, Denmark
94. E. A. Reid, Jr., Columbia Gas System Service Corporation, 1600 Dublin Road, Columbus, OH 43215
95. P. Riggle, Joint Center for Graduate Study, University of Washington, 100 Sprout Road, Richland, WA 99352
96. J. D. Ryan, Energy Conversion Equipment Branch, CE-112, GF-217/FORS, Department of Energy, 1000 Independence Avenue SW, Washington, DC 20585
97. J. G. Schreiber, NASA-Lewis Research Center, 21000 Brookpark Road, Cleveland, OH 44135
98. J. R. Senft, Department of Mathematics/Computer Science, University of Wisconsin, River Falls, WI 54022
99. J. G. Slaby, NASA-Lewis Research Center, 21000 Brookpark Road, Cleveland, OH 44135
100. J. L. Smith, Jr., Mechanical Engineering Department, Massachusetts Institute of Technology, Cambridge, MA 02139
101. P. F. Swenson, The East Ohio Gas Company, East 9th Avenue at Superior, P.O. Box 5759, Cleveland, OH 44101
102. D. R. Taylor, Royal Naval Engineering College, Manadon Plymouth, Devon PL5 3AQ, England
103. W. P. Teagan, Arthur D. Little, Inc., 20 Acorn Park, Cambridge, MA 02140
104. R. C. Tew, NASA-Lewis Research Center, 21000 Brookpark Road, Cleveland, OH 44135

105. W. M. Toscano, Aspen Systems, Inc., 275 Boston Post Road, Marlborough, MA 01752
106. V. J. Van Griethuysen, Air Force Wright Aeronautical Laboratories, Wright-Paterson Air Force Base, OH 45433
107. D. A. Vaughn, Belvoir R&D Center, Ft. Belvoir, VA 22060, ATTN: STRBE-EMP
108. G. Walker, University of Calgary, Department of Mechanical Engineering, 2500 University Drive NW, Calgary, Canada T2N1N4
109. B. P. Wang, Mechanical Engineering Department, University of Texas at Arlington, P.O. Box 19023, Arlington, TX 76019
110. M. A. White, University of Washington, Joint Center for Graduate Study, 100 Sprout Road, Richland, WA 99352
111. L. Williams, Logan Lewis Library, Research Division, Carrier Corporation, Carrier Parkway, Syracuse, NY 13221
112. J. Wurm, Institute of Gas Technology, 3424 South State Street, Chicago, IL 60616
113. Y. Yamashita, New Energy Development Organization, Sunshine 60 29F, 101 3-Chome Higashi-Ikebukuro, Toshima-Ku, Tokyo 170 Japan
114. Institute for Energy Analysis, ORAU-Library, Oak Ridge, TN 37831
115. Office of the Assistant Manager for Energy R&D, U.S. Department of Energy, Oak Ridge Operations, Oak Ridge, TN 37831

116-337. Given distribution for Category UC-95d.

☆U.S. GOVERNMENT PRINTING OFFICE 1987—548-118/60119